2013

Fast and reliable detection of incumbent users in cognitive radios

Mahdi Orooji
Louisiana State University and Agricultural and Mechanical College

FAST AND RELIABLE DETECTION OF INCUMBENT USERS IN COGNITIVE RADIOS

A Dissertation

Submitted to the Graduate Faculty of the
Louisiana State University and
Agricultural and Mechanical College
in partial fulfillment of the
requirements for the degree of
Doctor of Philosophy

in

The School of Electrical Engineering and Computer Sciences

by
Mahdi Orooji
B.Sc., University of Tehran, 2003
M.Sc., Iran University of Science and Technology, 2006
M.Sc., Louisiana State University, 2011
March 2013

To my beloved wife, Maryam,
and our lovely daughter, Rose.

Acknowledgments

First and foremost, I would like to express my sincerest gratitude to my supervisor, Dr. Morteza Naraghi Pour for his invaluable and insightful guidance throughout the course of my PhD study at the Louisiana State University. He gave me the main idea of this work, and without his continuous encouragement next to his deep knowledge of communication and mathematics, this thesis could not have been accomplished. I am always thankful for his support and all I have learned from his great professional vision and scientific insight. Also in three courses I have had with him, Wireless Communication Networks, Error Control Coding, and Random Process-II, he taught me how to face difficult problems in my researches and developed the true research spirit in me. Besides all he had done in my PhD studies, I always remember his fatherly manners in my life's difficulties from the day I entered the USA. All he has done to help me through this arduous task is more than what I would have expected to find in an advisor and will never be forgotten.

I want to express my special thanks to my thesis committee, Dr. Shuangqing Wei, Dr. Xuebin Liang, Dr. Guoxiang Gu, and Dr. Thomas Dean for patiently attending my general and final exams and providing me with their thoughtful comments and suggestions. Your help has always been constructive, beneficial, and very valuable to me. I would also like to thank Dr. Shuangqing Wei for his courses, Digital Communication and the Detection and Estimation Theory, and Dr. Xuebin Liang for his course, MIMO Systems. Your fruitful classes had great influence on my research insight, and I frequently used the materials of these courses in my PhD thesis.

I would like to express my thanks to my parents, Mohammadreza Orooji and Mansooreh Rabiee who taught me to be self-motivated, have a strong work ethic, and take pride in my work. Their supports and prayers have been invaluable.

Most certainly, this thesis would not have been possible without the love, encouragement and support of my wife, Dr. Maryam Rezai Rad. Her sacrifice for this project was much more than anticipated and far more than fair.

I want to thank my father-in-law Dr. Rezai Rad and my mother-in-law Dr. Nikravesh for their encouragements and supports through all of my educational years. I also want to thank my sisters and their families, and my brother-in-law for their unconditional love and devotion.

I also would like to acknowledge my colleagues, Erfan Soltanmohammadi, Yahya Sowti Khiabani, Reza Soosahabi, and Iman Khademi for their warm friendship and provided support in a variety of ways. And finally, I appreciate all my instructors in the School of Electrical Engineering and Computer Sciences and in the Department of Math. Their classes had great impact on my knowledge.

Table of Contents

List of Tables

List of Figures

Abstract

Fast and reliable Spectrum Sensing (SS) plays a crucial role in the cognitive radio (CR) technology in order to prevent unwanted interference to the primary users (PU) and to reliably and quickly detect the white spaces in the spectrum for opportunistic access by the secondary users (SU).

Spectrum Sensing must often be performed in the absence of information such as PU signaling scheme, noise level and channel fading coefficients. While these parameters can be estimated in the SU, estimation errors significantly deteriorates the performance of SS techniques. In this thesis, we introduce and evaluate the performance of two novel blind spectrum sensing algorithms which do not rely on knowledge of these parameters.

The first is a SS technique for signaling schemes which introduce controlled intersymbol interference in the transmitter. The second is for cases when the receiver of the SU is equipped with a multiantenna system. This approach exploits the path correlation among the signals received at different antennas.

Next we analyze the performance of Spectrum Monitoring (SM), an new technique which allows the SU to detect the presence of the PU using its own receiver statistics. In contrast to SS, with SM, the SU does not need to interrupt its own transmission in order to detect the presence of the PU. We carefully construct the decision statistics for SM and evaluate its performance. The performance of a hybrid SM/SS system shows a significant improvement over SS alone.

Chapter 1
Introduction and Background

1.1 Opportunistic Spectrum Access

Today most of the radio spectrum is assigned to licensed users. However, while spectrum utilization is mainly concentrated around certain parts of the spectrum, a considerable portion of the spectrum is underutilized. The spectrum usage is more concentrated for the frequencies below 3GHz [2]. Figure 1.1 shows actual measurement of the power spectral density (PSD) of the received signal in a frequency band 6 GHz wide collected for a span of 50 μs and sampled at 20 GS/s [1]. It can be observed that spectrum utilization is more intense at frequencies below 3 GHz whereas the spectrum is under-utilized in the 3-6 GHz bands.

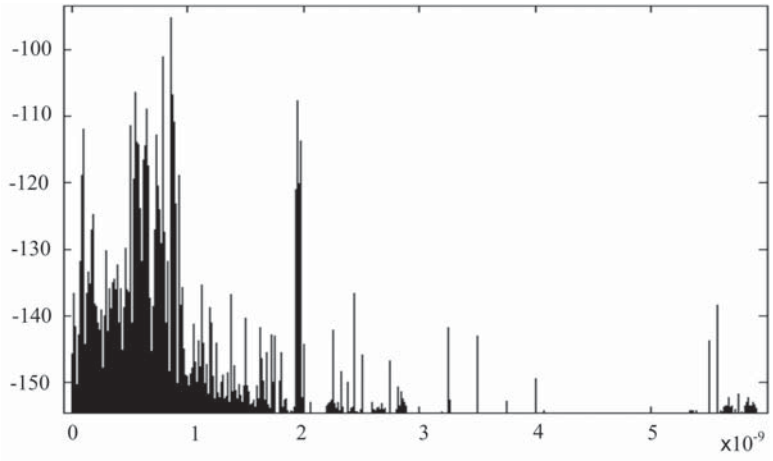

FIGURE 1.1. Actual measurement of 0-6 GHz spectrum utilization [1]

According to Federal Communications Commissions (FCC) [3], the spectrum utilization in different locations and frequencies is varying from 15% to 85%. Fixed spectrum allocation policies do not allow unlicensed users to reuse the mostly vacant bands which are allocated to licensed users. The limited available spectrum, inefficiently regulated bands and overcrowding of the radio spectrum coupled with

the ever increasing demand for wireless services has led to the introduction of a new paradigm in spectrum management, namely opportunistic spectrum access (OSA).

In OSA a secondary user (SU) can identify and utilize the portions of the licensed spectrum that are currently unused by the primary users (PU). Cognitive Radio (CR), first introduced in [4], has been proposed as the enabling technology for opportunistic spectrum access. Afterward many efforts have been made to clearly define the functionalities of CRs and many efforts have been made to standardize it [5]. However, most of them have focused on theoretical analysis, and only a few of them have been validated in practical system.

1.2 Cognitive Radios

Cognitive radio networks provide an opportunity to create time and location dependent virtual unlicensed bands (bands that have been shared with the PU), and to have dynamic spectrum management to prevent destructive interference to the PUs. Even though no CR-based commercial devices have been introduced yet, FCC allows the use of the unused television spectrum [6]. The Institute of Electrical and Electronics Engineers (IEEE) has also supported the cognitive radio by developing the IEEE-802.22 standard for Wireless Regional Area Network (WRAN) which works in unused TV channels [7]. In the following, we are going to explain two fundamental functionalities of cognitive radios, namely *Cognitive Capability* and *Reconfigurability*.

1.2.1 Cognitive Capability

The cognitive capability enables the secondary users to acquire necessary information from their radio environment. Transmitted waveforms, radio frequency spectrum, communication network protocol, security policies, and locally avail-

able resources are some examples of the information that the secondary user can gain from the licensed networks [8]. No standard duty cycle algorithm for cognitive radio has been established yet. However, Figure 1.2 demonstrates a typical cognitive cycles [9]. The steps of cognitive cycle defined in Figure 1.2 are,

- Spectrum sensing: In a cognitive radio network a secondary user must reliably sense the channel to determine whether in a specific band another user's signal (primary or secondary) is present or not.
- Spectrum analysis: The cognitive radio should evaluate the parameters of the potentially available band such as channel capacity, or noise level.
- Spectrum decision: In the absence of another signal, the secondary user adapts its operating parameters (e.g., carrier frequency, transmit power, modulation, coding, etc.) in order to make best use of the available spectrum hole and provide the desired quality of service.

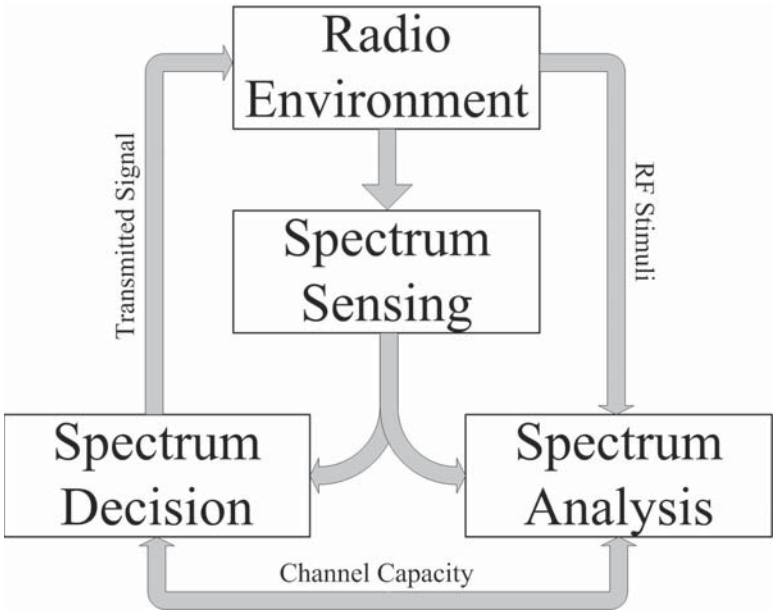

FIGURE 1.2. Duty cycle for cognitive radios

At the end of the cognitive cycle, the available spectrum is determined and the secondary user initiates transmission. As long as the secondary user wishes

to transmit, this cycle runs to keep track of the changes in the current transmitting band. Figure 1.3 demonstrates how the secondary user utilizes the available spectrum holes.

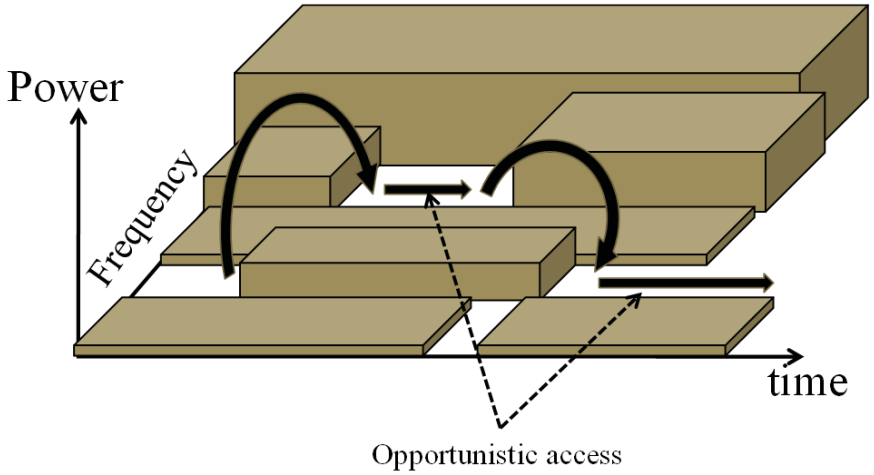

FIGURE 1.3. Opportunity Spectrum Access

1.2.2 Reconfigurability

The Reconfigurability of the cognitive radios means cognitive radio's transmitter and receiver should be capable of adjusting their operating parameters such as transmission power, carrier frequency or modulation scheme to take maximum advantage of the available radio resources in their environment [10]. The SUs should have the capability of adjusting their operating functions only by doing software adaptation and with no hardware modifications. This adjustment should happen not only at the initialization of the transmission but also during the communication, due to the fact that the secondary user may switch between available spectrum holes. Some examples of parameters that the secondary user should reconfigure frequently are,

- Transmission Power: The secondary user should adjust its transmission amplifier gains to first avoid an interference to the primary user who may be present in the band but has not been sensed due to misdetection (because

of for example large fading). Second to open up an opportunity to the other secondary users to access the available spectrum.

- Operating Frequency: Switching between spectral holes implies that the secondary user should have the capability of changing its operating frequency.
- Modulation: Based on the service that the secondary user receiver needs, the secondary user should adjust its modulation. On the other hand, the secondary user may also change its modulation based on available spectrum condition.

1.3 Spectrum Sensing in Cognitive Radios

As it was described, the first required capability of cognitive radio systems is spectrum sensing. In SS, two metrics of the probability of detection and the probability of false alarm are widely used in order to assess and compare the performance of different approaches. The probability of detection is defined as the probability that the SS algorithm is capable of detecting the existence of the PU. The probability of false alarm indicates the probability that the detector falsely alarms the existence of the PU when it is not present.

Spectrum sensing is performed for out-of-band channels (out-of-band sensing) in order to determine if they are vacant of the PU signals, and for the in-band channel so that the SU can promptly vacate the channel in which the PU has emerged (in-band sensing). Since protection of incumbent users is paramount, strict requirements are imposed on in-band sensing. For example in IEEE 802.22, the Wireless Regional Area Networks (WRAN) standard, a PU should be detected within 2 secs [5, 7] after it starts transmission. This requirement (referred to as detection time) implies that the transmission intervals of the SU must be shorter than two secs., and must be periodically interrupted by spectrum sensing intervals. If spectrum sensing determines that the channel is vacant of the incumbent users,

then a new transmission interval resumes followed by another sensing interval, and so on.

During the sensing intervals the communication of the SUs is suspended resulting in loss of quality of service (QoS) in the secondary network. Therefore, it is desired to make the sensing periods as short as possible and to reduce their frequency. However, duration of the spectrum sensing period affects the performance of the sensing algorithm as expressed by the detection and false alarm probabilities. Detection probability should be large (e.g., $> .9$ for IEEE 802.22 standard) since with misdetection the SU will continue to transmit causing interference to incumbent users. On the other hand, the probability of false alarm must be small (e.g., $< .1$ for IEEE 802.22 standard) as it results in loss of throughput in the secondary network. In addition, during its transmission intervals the SU does not try to detect the presence of the PU signal. Therefore if the PU emerges, not only will the SU cause undue interference to the PU, but also its own communication may be disrupted due to the interference from the PU. Spectrum sensing has received a great deal of attention in recent years and many algorithms have been proposed. A survey of some recent algorithms appears in [9, 11, 12] and the references therein.

1.4 Blind Spectrum Sensing

Based on the available prior knowledge of the signaling scheme used by the PU, the noise power, or the channel path coefficients, spectrum sensing techniques may be classified into two categories; feature detection and blind detection.

- Feature detection techniques: These algorithms utilize specific characteristics of the primary signal, noise and/or channel parameters (such as channel fading coefficients). Clearly as more knowledge of the primary signal, noise or channel is assumed, better performance can be achieved at the expense of additional complexity and less generality.

- Blind detection algorithms: These algorithms assume a minimal prior information of the primary signal parameters (e.g., bandwidth, modulation scheme, etc.), noise information (e.g., noise power) or the channel information (e.g., channel fading coefficients).

Cyclo-stationary detectors are examples of feature detectors, which require more information on the primary signal parameters and are more computationally intensive [13, 14, 15, 16, 17]. Energy Detector (ED) is the most typical example of spectrum sensing algorithm [18, 19]. Despite its easy implementation, selection of a threshold in ED to achieve a given false alarm probability requires precise knowledge of the noise power (in this sense, ED is considered as a feature detection algorithm). In the presence of noise power uncertainty, the performance of ED is severely degraded due to a phenomenon referred to as "SNR wall" [20]. To avoid the problem of noise power uncertainty in energy detectors, a generalized likelihood ratio test (GLRT) algorithm may be employed [15, 21]. Even though GLRT based energy detector is a blind spectrum sensing algorithm, the performance of such algorithms at low SNR values are generally poor.

Recently several autocorrelation-based algorithms have appeared in the literatures which are robust to noise uncertainty and exploit the fact that while white noise samples are uncorrelated, most communication signals exhibit non-zero correlation. However, these algorithms either assume a specific modulation scheme, [22, 23], or rely on oversampling (with respect to the modulation symbol period) of the received signal [24, 25, 26].

1.5 Spectrum Sensing Using Multiple Antennas

Multiple antenna systems have been widely used in wireless communication to increase channel capacity and to improve transmission reliability. Recently, several

authors have considered using multiple antenna systems for spectrum sensing [19, 26, 27, 28, 29, 30].

In [28] the authors employ GLRT based multiple antenna algorithm. Their algorithm is blind and it is shown that the system is robust to noise power uncertainty. A multiple-antenna system is also employed in [29] where an eigenvalue-based signal detection scheme is developed under noise power and/or signal correlation uncertainty. In [31], it is shown that in the presence of an unknown number of interferers, single-user multiple-antenna systems still suffer from SNR wall phenomenon. Recognizing that low-power interferers are local whereas the primary user has a global footprint, the authors propose a collaborative spectrum sensing technique to exploit what they refer to as "interference diversity".

1.6 Thesis Organization and Contributions

In Chapter 2, we propose a spectrum sensing technique for signaling schemes which introduce controlled intersymbol interference in the transmitter. Examples include correlative coding or partial response signaling techniques which have an inherent memory in the transmitted signal. A decision statistic is introduced based on the autocorrelation of the received signal and its performance in terms of the probabilities of false alarm and detection is evaluated for AWGN and Rayleigh fading channels. It is shown that the proposed method is a constant false alarm detector. The numerical results from simulation and analysis are presented to demonstrates the accuracy of our analysis.

Coexistence of the primary users and the secondary users in cognitive networks leads to increases in co-channel interference (CCI) which needs to be appropriately mitigated. CCI is often modeled as a white Gaussian noise process and assumed to simply reduce the signal-to-noise (plus interference) ratio. In Chapter 3, we consider the effect of CCI by a careful examination of the samples at the output of the

matched filter receiver. We show that the timing offset between the interference and the desired signals may result in the correlation of adjacent samples. We evaluate the bit error rate (BER) resulting from CCI as well as the distribution of the total number of errors in a packet. We use this result to introduce spectrum monitoring scheme. However, our results can be employed for more accurate evaluation of CCI and in developing techniques for CCI mitigation such as design of precoders or forward error correction codes.

In Chapter 4, using the receiver statistics, we introduce a decision statistic to enable the SU to detect the emergence of the PU without having to interrupt its own communication. The proposed algorithm is not an alternative spectrum sensing techniques. Rather it is intended to enhance an existing spectrum sensing by increasing channel utilization for the SU and reducing detection delay for the PU. We derive closed form formulas for channel utilization and detection delay using two Markov chain models. The limits of the introduced decision statistic is derived and an optimization problem is solved to maximize channel utilization with a constraint on detection delay. Numerical results are presented from analysis and simulation which show the accuracy of the analysis and the proficiency of the proposed method.

In Chapter 5, we consider the problem of blind spectrum sensing when the receiver of the secondary user is equipped with a multiantenna system. Using an estimate of the cross correlation among the signals received at different antenna elements, we propose a blind detection method which assumes no prior knowledge of the signaling scheme used by the PU, the noise power, or the channel path coefficients. The cross correlation among the received signals is a result of the correlation among the channel path coefficients from the primary user transmitter to different antenna elements of the secondary receiver. The detection and false

alarm probabilities of the proposed algorithms are evaluated using an asymptotic analysis, and the results are compared with simulation results.

Finally, the thesis is concluded in Chapter 6 by presenting some final remarks.

Chapter 2

Blind, Constant False Alarm Spectrum Sensing for Correlative Coding Signaling

2.1 Introduction and Background

The proficiency of the blind spectrum sensing in cognitive radios has been explained in Chapter 1. Recently several covariance and autocorrelation-based algorithms have appeared in the literature which are robust to noise uncertainty and exploit the fact that while white noise samples are uncorrelated, most communication signals exhibit non-zero correlation. These algorithms either assume a specific modulation scheme, [22, 23], or rely on oversampling (with respect to the modulation symbol period) of the received signal [25, 26, 24].

In this Chapter, we exploit the correlation present in communication signals resulting from correlated signaling or coding to introduce a novel blind spectrum sensing technique. We develop a decision statistic based on the autocorrelation of the received signal samples. The proposed method is constant false alarm rate in that its false alarm rate can be set by selecting the number of observation samples. The false alarm and detection probabilities are evaluated analytically for AWGN and Rayleigh fading channels and compared with results from simulation.

2.2 Autocorrelation or the Received Signal at the Secondary User Receiver

The baseband complex envelope of the primary user transmitted signal is given by [32],

$$s(t) = \sum_{n=-\infty}^{\infty} h_a(t - nT_s)\mathfrak{F}(X_n) \tag{2.1}$$

$$X_n = [x_n, x_{n-1}, \cdots, x_{n-K}], \tag{2.2}$$

where $\{x_n\}$ is the sequence of zero-mean independent and identically distributed transmitted symbols, $h_a(t)$ for $t \in [0, T_s)$ is the pulse shape, T_s is the symbol duration and K is a non-negative integer. Finally $\mathfrak{F}(.)$ is a function defined based on the modulation scheme and the forward error correction (FEC) code utilized by the PU. If $K = 0$ corresponds to full-response signaling, while $K \geq 1$ define partial response signaling for which there is an inherent memory in the modulated signal. *Correlative coding*, *continuous phase modulation*, and *trellis coded modulation* are some schemes which introduce memory into the transmitted signal. This Chapter will focus on correlative coding.

Correlative coding, also called partial response signaling or controlled intersymol-interference (CISI) signaling is introduced in [33] in which the data sequence is passed through a finite impulse response (FIR) filter denoted by f_{CISI} where $f_{\text{CISI}}(z) = \sum_{k=0}^{K-1} f_k z^{-k}$. Due to their simplicity and their useful spectral shapes, *Doubinary* signaling with $f_{\text{CISI}}(z) = 1+z^{-1}$, and *Modified doubinary* signaling with impulse response $f_{\text{CISI}}(z) = 1-z^{-2}$ are the most commonly used correlative coding schemes [34]. The transmitted signal with correlative coding and linear modulation is given by

$$s(t) = \sum_{n=-\infty}^{\infty} h_a(t - nT_s) \left(\sum_{k=0}^{K-1} x_{n-k} f_k \right) \tag{2.3}$$

The autocorrelation function of $s(t)$ is given by

$$\begin{aligned} \Phi_{ss}(\tau) &= \frac{1}{T_s} \int_0^{T_s} E\left[s(t+\tau)s^*(t)\right] dt \qquad (2.4) \\ &= \frac{1}{2T_s} \sum_{n=-\infty}^{\infty} \sum_{m=-\infty}^{\infty} \left(\int_0^{T_s} h_a(t+\tau-mT_s) h_a^*(t-nT_s) \right. \\ &\qquad \left. \times \sum_{p=0}^{K-1} \sum_{q=0}^{K-1} f_q f_p^* E[x_{m-p} x_{n-q}^*] \;\; dt \right) \end{aligned}$$

$$= \frac{1}{2T_s} \sum_{n=-\infty}^{\infty} \sum_{m=-\infty}^{\infty} \left(\int_{-nT_s}^{-nT_s+T_s} h_a(t+\tau-(m-n)T_s) h_a^*(t) \right. \tag{2.5}$$
$$\left. \times \mathcal{E}_x \sum_{p=0}^{K-1} \sum_{q=0}^{K-1} f_q f_p^* \delta(m-n+q-p)\ dt \right)$$
$$= \frac{1}{2T_s} \sum_{i=-\infty}^{\infty} \left(\int_{-\infty}^{\infty} h_a(t+\tau-iT_s) h_a^*(t) dt \right.$$
$$\left. \times \mathcal{E}_x \sum_{p=0}^{K-1} \sum_{q=0}^{K-1} f_q f_p^* \delta(i+q-p) \right)$$
$$= \frac{1}{2T_s} \sum_{i=-\infty}^{\infty} \left(\mathcal{G}_a(\tau - iT_s)\ \mathcal{E}_x \sum_{p=0}^{K-1} \sum_{q=0}^{K-1} f_q f_p^* \delta(i+q-p) \right)$$

where $\delta(k) = 1$ for $k = 0$ and 0 otherwise, $\mathcal{E}_x$ is the average energy of the transmitted symbols and $\mathcal{G}_a(t) \triangleq h_a(t) * h_a^*(-t)$, where $*$ between two signals denotes convolution and $h_a^*(t)$ is the conjugate of $h_a(t)$. Assuming $\mathcal{G}_a(-T_s) = \mathcal{G}_a(T_s) = 0$, $\mathcal{G}_a(t)$ is a function defined on $[-T_s, T_s]$ which implies that in 2.4, i assumes one of two values, i.e.,

$$i \in \{\lfloor \tau/T_s \rfloor, \lfloor \tau/T_s \rfloor + 1\} \tag{2.6}$$

where $\lfloor . \rfloor$ is the floor function. After some manipulations one can show that,

$$\Phi_{ss}(\tau) = \frac{\mathcal{E}_x}{2T_s} \left(\mathcal{G}_a(\mathcal{T}) \sum_{p=0}^{K-1-\mathcal{T}} f_{p+\mathcal{T}}\ f_p^* \right. \tag{2.7}$$
$$\left. + \mathcal{G}_a(\mathcal{T} - T_s) \sum_{p=0}^{K-2-\mathcal{T}} f_{p+\mathcal{T}+1}\ f_p^* \right)$$

where $\mathcal{T} \triangleq \tau - \left\lfloor \frac{\tau}{2T_s} \right\rfloor T_s$, and $0 \leq \mathcal{T} < T_s$.

If there is no over-sampling in spectrum sensing, we would have $\tau = lT_s$. Consequently, $\mathcal{T} = 0$ which results in for $0 \leq l \leq K-1$ we have,

$$\Phi_{ss}(lT_s) = \bar{\mathcal{E}}_h\ \mathcal{E}_x \sum_{p=0}^{K-l-1} f_{p+l} f_p^* \tag{2.8}$$

where

$$\bar{\mathcal{E}}_h \triangleq \frac{1}{T_s}\int_0^{T_s} |h_a(t)|^2 dt \tag{2.9}$$

2.2.1 Correlation of the Received Signal

Let H_0 and H_1 denote the absence and the presence of the PU, respectively. We assume block fading in that the channel coefficient, denoted by g, is fixed during the sensing period. The baseband complex envelope of the received signal at the SU receiver under hypothesis H_η, $\eta \in \{0, 1\}$, is given by

$$r(t) = \eta g s(t) + v(t). \tag{2.10}$$

where $\{v(t)\}$ is the white Gaussian noise process with zero mean and variance N_0 which is independent of $s(t)$. It can be seen that the correlation of the received signal under hypothesis H_η is given by

$$\Phi_{rr}^{(\eta)}(\tau) = \eta |g|^2 \Phi_{ss}(\tau) + N_0 \delta(\tau) \tag{2.11}$$

where $\delta(\tau)$ is the impulse function.

2.3 Decision Statistic

Spectrum sensing is performed on N consecutive samples of the received signal, $\mathbf{r} \triangleq \{r_0, r_1, \cdots, r_{N-1}\}$, where $r_n \triangleq r(nT_s)$. The correlation of the received signal is estimated as,

$$\hat{\Phi}_{rr}(\tau) \triangleq \begin{cases} \frac{1}{N-\tau} \sum_{n=0}^{N-\tau-1} r_{n+\tau} r_n^* & \text{if } \tau \geq 0 \\ \hat{\Phi}_{rr}^*(-\tau) & \text{if } \tau < 0 \end{cases} \tag{2.12}$$

One can verify that $\hat{\Phi}_{rr}(\tau)$ under H_η is a consistent and unbiased estimate of $\Phi_{rr}^{(\eta)}(\tau)$. The real and imaginary parts of $\hat{\Phi}_{rr}(\tau)$ are denoted by $\hat{\xi}(\tau)$ and $\hat{\chi}(\tau)$,

respectively. The proposed decision statistic is now given by

$$T = \sum_{\tau=1}^{K-1} \left[\Omega_\tau^{(R)} \hat{\xi}(\tau) + \Omega_\tau^{(I)} \hat{\chi}(\tau) \right] - \lambda \hat{\xi}(0) \underset{H_0}{\overset{H_1}{\gtrless}} 0 \tag{2.13}$$

where $\Omega_\tau \triangleq \Omega_\tau^{(R)} + j\Omega_\tau^{(I)}$ for $\tau \in \{1, 2, \cdots, K-1\}$ are coefficients which have to be appropriately selected and λ is the real-valued threshold which is chosen to achieve the desired probability of false alarm. One notes that $\hat{\Phi}_{rr}(0)$ is the average energy of the received signal and thus $\hat{\chi}(0) = 0$.

The performance of the proposed algorithm is evaluated in terms of the probabilities of false alarm and detection denoted by p_0 and p_1, respectively. To this end we need to find the distribution of T under each hypothesis.

2.3.1 Distribution of the Proposed Decision Statistic

The correlation of the received signal in (2.11) is a function of the power of the channel, $|g|^2$. As a result $\hat{\xi}(\tau)$, $\hat{\chi}(\tau)$, and consequently the decision statistic are functions of $|g|^2$. Therefore we first compute all the distributions conditioned on $|g|^2$. The unconditional distributions are computed in the next section. For ease of notation in this subsection, we drop the conditioning on $|g|^2$ from our notations.

From (2.10), the memory of the received signal is limited and is at most KT_s. Therefore the received sequence $\{r_n\}$ although correlated has a finite memory. More precisely, this an identically distributed sequence for which r_n and r_m are independent if $|n - m| > K$. Therefore by the central limit theorem for strongly mixing random processes the distribution of $\hat{\Phi}_{rr}(\tau)$ under H_η converges to a Gaussian distribution $\mathcal{CN}(\mu_{\hat{\Phi}|\eta}(\tau), \sigma^2_{\hat{\Phi}|\eta}(\tau))$. This implies,

$$\hat{\xi}(\tau) \mid \eta \sim \mathcal{N}(\mu_{\hat{\xi}|\eta}(\tau), \sigma^2_{\hat{\xi}|\eta}(\tau)) \tag{2.14}$$

$$\hat{\chi}(\tau)|\eta \sim \mathcal{N}(\mu_{\hat{\chi}|\eta}(\tau), \sigma^2_{\hat{\chi}|\eta}(\tau)) \tag{2.15}$$

From (2.12) it is easy to show $\mu_{\hat{\Phi}|\eta}(\tau) = \Phi_{rr}^{(\eta)}(\tau)$. So,

$$\mu_{\hat{\xi}|\eta}(\tau) = \xi^{(\eta)}(\tau) \tag{2.16}$$

$$\mu_{\hat{\chi}|\eta}(\tau) = \chi^{(\eta)}(\tau) \tag{2.17}$$

where $\xi^{(\eta)}(\tau)$ and $\chi^{(\eta)}(\tau)$ are the real and imaginary parts of $\Phi_{rr}^{(\eta)}(\tau)$, respectively.

From (2.13), we see that T also Gaussian. For ease of notation let us define $\Omega_0 \triangleq -\lambda$. Therefore the mean of T is given by

$$\begin{aligned} \mu_{T|\eta} &\triangleq E[\ T \mid H_\eta] \qquad (2.18)\\ &= \sum_{\tau=1}^{K-1} \Omega_\tau^{(R)} \xi^{(\eta)}(\tau) + \Omega_\tau^{(I)} \chi^{(\eta)}(\tau) - \lambda \xi^{(\eta)}(0) \\ &= \bar{\mathbf{1}} \Xi_\eta + \bar{\mathbf{1}} X_\eta \end{aligned}$$

where $\bar{\mathbf{1}}$ is $1 \times K$ vector with all elements of 1, and vectors Ξ_η and X_η are defined as

$$\Xi_\eta \triangleq [\Omega_0^{(R)} \xi^{(\eta)}(0), \cdots, \Omega_{K-1}^{(R)} \xi^{(\eta)}(K-1)]^\dagger \tag{2.19}$$

$$X_\eta \triangleq [\Omega_0^{(I)} \chi^{(\eta)}(0), \cdots, \Omega_{K-1}^{(I)} \chi^{(\eta)}(K-1)]^\dagger, \tag{2.20}$$

where $A^\dagger$ is the conjugate transpose of A.

To find the variance of T, define the covariance matrix of $\Omega_\tau^{(R)} \hat{\xi}(\tau)$, and $\Omega_\tau^{(I)} \hat{\chi}(\tau)$ for $\tau \in \{0, 1, \cdots, K-1\}$ under hypothesis H_η as $\Gamma_{\hat{\xi}|\eta} = \left[\gamma_{\hat{\xi}|\eta}(i,j)\right]_{K \times K}$ and $\Gamma_{\hat{\chi}|\eta} = \left[\gamma_{\hat{\chi}|\eta}(i,j)\right]_{K \times K}$, respectively. The elements of these matrices have been evaluated in Appendix A From (2.13), and after some manipulation we have,

$$E[\ T^2 \mid H_\eta] = \bar{\mathbf{1}} \left(\Gamma_{\hat{\xi}|\eta} + \Gamma_{\hat{\chi}|\eta} + \Xi_\eta X_\eta^\dagger + X_\eta \Xi_\eta^\dagger \right) \bar{\mathbf{1}}^\dagger, \tag{2.21}$$

which results in,

$$\begin{aligned} \sigma_{T|\eta}^2 &\triangleq E[\ T^2 \mid H_\eta] - \mu_{T|\eta}^2 \qquad (2.22)\\ &= \bar{\mathbf{1}} \left(\Gamma_{\hat{\xi}|\eta} + \Gamma_{\hat{\chi}|\eta} - \Xi_\eta \Xi_\eta^\dagger - X_\eta X_\eta^\dagger \right) \bar{\mathbf{1}}^\dagger. \end{aligned}$$

And finally, the distribution of T under hypothesis H_η conditioned on $|g|^2$ is given by, $T \mid \eta \sim \mathcal{N}\left(\mu_{T|\eta}, \sigma^2_{T|\eta}\right)$. Note that under H_1 both $\mu_{T|\eta}$ and $\sigma^2_{T|\eta}$ depend on $\alpha \triangleq |g|^2$. Now the conditional probabilities of false alarm and detection (conditioned on α) are

$$p_{\eta|\alpha} = \mathcal{Q}(-\frac{\mu_{T|\eta}}{\sigma_{T|\eta}}) \tag{2.23}$$

where $\mathcal{Q}(x) = 1/\sqrt{2\pi}\int_x^\infty \exp(-u^2/2)du$, is the Q-function. Finally the unconditional probabilities of false alarm and detection are given by,

$$p_\eta = \int p_{\eta|x} f_\alpha(x)dx \tag{2.24}$$

where $f_\alpha(.)$ is probability density function of α.

2.3.2 Constant False Alarm Ratio Detection

The received signal under H_0 is the white Gaussian noise process. Therefore

$$\Phi^{(0)}_{rr}(\tau) = N_0\delta(\tau) \tag{2.25}$$

which results in

$$\Xi_0 = [-\lambda N_0, 0, \cdots, 0]^\dagger \tag{2.26}$$

$$X_0 = [0, 0, \cdots, 0]^\dagger \tag{2.27}$$

Substituting the values of $\xi^{(0)}(i)$ and $\chi^{(0)}(i)$ from (2.26) and (2.27) into (6.3), and (6.4), followed by some manipulations one can verify that for $i, k \in \{0, 1, \cdots, K-1\}$,

$$\gamma_{\hat{\xi}|\eta}(i,k) = \lambda^2 N_0^2 \delta(i)\delta(k)\left(1 + \frac{1}{2N}\right) + \frac{N_0^2 {\Omega_i^{(R)}}^2}{2(N-i)}\delta(i-k) \tag{2.28}$$

$$\gamma_{\hat{\chi}|\eta}(i,k) = \frac{N_0^2 {\Omega_i^{(I)}}^2}{2(N-i)}\delta(i-k) \tag{2.29}$$

Moreover,

$$\mu_{T|0} = -\lambda N_0. \tag{2.30}$$

By substituting (2.28) and (2.29) into (2.22) we get,

$$\sigma^2_{T|0} = N_0^2 \left(\frac{\lambda^2}{N} + \sum_{i=1}^{K-1} \frac{{\Omega_i^{(R)}}^2 + {\Omega_i^{(I)}}^2}{2(N-i)} \right) \tag{2.31}$$

Therefore from (2.24), the probability of false alarm is given by,

$$p_0 = \mathcal{Q} \left(\frac{\lambda}{\sqrt{\frac{\lambda^2}{N} + \sum_{i=1}^{K-1} \frac{{\Omega_i^{(R)}}^2 + {\Omega_i^{(I)}}^2}{2(N-i)}}} \right) \tag{2.32}$$

It is clear from (2.32) that the probability of false alarm is not a function of N_0 or g, and can be fixed by choosing proper values of N and λ. This is why the proposed algorithm is a constant false alarm ratio (CFAR) technique.

If $p_0 = \mathfrak{P}_0$ is the desired false alarm rate, then for a given number of samples N the threshold λ can be chosen as

$$\lambda = \sqrt{\frac{\sum_{i=1}^{K-1} \frac{{\Omega_i^{(R)}}^2 + {\Omega_i^{(I)}}^2}{2(N-i)}}{\frac{1}{\left[\mathcal{Q}^{-1}(\mathfrak{P}_0)\right]^2} - \frac{1}{N}}} \tag{2.33}$$

2.4 System Optimization

To improve the proficiency of the proposed decision statistic, we can optimize the performance by appropriately selecting the vector $\mathbf{\Omega} = [\Omega_1, \cdots, \Omega_{K-1}]$. The distribution of T under H_η is a function of $\mathbf{\Omega}$ which means the probabilities of false alarm and detection are also functions of $\mathbf{\Omega}$. The correlation of the received signal is function of the coefficient of the channel from the PU to the SU which

is unknown. For a given channel coefficient, T and (as a result) false alarm and detection probabilities are functions of $\mathbf{\Omega}$ and λ. To show this dependency, we subsequently use the notation $\mu_{T|\eta}(\mathbf{\Omega}, \lambda)$, $\sigma^2_{T|\eta}(\mathbf{\Omega}, \lambda)$, $p_0(\mathbf{\Omega}, \lambda)$, and $p_1(\mathbf{\Omega}, \lambda)$.

One approach to optimize the performance over $\mathbf{\Omega}$ is to maximize the detection probability with a constraint on the probability of false alarm, i.e., a Neyman-Pearson criterion. Considering the fact that multiplying $\mathbf{\Omega}$ by a constant factor will not change the decision statistic, and each Ω_i in (6.3) and (6.4) is divided by $N - i$, the constrained optimization problem is given by,

$$\text{Maximize:} \quad p_1(\mathbf{\Omega}, \lambda) \tag{2.34}$$

$$\text{Subject to:} \quad \begin{cases} p_0(\mathbf{\Omega}, \lambda) \leq \mathfrak{P}_{\text{opt}} \\ \displaystyle\sum_{i=0}^{K-1} \frac{{\Omega_i^{(R)}}^2 + {\Omega_i^{(I)}}^2}{N-i} = \mathcal{W} \end{cases} \tag{2.35}$$

As p_1 is an increasing function of p_0, the maximum of p_1 occurs when $p_0 = \mathfrak{P}_{\text{opt}}$, and from (2.32) we can find the corresponding λ_{opt}. To maximize the integral in (2.24), we maximize the integrand. Now since $\mathcal{Q}(x)$ is a deceasing function of x, the optimization problem can be rewritten as

$$\text{Maximize:} \quad \frac{\mu_{T|1}(\mathbf{\Omega}, \lambda_{\text{opt}})}{\sigma_{T|1}(\mathbf{\Omega}, \lambda_{\text{opt}})} \tag{2.36}$$

$$\text{Subject to:} \quad \begin{cases} \lambda_{\text{opt}} = \sqrt{\dfrac{\displaystyle\sum_{i=1}^{K-1} \frac{{\Omega_i^{(R)}}^2 + {\Omega_i^{(I)}}^2}{2(N-i)}}{\dfrac{1}{\left[\mathcal{Q}^{-1}(\mathfrak{P}_{\text{opt}})\right]^2} - \dfrac{1}{N}}} \\ \displaystyle\sum_{i=0}^{K-1} \frac{{\Omega_i^{(R)}}^2 + {\Omega_i^{(I)}}^2}{N-i} = \mathcal{W} \end{cases} \tag{2.37}$$

This optimization problem is too complicated to be tractable. However, we can approximate (2.36) for low-SNR regime which is the reasonable in the SS. After

some manipulation from (2.22), we get

$$\sigma^2_{T|1} \approx \lambda_{\text{opt}} \left(\frac{1}{N} - 2N_0^2 \right) + \sum_{i=1}^{K-1} \frac{{\Omega_i^{(R)}}^2 + {\Omega_i^{(I)}}^2}{2(N-i)} \tag{2.38}$$

Define $\mathcal{O}_i = \mathcal{O}_i^R + j\mathcal{O}_i^I \triangleq \frac{\Omega_i^R + j\Omega_i^I}{N-i}$ for $0 \leq i \leq K-1$, and $\mathbf{O} \triangleq [\mathcal{O}_0, \cdots, \mathcal{O}_{K-1}]$. Using Lagrange multiplier and approximation in (2.38) Define the Lagrangian as

$$\begin{aligned} \mathcal{L} = &\sum_{\tau=1}^{K-1} (N-i) \left(\mathcal{O}_i^R \xi^{(1)}(\tau) + \mathcal{O}_i^I \chi^{(1)}(\tau) \right) \\ &- N\lambda_{\text{opt}} \left(\xi^{(1)}(0) + \chi^{(1)}(0) \right) - \ell \left(\mathbf{O}\mathbf{O}^\dagger - 2\mathcal{W} \right) \end{aligned} \tag{2.39}$$

Setting the derivative of the Lagrangian with respect to $\mathcal{O}^R(\tau)$ to zero,

$$\frac{\partial \mathcal{L}}{\partial \mathcal{O}_\tau^R} = \xi^{(1)}(\tau)(N-\tau) - 2\ell \mathcal{O}_\tau^R = 0 \tag{2.40}$$

which results in,

$$\mathcal{O}_\tau^R = \frac{N-\tau}{2\ell} \xi^1(\tau) \tag{2.41}$$

Similarly, one can get evaluate $\mathcal{O}_\tau^I$. Note that this result is for a given $|g|^2$, however multiplying the optimization coefficients by a constant factor does not change the performance, so let us multiply it by $2\ell/(|g|^2(N-\tau))$ and we get,

$$\Omega(\tau) = \Phi_{ss}(\tau), \qquad \text{for} \quad 1 \leq \tau \leq K-1. \tag{2.42}$$

2.5 Performance Evaluation

In this section, we evaluate the performance of the proposed algorithm via simulation and compare it with derived analytical results. Simulation results are obtained from 10^4 independent trials. The PU uses 16-QAM with rectangular pulse shape. Two types of channels, Rayleigh Fading and additive white Gaussian noise (AWGN), are considered.

Fig 2.1 demonstrates the probability of detection of the proposed method, when $\mathfrak{P}_0 = 0.1$, for doubinary signaling, and different values of N. It is clear that by

increasing the value of N the performance improves. It can also be seen that the performance in AWGN channel outperform the performance in Rayleigh fading channel. In particular, to achieve the operating region of $p_d \geq 0.9,\ p_f \leq 0.1$, when $N = 512$ the required SNR for Rayleigh fading channel and AWGN channel should be at least -6.5 dB and -12.7 dB, respectively.

Fig 2.2 demonstrates the receiver operating characteristic (ROC) curves for AWGN and Rayleigh fading channel for two different values of N and SNR=-8dB. Doubinary signaling is assumed.

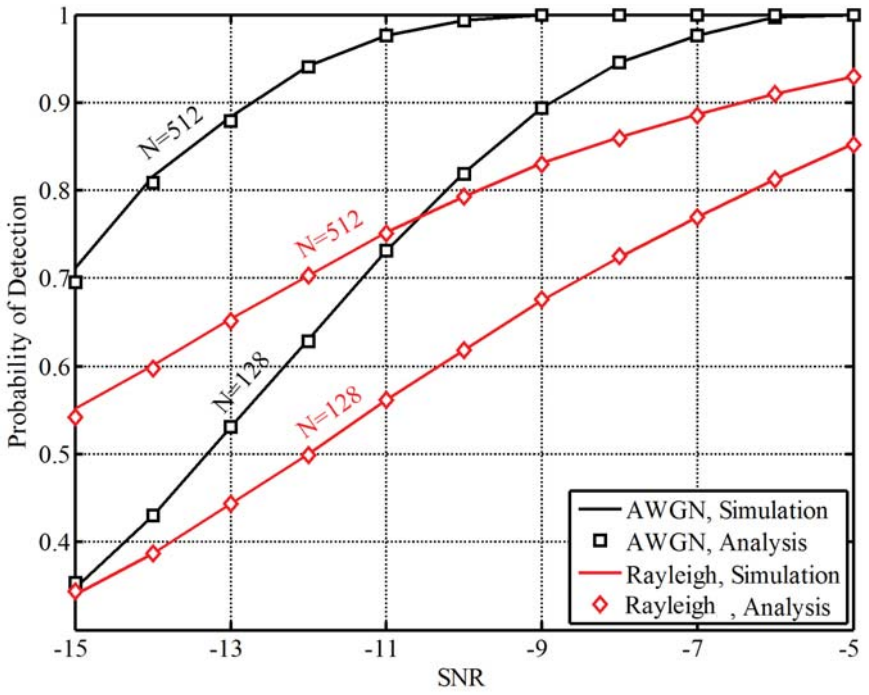

FIGURE 2.1. p_1 versus SNR for Rayleigh and AWGN channel, doubinary signaling, and different values of N

Finally, Fig 2.3 shows probability of detection versus SNR for $p_0 = .1$ and different correlative coding techniques. In particular we employed *doubinary*, *Kabal*, *Kretzmer*, and *Kretzmer2* with FIR transfer functions given by $1 + z^{-1}$, $1 + z^{-1} - z^{-2} - z^{-3}$, $1 + 2z^{-1} + z^{-2}$, and $2 + z^{-1} - z^{-2}$, respectively. The proficiency of these methods have been evaluated in [33].

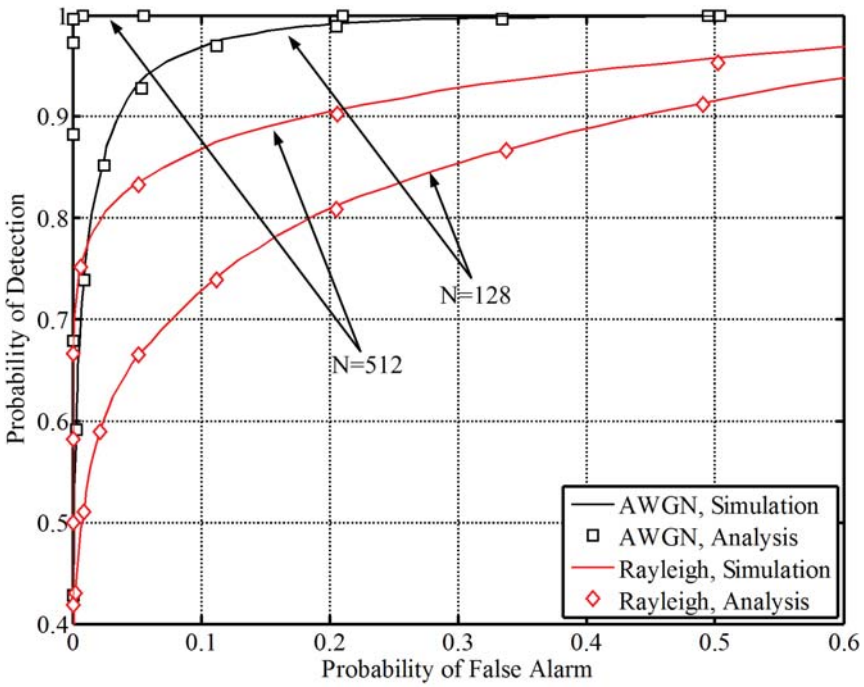

FIGURE 2.2. ROC for Rayleigh and AWGN channel, doubinary signaling, and different values of N

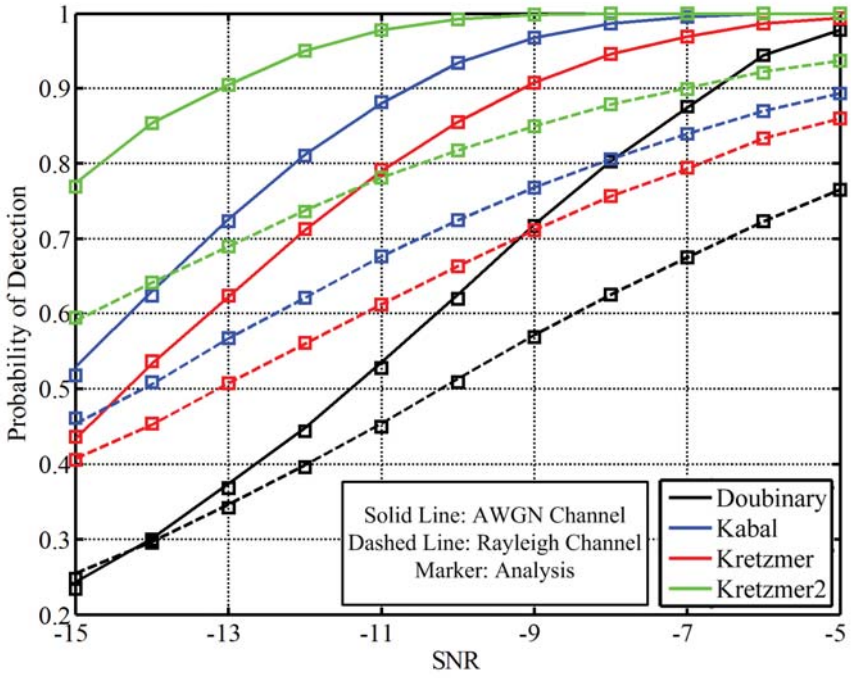

FIGURE 2.3. p_1 versus SNR for Rayleigh and AWGN channel, different values of N

Chapter 3

Evaluating the Effect of Co-Channel Interferer Signals in the Wireless Networks

3.1 Introduction and Background

The ever growing popularity of wireless services coupled with the limited spectrum have resulted in an increase in the spacial reuse of the radio spectrum where many wireless services, applications or users coexist in the same frequency band. For example in cellular mobile networks frequency reuse enables the users to share the same frequency band as long as they are sufficiently apart. Another example is in the overcrowded 2.4 GHz ISM band in which WLAN, Bluetooth, wireless headsets, and cordless phones may share the same band. More recently dynamic spectrum access has been proposed by FCC where unlicensed users can share the spectrum with licensed users. One approach is the so-called underlay cognitive radio networks where secondary unlicensed users may coexist with the primary licensed users provided that they adapt their transmission parameters in order to limit their interference to the primary users [35].

Coexistence of users in the same frequency band results in co-channel interference which can severely degrade the performance of wireless transceivers. Co-Channel Interference (CCI) has been the subject of many studies in the literature. Effects of CCI in WLAN with multiple access points is addressed in [36] and [37]. CCI in wireless sensor networks has been studied in [38] and [39]. For cellular networks the radio link performance is usually limited by CCI rather than noise, and the outage probability due to CCI is of primary concern [32], where CCI can meaningfully degrade the performance of users especially near the border of the cells [40, 41].

In cognitive radios several authors have investigated the effects of interference caused by the secondary users on the primary user [42, 37, 43, 44]. Several authors have proposed methods to mitigate the effects of CCI [45, 46, 47, 48] or to exploit the effects of CCI on the secondary user receiver statistics in order to detect the emergence of the primary user [49, 50].

In the study of the effects of CCI, the interference signal is often modeled as a white Gaussian process. As a result it can be added to the thermal noise and accounted for by appropriately reducing the signal to noise (plus interference) ratio (SNIR). However, this is not a good model owing to the fact that the interference signal is generated from a finite set of modulation symbols.

In this Chapter, we evaluate the effect of CCI on the bit error rate (BER), and the distribution of the total number of errors in a packet by a careful examination of the samples at the output of the matched filter receiver. It is demonstrated that due to the timing offset between the desired and the interference signals, the adjacent samples may be correlated. We show that BER and the distribution of the total number of errors highly depend on this timing offset and identify the best and worst cases for BER. This result can be exploited to reduce CCI in cooperative networks. Our results can also be employed for more accurate evaluation of CCI effects and in developing techniques for CCI mitigation such as design of precoders [51, 52] or forward error correction codes. In this thesis, we use CCI to detect the emergence of the primary user during the signal reception in the secondary user receiver in Chapter 4.

3.2 Probability of Bit Error

We consider two transmitters denoted U_1 and U_2 transmitting in the same frequency band. A receiver is interested in detecting the signal from U_1 and experiences interference from U_2's transmission. To make the analysis tractable, BPSK

or QPSK modulation are assumed for U_1 whereas U_2 may employ an arbitrary M-array linear digital modulation scheme. The received signals from U_1 and U_2 are, respectively, given by

$$s_1(t) = \sqrt{\frac{E_1}{T_s}} \sum_{n=-\infty}^{\infty} a_n e^{j\omega_c t} p_1(t - nT_s) \tag{3.1}$$

and

$$\begin{aligned} s_2(t) &= \sqrt{\frac{E_2}{T_s}} \sum_{n=-\infty}^{\infty} b_n e^{j\omega_c(t+\tau)+j\zeta} p_2(t + \tau - nT_s) \\ &= \sqrt{\frac{E_2}{T_s}} \sum_{n=-\infty}^{\infty} b_n e^{j(\omega_c t+\theta)} p_1(t + \tau - nT_s), \end{aligned} \tag{3.2}$$

where, for $i = 1, 2$, E_i, $p_i(t)$ and $\mathcal{S}_i$ denote the energy, pulse shape and set of constellation points of U_i, respectively. Also τ and ζ are the time offset and phase offset between two received signals, and T_s denotes the symbol duration. Finally $a_n \in \mathcal{S}_1$ and $b_n \in \mathcal{S}_2$ are the transmitted symbols by U_1 and U_2 modulation, respectively, and $\theta \triangleq \omega_c\tau + \zeta$. It is assumed that the sequences $\{a_n\}$ and $\{b_n\}$ are independent and identically distributed (iid) and are independent of each other. Furthermore, all the symbols are equally likely. Note that if $\tau \neq 0$, then two adjacent bits of U_1 receive interference from the same symbol of the U_2 resulting in the correlation of the error events for adjacent bits . The output of the matched filter at the receiver is given by

$$\begin{aligned} r_n &= \sqrt{E_1}\, a_n + \nu_n + \sum_{k=-\infty}^{\infty} \int_{nT_s}^{(n+1)T_s} \frac{\sqrt{E_2}}{T_s} b_k e^{j\theta} p_2(t + \tau - kT_s) p_1(t - nT_s) dt \\ &= \sqrt{E_1}\, a_n + \nu_n + \frac{\sqrt{E_2}}{T_s} e^{j\theta} \sum_{k=-\infty}^{\infty} b_k \int_{-\infty}^{\infty} p_2(t + \tau - kT_s) p_1(t - nT_s) dt \\ &= \sqrt{E_1}\, a_n + \nu_n + \sqrt{E_2} e^{j\theta} \sum_{k=-\infty}^{\infty} b_k \psi((k - n)T_s - \tau) \end{aligned} \tag{3.3}$$

where $\{\nu_n\}$ is assumed to be the iid Gaussian noise process. Moreover

$$\psi(t) \triangleq \frac{1}{T} p_1(-t) * p_2(t), \tag{3.4}$$

where $*$ denotes convolution. Using the above notation and the fact that $p_i(t) = 0$ for $t \notin [0, T]$, (3.3) can be written as

$$r_n = \sqrt{E_1}a_n + \nu_n + \sqrt{E_2}e^{j\theta}\left(b_n\psi(-\tau) + b_{n+1}\psi(T_s - \tau)\right) \tag{3.5}$$

We first consider BPSK or the in-phase component of QPSK modulation. Consider the received signal in (3.5) and let $x_n = 1$ if the nth bit in the received sequence is in error, and $x_n = 0$ otherwise. Then,

$$\begin{aligned} p_{b,1} &\triangleq Pr(x_n = 1) \\ &= Pr\left(\Re\left\{\nu_n + \sqrt{E_2}e^{j\theta}(b_n\psi(-\tau) + b_{n+1}\psi(T_s - \tau))\right\} > \sqrt{E_1}\right) \end{aligned} \tag{3.6}$$

where $\Re\{.\}$ denotes the real part. Here and subsequently, superscripts R and I represent the real and imaginary parts of a signal, respectively. Rewriting (3.6) we have,

$$\begin{aligned} p_{b,1} =& Pr\left(\nu_n^R + \sqrt{E_2}\cos\theta\left(b_n^R\psi(-\tau) + b_{n+1}^R\psi(T_s - \tau)\right)\right. \\ -& \quad \left.\sqrt{E_2}\sin\theta\left(b_n^I\psi(-\tau) + b_{n+1}^I\psi(T_s - \tau)\right) > \sqrt{E_2}\right) \\ =& Pr\left(\nu_n^R + \sqrt{E_2}\psi(-\tau)\left(b_n^R\cos\theta - b_n^I\sin\theta\right)\right. \\ +& \quad \left.\sqrt{E_2}\psi(T_s - \tau)\left(b_{n+1}^R\cos\theta - b_{n+1}^I\sin\theta\right) > \sqrt{E_1}\right) \end{aligned} \tag{3.7}$$

Denote by $\mathcal{S}_2^\theta$ a new constellation obtained from a rotation of $\mathcal{S}_2$ by θ and let $\mathcal{S}_2^{(\text{eff})}$ be the set of points obtained from projection of $\mathcal{S}_2^\theta$ onto the real line. Then

$$p_{b,1} = \frac{1}{M^2} \times \sum_{\alpha \in \mathcal{S}_2^{(\text{eff})}} \sum_{\beta \in \mathcal{S}_2^{(\text{eff})}} Q\left(\frac{\sqrt{E_1} - \sqrt{E_2}\left(\psi(-\tau)\alpha - \psi(T_s - \tau)\beta\right)}{\sqrt{N_0/2}}\right) \tag{3.8}$$

where M is the size of the constellation $\mathcal{S}_2$.

Define $\Psi(\alpha, \beta) \triangleq \psi(-\tau)\alpha + \psi(T_s - \tau)\beta$ and assume that the constellation $\mathcal{S}_2$ has the symmetry property that if $a \in \mathcal{S}_2$, then $-a$ and $\sqrt{-1}a \in \mathcal{S}_2$[1]. Then the bit

[1]Note that all practical constellations such as MPSK and QAM satisfy this property.

error probability can be written as,

$$p_{b,1} = \frac{1}{2M^2} \sum_{\alpha \in \mathcal{S}_2^{(\text{eff})}} \sum_{\beta \in \mathcal{S}_2^{(\text{eff})}} \left\{ Q\left(\sqrt{2\gamma_1}\sqrt{2\gamma_2}\Psi(\alpha,\beta)\right) + Q\left(\sqrt{2\gamma_1} - \sqrt{2\gamma_2}\Psi(\alpha,\beta)\right)\right\} \tag{3.9}$$

where $\gamma_i \triangleq E_i/N_0$ for $i \in \{1,2\}$ is signal to noise ratio. Using Taylor's expansion of the two terms in (3.9) around $2\gamma_1$ we get

$$\begin{aligned} p_{b,1} &= Q(\sqrt{2\gamma_1}) \\ &+ Q^{(2)}(\sqrt{2\gamma_1})\frac{2\gamma_2}{2!M^2} \sum_{\alpha \in \mathcal{S}_2^{(\text{eff})}} \sum_{\beta \in \mathcal{S}_2^{(\text{eff})}} \Psi^2(\alpha,\beta) \\ &+ Q^{(4)}(\sqrt{2\gamma_1})\frac{4\gamma_2^2}{4!M^2} \sum_{\alpha \in \mathcal{S}_2^{(\text{eff})}} \sum_{\beta \in \mathcal{S}_2^{(\text{eff})}} \Psi^4(\alpha,\beta) + \cdots \end{aligned} \tag{3.10}$$

where $Q^{(n)}(.)$ denotes the nth derivative of $Q(.)$. For small γ_2, we can approximate Taylor's expansion of $p_{b,1}$ by its first three terms. Using Lemmas 1 and 2, (3.10) is approximated by,

$$p_{b,1} \approx Q(\sqrt{2\gamma_1}) + \sqrt{\frac{\gamma_1}{\pi}}\, e^{-\gamma_1} \frac{\gamma_2}{M^2} \times \sum_{\alpha \in \mathcal{S}_2^{(\text{eff})}} \sum_{\beta \in \mathcal{S}_2^{(\text{eff})}} \left(\alpha^2\psi^2(-\tau) + \beta^2\psi^2(T_s - \tau)\right) \tag{3.11}$$

$$= Q(\sqrt{2\gamma_1}) + \sqrt{\frac{\gamma_1}{\pi}} e^{-\gamma_1} \frac{\bar{\gamma}_2}{2} \left(\psi^2(-\tau) + \psi^2(T_s - \tau)\right)$$

where $\bar{\gamma}_2$ is the average signal to noise ratio of U_2 given by,

$$\bar{\gamma}_2 \triangleq \frac{\gamma_2}{M} \sum_{a \in \mathcal{S}_2} |a|^2, \tag{3.12}$$

One would note that the first term in (3.11) is the effect of noise and the second term is due to the CCI from U_2. In addition $p_{b,1}$ is independent of θ. From this it follows that for QPSK modulation the errors in the in-phase and quadrature components are independent and identically distributed.

Lemma 1. *For the constellation $\mathcal{S}_2$ with the symmetry property that if $a \in \mathcal{S}_u$, then $-a$ and $\sqrt{-1}a \in \mathcal{S}_2$, the following equality holds.*

$$\sum_{\alpha \in \mathcal{S}_2^{(\text{eff})}} \sum_{\beta \in \mathcal{S}_2^{(\text{eff})}} \Psi^2(\alpha, \beta) = M \left(\psi^2(-\tau) + \psi^2(T_s - \tau) \right) \sum_{\alpha \in \mathcal{S}_2} |\alpha|^2 \tag{3.13}$$

Proof. Regardless of the value of θ, $\alpha \in \mathcal{S}_2^{(\text{eff})}$ implies that $-\alpha \in \mathcal{S}_2^{(\text{eff})}$. Thus

$$\begin{aligned} &\sum_{\alpha \in \mathcal{S}_2^{(\text{eff})}} \sum_{\beta \in \mathcal{S}_2^{(\text{eff})}} (\alpha\psi(-\tau) + \beta\psi(T_s - \tau)) = \\ &\frac{1}{2} \Bigg[\sum_{\alpha \in \mathcal{S}_2^{(\text{eff})}} \sum_{\beta \in \mathcal{S}_2^{(\text{eff})}} (\alpha\psi(-\tau) + \beta\psi(T_s - \tau)) \\ &+ \sum_{\alpha \in \mathcal{S}_2^{(\text{eff})}} \sum_{\beta \in \mathcal{S}_2^{(\text{eff})}} (-\alpha\psi(-\tau) + \beta\psi(T_s - \tau)) \Bigg] \\ &= 0 \end{aligned} \tag{3.14}$$

which implies,

$$\begin{aligned} &\sum_{\alpha \in \mathcal{S}_2^{(\text{eff})}} \sum_{\beta \in \mathcal{S}_2^{(\text{eff})}} \Psi^2(\alpha, \beta) \\ &= \sum_{\alpha \in \mathcal{S}_2^{(\text{eff})}} \sum_{\beta \in \mathcal{S}_2^{(\text{eff})}} (\alpha^2\psi^2(-\tau) + \beta^2\psi^2(T_s - \tau)) \\ &= \frac{1}{2} \left(\psi^2(-\tau) + \psi^2(T_s - \tau) \right) \sum_{\alpha \in \mathcal{S}_2^{(\text{eff})}} \sum_{\beta \in \mathcal{S}_2^{(\text{eff})}} \alpha^2 + \beta^2 \\ &= M \left(\psi^2(-\tau) + \psi^2(T_s - \tau) \right) \sum_{\alpha \in \mathcal{S}_2^{(\text{eff})}} \alpha^2 \end{aligned} \tag{3.15}$$

□

Lemma 2. *For the constellation $\mathcal{S}_2$ which has the symmetry property in Lemma 1, we have*

$$\sum_{\alpha \in \mathcal{S}_2^{(\text{eff})}} \alpha^2 = \sum_{\alpha \in \mathcal{S}_2} |\alpha|^2 \tag{3.16}$$

Proof. For symmetry constellation we have,

$$\sum_{\alpha\in\mathcal{S}_2}\left(\alpha^R\right)^2=\sum_{\alpha\in\mathcal{S}_2}\left((\sqrt{-1}\alpha)^R\right)^2=\sum_{\alpha\in\mathcal{S}_2}\left(\alpha^I\right)^2 \tag{3.17}$$

$$\sum_{\alpha\in\mathcal{S}_2}\alpha^R\alpha^I=\frac{1}{2}\left(\sum_{\alpha\in\mathcal{S}_2}\alpha^R\alpha^I+\sum_{\alpha\in\mathcal{S}_2}-\alpha^R\alpha^I\right)=0 \tag{3.18}$$

So, we can write,

$$\sum_{\alpha\in\mathcal{S}_2^{(\text{eff})}}\alpha^2=\sum_{\alpha\in\mathcal{S}_2}\left(\alpha^R\cos(\theta)-\alpha^I\sin(\theta)\right)^2 \tag{3.19}$$

$$=\cos^2(\theta)\sum_{\alpha\in\mathcal{S}_2}(\alpha^R)^2+\sin^2(\theta)\sum_{\alpha\in\mathcal{S}_2}(\alpha^R)^2-\sin(2\theta)\sum_{\alpha\in\mathcal{S}_2}\alpha^R\alpha^I=\sum_{\alpha\in\mathcal{S}_2}|\alpha|^2$$

□

In the case of non-zero time offsets, the events of two consecutive errors are dependent. Define $P_{2b,1}$ as the probability of two consecutive bits being in error. Then

$$\begin{aligned}p_{2b,1}&\triangleq P(x_n=1,x_{n+1}=1)\\&=\frac{1}{2}\left[P(x_n=1,x_{n+1}=1|a_n=1,a_{n+1}=1)\right.\\&\left.+P(x_n=1,x_{n+1}=1|a_n=1,a_{n+1}=-1)\right],\end{aligned} \tag{3.20}$$

Note that

$$\begin{aligned}&P(x_n=1,x_{n+1}=1|a_n=i,a_{n+1}=j)\\&=P(x_n=1,x_{n+1}=1|a_n=-i,a_{n+1}=-j)\end{aligned} \tag{3.21}$$

The first term of (3.20) is evaluated as,

$$\begin{aligned}&P(x_n=1,x_{n+1}=1|a_n=1,a_{n+1}=1)\\&=P\left(\nu_n^R+\sqrt{E_2}\left(\psi(-\tau)b_n^{(\text{eff})}+\psi(T_s-\tau)b_{n+1}^{(\text{eff})}\right)>\sqrt{E_1},\right.\\&\qquad\left.\nu_{n+1}^R+\sqrt{E_2}\left(\psi(-\tau)b_{n+1}^{(\text{eff})}+\psi(T_s-\tau)b_{n+2}^{(\text{eff})}\right)>\sqrt{E_1}\right)\end{aligned} \tag{3.22}$$

$$= \frac{1}{M} \sum_{\beta \in \mathcal{S}_2^{(\text{eff})}} \Big[P\left(\nu_n^R + \sqrt{E_2}\left(\psi(-\tau) b_n^{(\text{eff})} + \psi(T_s - \tau)\beta\right) > \sqrt{E_1} \;\; | \, b_{n+1}^{(\text{eff})} = \beta \right)$$

$$\times P\left(\nu_{n+1}^R + \sqrt{E_2}\left(\psi(-\tau)\beta + \psi(T_s - \tau) b_{n+2}^{(\text{eff})}\right) > \sqrt{E_1} \;\Big|\; b_{n+1}^{(\text{eff})} = \beta \;\right) \Big] \tag{3.23}$$

$$= \frac{1}{M^3} \sum_{\alpha \in \mathcal{S}_2^{(\text{eff})}} \sum_{\beta \in \mathcal{S}_2^{(\text{eff})}} \sum_{\delta \in \mathcal{S}_2^{(\text{eff})}} Q\left(\sqrt{2\gamma_1} - \sqrt{2\gamma_2}\Psi(\alpha, \beta) \right)$$

$$\times Q\left(\sqrt{2\gamma_1} - \sqrt{2\gamma_2}\Psi(\beta, \delta) \right) \tag{3.24}$$

$$= \frac{1}{2M^3} \sum_{\alpha \in \mathcal{S}_2^{(\text{eff})}} \sum_{\beta \in \mathcal{S}_2^{(\text{eff})}} \sum_{\delta \in \mathcal{S}_2^{(\text{eff})}} Q\left(\sqrt{2\gamma_1} - \sqrt{2\gamma_2}\Psi(\alpha, \beta) \right)$$

$$\times Q\left(\sqrt{2\gamma_1} - \sqrt{2\gamma_2}\Psi(\beta, \delta) \right)$$

$$+ \frac{1}{2M^3} \sum_{\alpha \in \mathcal{S}_2^{(\text{eff})}} \sum_{\beta \in \mathcal{S}_2^{(\text{eff})}} \sum_{\delta \in \mathcal{S}_2^{(\text{eff})}} Q\left(\sqrt{2\gamma_1} + \sqrt{2\gamma_2}\Psi(\alpha, \beta) \right)$$

$$\times Q\left(\sqrt{2\gamma_1} + \sqrt{2\gamma_2}\Psi(\beta, \delta) \right) \tag{3.25}$$

From (3.22) to (3.23) we use the independence of x_n and x_{n+1} conditioned on b_{n+1}. To simplify (3.25), we approximate it by substituting the first three terms of Taylor's expansion around $\sqrt{2\gamma_1}$ for each Q-function in (3.25). Using the same approach for the second term of (3.20) and after some manipulations,

$$P(x_n = 1, x_{n+1} = 1 | a_n = 1, a_{n+1} = \pm 1) \tag{3.26}$$

$$\approx Q^2(\sqrt{2\gamma_1}) + \frac{2\gamma_2}{M^3} Q(\sqrt{2\gamma_1}) Q^{(2)}(\sqrt{2\gamma_1})$$

$$\times \sum_{\alpha \in \mathcal{S}_2^{(\text{eff})}} \sum_{\beta \in \mathcal{S}_2^{(\text{eff})}} \sum_{\delta \in \mathcal{S}_2^{(\text{eff})}} \left(\frac{\Psi^2(\alpha, \beta) + \Psi^2(\beta, \delta)}{2} \right)$$

$$\pm \frac{2\gamma_2 (Q^{(1)}(\sqrt{2\gamma_1}))^2}{M^3} \sum_{\alpha \in \mathcal{S}_2^{(\text{eff})}} \sum_{\beta \in \mathcal{S}_2^{(\text{eff})}} \sum_{\delta \in \mathcal{S}_2^{(\text{eff})}} \Psi(\alpha, \beta)\Psi(\beta, \delta)$$

Therefore $p_{2b,1}$ is given by,

$$p_{2b,1} \approx Q^2(\sqrt{2\gamma_1}) + Q(\sqrt{2\gamma_1}) \sqrt{\frac{\gamma_1}{\pi}} e^{-\gamma_1} \frac{2\gamma_2}{M^2} \sum_{\alpha \in \mathcal{S}_2^{(\text{eff})}} \sum_{\beta \in \mathcal{S}_2^{(\text{eff})}} \Psi^2(\alpha, \beta). \tag{3.27}$$

Using Lemma 1, Equations (3.11)-(3.15), and after some manipulations (3.27) is given by,

$$p_{2b,1} \approx Q(\sqrt{2\gamma_1}) \left(2p_{b,1} - Q(\sqrt{2\gamma_1})\right) \tag{3.28}$$

Consider a packet transmission system in which users U_1 and U_2 transmit their messages using packets of length N bits. Let $e = \sum_{n=1}^{N} x_n$ denote the number of errors in a received packet of U_1. We would like to find the distribution of e, namely $P(e = \ell)$. Since adjacent errors are dependent, $\{x_n\}$ is not a Bernoulli sequence and thus the distribution of e is not binomial. However, e is the sum of identically distributed random variables which are weekly dependent [53]. More specifically, $\{x_n\}$ is strongly mixing in that x_n and x_m are independent if $|m - n| > 1$. Thus using the central limit theorem for strongly mixing sequences, [53], we conclude that e converges in distribution to a Gaussian distribution $\mathcal{N}(m_1, \sigma_1^2)$, where $m_1 = \sum_{n=1}^{N} \mathbb{E}x_n = Np_{b,1}$, and $\sigma_1^2 = \sum_{i=1}^{N} \sum_{j=1}^{N} \mathrm{Cov}(x_i, x_j)$. It follows that,

$$\sigma_1^2 = N(p_{b,1} - p_{b,1}^2) + 2(N - \mathcal{M}) \left(p_{2b,1} - p_{b,1}^2\right) \tag{3.29}$$

where $\mathcal{M}$ is the number of bits per transmitted symbol of U_1.

3.2.1 The Worst Case

In section 3.2 we calculate the probability of bit error and the distribution of the total number of errors in a packet. These quantities depend on the timing offset τ. In particular the average number of errors per packet depends on τ. To determine the worst case for the average number of errors we set $\partial p_{b,1}/\partial\tau = 0$ which results,

$$\frac{\partial}{\partial\tau} \left(\psi^2(-\tau) + \psi^2(T_s - \tau)\right) = 0. \tag{3.30}$$

The result depends on the pulse shapes of U_1 and U_2. For the case that they use the same pulse shape, one can verify that

$$\psi(-t) = \psi(T_s - t) \tag{3.31}$$

$$\frac{\partial}{\partial t}\psi(-t) = -\frac{\partial}{\partial t}\psi(t). \tag{3.32}$$

Using the above, it can be shown that $\psi^2(-\tau) + \psi^2(T_s - \tau)$ is convex for $0 \leq \tau \leq T_s$. Therefore its maximum occurs on the boundaries and its values on $\tau = 0$ and $\tau = T_s$ are equal. Consequently the average number of errors per packet is maximized when U_1 and U_2 are synchronized.

3.3 Simulation Results

In this section we validate our modeling assumptions by comparing the analytical results obtained in the previous section with those from simulation. We assume users U_1 and U_2 employ QPSK and 16-QAM modulation schemes, respectively and both use rectangular pulse shapes. Fig. 3.1 compares the distribution of the total number of errors derived from analysis with the histogram obtained from simulations for SNR values of $\gamma_1 = 2$dB and $\gamma_2 = -3$dB and for three different values of the timing offset τ. The figures show a close match between the results from analysis and simulation. As the figure shows, the average number of errors is largest for $\tau = 0$ (maximum $p_{b,1}$) and smallest for $\tau = \frac{T_2}{2}$ (minimum $p_{b,1}$). A significant difference can be observed in the average number of errors as well as the distribution of the number of errors between the best and the worst case. This implies that in cooperative systems where the timing offsets can be adjusted, it is desirable to set $\tau = T_s/2$. On the other hand for system design in non-cooperative networks, one should consider the worst case corresponding to $\tau = 0$.

Cramer−von Mises criterion, [54, 55], provides a metric to test the goodness of fit of a distribution compared to the empirical distribution. For the distribution of the number of errors in a packet of length N this metric is given by

$$\mathcal{D}_f \triangleq \frac{1}{N+1}\sum_{n=0}^{N}[\mathfrak{F}_y(n) - F_y(n)]^2\mathfrak{p}_y(n) \tag{3.33}$$

where $\mathfrak{F}_y$, $\mathfrak{p}_y$, and F_y are the empirical cumulative distribution function (CDF), the empirical probability density function (PDF), and the CDF of number of errors from analysis in a received packet, respectively. Fig. 3.2 shows the value of $\mathcal{D}_f$ versus γ_2 for different values of τ when $N = 1024$, $\gamma_1 = 3$dB. Fig. 3.2 demonstrates that $\mathcal{D}_f$ is quite small but increases with γ_2 and decreases from $\tau = 0$ to $\tau = T_s/2$. This is due to the fact that the approximation of $p_{b,1}$ in (3.11) is less accurate for larger values of $p_{b,1}$.

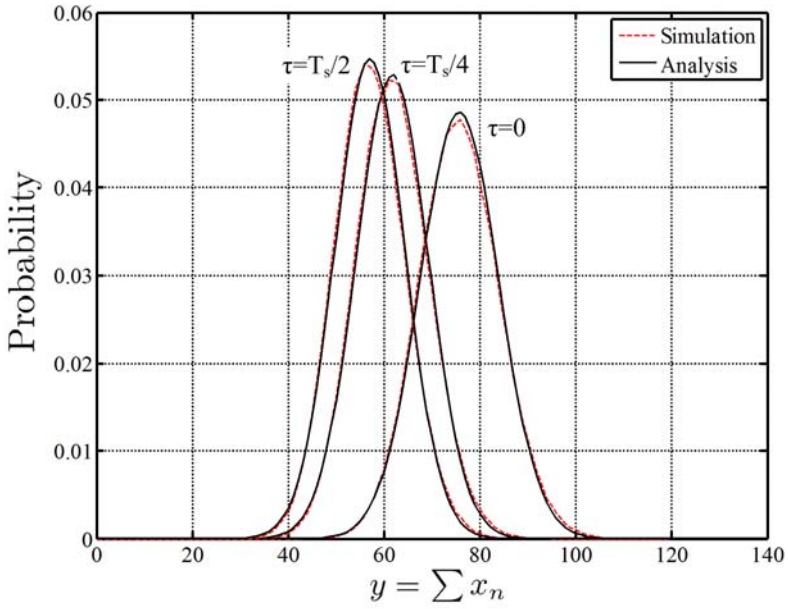

FIGURE 3.1. Distribution of Number of Errors in a packet with length $N = 1024$, when $\gamma_1 = 2$dB, $\gamma_2 = -3$dB and U_1 and U_2 uses QPSK and 16-QAM respectively

In the following example we consider the problem of code design for user U_1. Suppose U_1 and U_2 employ QPSK and 64-QAM modulation schemes, respectively and that U_1 uses a $(1023, \mathcal{K})$ BCH code for forward error correction. We are interested in the largest value of $\mathcal{K}$ (highest code rate) which guarantees an average packet error rate below $\eta\%$ in the presence of CCI from U_2. TABLE 3.1 demonstrates these values for the parameters $\gamma_1 = 5$dB, $\gamma_2 = 0$dB and $\gamma_1 = 4$dB, $\gamma_2 = -1$dB,

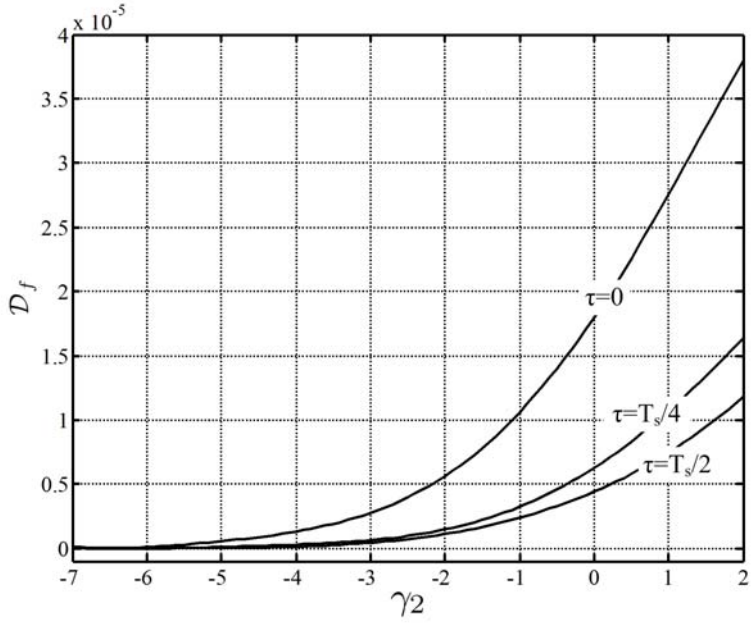

FIGURE 3.2. Cramrvon Mises test to measure the accuracy of estimated distribution of number of errors in a packet when $N = 1024$, $\gamma_1 = 3$dB and U_1 and U_2 uses QPSK and 16-QAM respectively

and the average packet error probability $\mathcal{P}_{\text{th}}$. We would like to point out the more than 20% increase in code rate from the worst case to the best case.

TABLE 3.1. Minimum $\mathcal{K}$ and required coding rate $\gamma_1 = 5$dB, $\gamma_2 = 0$dB and $\gamma_1 = 4$dB, $\gamma_2 = -1$dB

		$\gamma_1 = 5, \gamma_2 = 0$		$\gamma_1 = 4, \gamma_2 = -1$	
	$\mathcal{P}_{\text{th}}$	$\mathcal{K}$	Rate	$\mathcal{K}$	Rate
Worst Case	0.1%	618	0.60411	473	0.462366
	1%	648	0.63343	513	0.501466
($\tau = 0$)	10%	708	0.69208	573	0.560117
Best Case	0.1%	738	0.72141	628	0.613881
	1%	768	0.75073	658	0.643206
($\tau = T_s/2$)	10%	808	0.78983	708	0.692082

Chapter 4

Enhancing Sensing-Throughput Tradeoff in Cognitive Radios Using Receiver Statistics

4.1 Introduction and Background

In overlay cognitive radio networks spectrum sensing is used by the SU determine whether the channel is occupied by the PU or not. During the sensing periods communication of the SU's is suspended resulting in loss of throughput in the secondary network. Therefore, it is desired to make the sensing periods as short as possible. However, the sensing periods cannot be too short since the performance of the sensing algorithm as expressed by misdetection and false alarm probabilities will be adversely affected. Misdetection increases the detection delay. Therefore misdetection probability should be small (e.g., $< .1$ for IEEE 802.22 standard). On the other hand, the probability of false alarm must also be small (e.g., $< .1$ for IEEE 802.22 standard) since false alarm results in loss of throughput in the secondary network.

It is evident that an intricate tradeoff is at work between protecting the incumbent users and the quality of service in the secondary network. This tradeoff, referred to as sensing-throughput tradeoff, has been formulated in [56]. Recently efforts have been underway to increase the throughput of SU without violating the maximum allowed detection delay. In [57] Zarrin *et al.* maximize the throughput with respect to the frame length when the quickest sensing algorithm is employed. In [58], Stergios *et al.* proposed a new receiver and frame structure for cognitive radios so as to perform spectrum sensing and the data transmission simultaneously in order to overcome the sensing-throughput tradeoff. Adaptive scheduling of spec-

trum sensing whereby the sensing period is adapted to the primary user activities has been investigated in [59] and [60] in order to improve the SU's throughput.

During its own transmission periods the SU does not attempt to detect the presence of the PU signal. This implies that if the PU emerges, not only will the SU cause undue interference to the PU, but also its own communication may be disrupted due to the interference from the PU. In [61] the authors proposed several physical-layer receiver statistics that a secondary radio can employ in order to detect the emergence of the PU signal during its own communication. These statistics can be easily derived after demodulation and/or decoding of each packet and are often available for other purposes such as performance improvement in adaptive transmission schemes. Some examples include the receiver error count (REC), the iteration count (IC) in systems using iterative decoding, and the signal-to-noise ratio. To contrast this with the usual spectrum sensing techniques, the authors referred to this approach as spectrum monitoring.

In this Chapter, we revisit the problem of sensing-throughput tradeoff by considering spectrum monitoring using the receiver statistics. A new decision statistic is introduced using a combination of the receiver error counts and the output of a CRC (cyclic redundancy check) code in order to detect the emergence of the primary user in the in-band channel. Using the proposed decision statistic, the probabilities of false alarm and detection are evaluated in closed form. We also evaluate both channel utilization [1] and detection delay of the hybrid spectrum sensing/spectrum monitoring system in closed form using two Markov chain models. The upper and lower limits of performance for this decision statistic are evaluated and an optimization problem is formulated to maximize channel utilization with a constraint on detection delay. Numerical results are presented from analy-

[1] Defined as the average fraction of time that under hypothesis H_0 the SU communicates over the channel.

sis and simulation which show the accuracy of the analytical formulation and the efficacy of the proposed algorithm. To present the performance of the algorithm with concrete examples we simulate the proposed system using two forward error correcting codes, namely a BCH code and a convolutional code. It is shown that the results from these simulations are closely matched with those from analysis.

4.2 System Model

The SU starts with a spectrum sensing interval (SSI) during which it attempts to detect the presence of the PU. If at the end of SSI, the SU decides that the PU signal is present, then another sensing interval begins anew. This process continues until the channel is sensed to be free of the PU signal at which time a spectrum monitoring interval (SMI) begins during which the SU will be receiving packets. After the reception of each packet the SU computes a decision statistic (described below) in order to determine whether the PU has emerged or not. If it is decided that the PU has emerged, the SU vacates the channel and starts a new SSI; otherwise, it continues in SMI mode until K_M packets are received. At that time a new sensing interval begins. In other words SMI is restricted to a maximum of K_M packets. It is assumed that time at the SU is slotted with the slot duration T_p equal to the transmission time of a single packet, and that the length of SSI is $T_S = K_S T_p$ for some integer $K_S \geq 1$.

Some remarks are in order. The system model described above does not require that spectrum sensing be repeatedly performed on the same channel when the channel is found to be occupied. Cognitive radios are envisioned to be equipped with agile radios capable of scanning the spectrum for white spaces. If at the end of an spectrum sensing interval the channel is found to be occupied, the secondary user may switch and begin its sensing operation in a new channel. The model and subsequent analysis presented here applies without change assuming that the

detection and false alarm probabilities are the same for all the channels. Next, for most spectrum sensing algorithms the sensing time (required to achieve the desired false alarm and detection probabilities) is determined by the number of observation samples and the sampling rate. Assuming a sampling rate equal to the symbol rate of the primary user (i.e., no oversampling) it can be seen that for an spectrum sensing interval of duration T_p, enough observation samples can be collected to complete the spectrum sensing operation. We have chosen the more general case where spectrum sensing interval has duration $K_S T_p$. In case the spectrum sensing interval duration is shorter than a packet time, then our results provide a very tight lower bound to channel utilization and detection delay. This is due to the fact that a fraction of packet time is very small compared to the detection delay mandated by the standards such as IEEE 802.22. Finally we should point out that spectrum monitoring is not a substitute for spectrum sensing, but it is intended to enhance the performance of (any) existing spectrum sensing algorithms by enabling the secondary user to detect the emergence of the prmary user during its sown communication.

4.3 Decision Statistic

At the source the information sequence is assumed to be first encoded using a CRC code (for error detection) followed by a forward error correction (FEC) scheme to obtain an N-bit packet[2]. At the receiver the packet is demodulated and decoded. The decoded packet is then checked by CRC and also encoded using a replica of the transmitter's encoder. The output of the encoder is compared to the output of the demodulator[3] to estimate the number of errors introduced by the channel.

[2]In today's communication systems error control coding is widely used to combat channel errors. Therefore there is no loss of throughput or increase in complexity due to FEC if it is already in use by the SU. Moreover, the throughput loss associated with the addition of CRC is small given the number of parity check bits compared to the length of the data string.

[3]If the decoder uses soft decision, then hard decision must be performed on the demodulator output before comparison with the encoder's output.

The number of errors thus calculated is referred to as receiver error count (REC) and is used in our decision statistic.

Consider a spectrum monitoring interval and let the hypotheses H_0 and H_1, respectively, represent the absence and the presence of the PU during the reception of the current packet. Also denote by $\mathcal{C}_{\rm v}$ (resp. $\mathcal{C}_{\rm nv}$) the events that the CRC is validated (resp. not validated) and let k denote the REC. The proposed decision rule is now given by,

$$\begin{cases} (\{k \geq \mu\} \cap \mathcal{C}_{\rm v}) \cup \mathcal{C}_{\rm nv} \ , & \text{Decide } H_1 \\ \text{else}, & \text{Decide } H_0 \end{cases} \tag{4.1}$$

where μ is the REC threshold. Denote by t the maximum number of errors in a packet that FEC is capable of correcting. In the sequel the threshold value μ in (4.1) is chosen such that $\mu \leq t$. Fig. 4.1 illustrates an implementation of the proposed decision rule[4].

If the decision is H_1, i.e., $\eta = 1$ in Fig. 4.1, the SMI is terminated. Otherwise it is decided that the PU has not emerged and SMI continues (up to K_M packets).

A number of CRC codes are incorporated into technical standards. The most commonly used are the 16- and the 32-bit CRCs, such as CCITT-16, CRC-32-Castagnoli and CRC-32-IEEE [62, 63, 64]. It is shown in [65] that for an L-bit CRC, used over a binary symmetric channel, the probability of undetected error (CRC failure) approaches 2^{-L} when the number of information bits is large (e.g., ≥ 100). For a 16-bit CRC this probability is around 1.5×10^{-5} and for a 32-bit CRC it is 2.3×10^{-10}.

Let the *actual number of errors* introduced by the channel in the current packet be denoted by e. The value of e is unknown since we do not know if the packet is correctly decoded or not. However, note that if the packet is correctly decoded,

[4]Note that as (4.1) and Fig. 4.1 show, the decision rule does not rely on the actual number of channel errors.

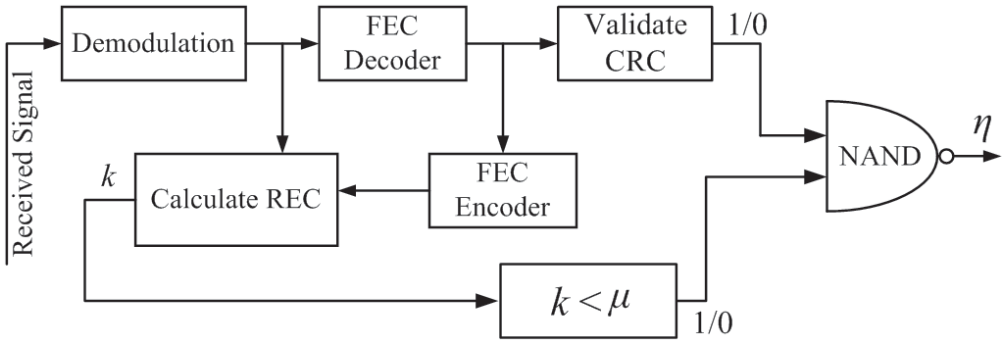

FIGURE 4.1. The proposed system model

then the CRC will rightfully indicate so and the value of REC is equal to the actual number of errors, i.e., $k = e$. On the other hand, if the packet is not decoded correctly, then the actual number of errors cannot be inferred from REC. In this case there are two possibilities. First, CRC is not validated, ($\mathcal{C}_{\text{nv}}$), and therefore succeeds in detecting that the packet is not correctly decoded. In this case REC is not used and it is decided that the PU has emerged (see Fig. 4.1). Second, CRC is validated ($\mathcal{C}_{\text{v}}$), i.e., it fails to detect that the packet is incorrectly decoded. In this case REC is used but it is not the same as the actual number of errors e. The probability of the event that the packet is incorrectly decoded (small probability event) and that this event is not detected by the CRC (probability less than 2^{-L} for an L-bit CRC) is clearly extremely low. If this event occurs under H_1, the system may fail to detect the emergence of the PU. It is not difficult to see that the additional (average) detection delay caused by such events would be less than 2^{-L} in packet time, i.e., $2^{-L} \times T_p$. On the other hand if this event occurs under H_0, the (average) loss in channel utilization for the SU will be less than $2^{-L} \times \frac{K_S}{K_M+K_S} \leq 2^{-L}$. In view of the above in subsequent analysis we ignore the event that the packet is decoded incorrectly and that such event goes undetected by the CRC. Therefore when the event $\mathcal{C}_{\text{v}}$ occurs, REC and the actual number of channel errors are assumed to be equal, i.e., $e = k$. It should be noted, however,

that the proposed method works even in the presence of CRC failures and as shown above and confirmed through simulations in section 4.7, the resulting effect on the system performance is negligible.

Let p_f and p_d denote the probabilities of false alarm and detection in the SMI, respectively. From (4.1) and assuming that $\mu \leq t$ we get,

$$\begin{aligned} p_f &= P[(\{k \geq \mu\} \cap \mathcal{C}_{\mathrm{v}}) \cup \mathcal{C}_{\mathrm{nv}} | H_0] \\ &= P((\{e \geq \mu\} \cap \mathcal{C}_{\mathrm{v}}) \cup (\{e \geq \mu\} \cap \mathcal{C}_{\mathrm{nv}}) | H_0) \\ &= P(e \geq \mu | H_0), \end{aligned} \tag{4.2}$$

and similarly, the probability of detection is given by,

$$p_d = P(\{e \geq \mu\} | H_1). \tag{4.3}$$

where the second equality in (4.2) follows from the fact that since μ is chosen such that $\mu \leq t$, $\mathcal{C}_{\mathrm{nv}}$ implies $\{e \geq \mu\}$.

4.4 Channel Utilization

Channel utilization is the average fraction of time that (under hypothesis H_0) the SU communicates over the channel. In the absence of the PU, the SU does not use the channel if the system is in spectrum sensing. In three cases the system leaves the SMI and enters the SSI. First, at the end of an SMI (after the transmission of K_M packets); next, if a false alarm occurs during SMI; and finally, when a false alarm occurs at the end of an SSI.

Under hypothesis H_0 the spectrum monitoring operation can be modeled by $K_M + 1$ states, $\{0, 1, \cdots, K_M\}$, where state 0 represents spectrum sensing and states $1, 2, \cdots, K_M$, represent the first, second and K_Mth packet of the SMI. The REC of each packet is independent of the REC of any other packet, hence, given the current state, the next state is independent of the past states. Consequently,

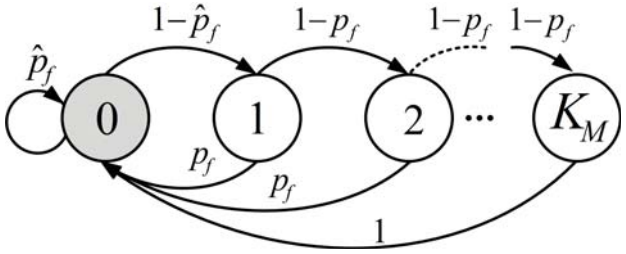

FIGURE 4.2. Markov chain model for spectrum monitoring in the absence of primary users.

under H_0, spectrum monitoring can be modeled by the Markov chain depicted in Fig. 4.2 where $\hat{p}_f$ denotes the false alarm probability of the spectrum sensing algorithm. We call this chain, whose probability transition matrix is given below, the Channel Utilization Markov Chain (CUMC).

$$P_{CUMC} = \begin{bmatrix} \hat{p}_f & 1-\hat{p}_f & 0 & 0 & \cdots & 0 \\ p_f & 0 & 1-p_f & 0 & \cdots & 0 \\ p_f & 0 & 0 & 1-p_f & \cdots & 0 \\ \vdots & \vdots & \vdots & 0 & \ddots & \vdots \\ p_f & 0 & 0 & 0 & \cdots & 1-p_f \\ 1 & 0 & 0 & 0 & \cdots & 0 \end{bmatrix} \tag{4.4}$$

It is clear that the CUMC is an irreducible, positive recurrent and aperiodic Markov chain with finitely many states. Therefore, it has an invariant distribution, $\underline{\pi} = [\pi_0, \cdots, \pi_{K_M}]$ which satisfies the following system of equations,

$$\underline{\pi} P_{CUMC} = \underline{\pi}, \quad \sum_{i=0}^{K_M} \pi_i = 1 \tag{4.5}$$

where π_i shows the long-run proportion of time the process spends in state i, [66]. Channel utilization is now given by the fraction of time that the process spends in states $1, 2, \cdots, K_M$. Considering the duration of SSI and SMI, channel utilization is given by,

$$U = \frac{\sum_{i=1}^{K_M} \pi_i}{\pi_0 K_S + \sum_{i=1}^{K_M} \pi_i} = \frac{1-\pi_0}{\pi_0 K_S + 1 - \pi_0} \tag{4.6}$$

From (4.5) we get,

$$\pi_0 = \frac{p_f}{p_f + (1-\hat{p}_f)[1-(1-p_f)^{K_M}]} \tag{4.7}$$

By substituting (4.7) into (4.6) we get,

$$U = \frac{(1-\hat{p}_f)[1-(1-p_f)^{K_M}]}{(1-\hat{p}_f)[1-(1-p_f)^{K_M}] + K_S p_f} \tag{4.8}$$

4.5 Detection Delay

Detection delay is defined as the average time it takes to detect the presence of the primary user after its emergence in the channel. Therefore, detection delay is evaluated under hypothesis H_1. Considering the fact that the total length of SSI and SMI is $(K_S + K_M)T_p$, we define a set of $K_M + K_S + 1$ states where for $0 \leq i \leq K_S - 1$, state i belongs to the SSI, i.e., iT_p shows the elapsed time from the beginning of SSI. For $K_S \leq i \leq K_S + K_M - 1$, state i represents the transmission of the $(i - K_S + 1)$th packet in the SMI. Finally, state $K_M + K_S$ indicates that detection has occurred.

The probability of detection in spectrum sensing algorithms depends on the duration of observation of the PU signal. Therefore during the SSI, the probability of detection denoted $\hat{p}_d(i)$ depends on the state $i = 0, 1, \cdots, K_S - 1$, in which the PU signal emerges. In Appendix E we have evaluated these probabilities assuming that for spectrum sensing, the SU employs an energy detector [18, 19]. However, a remark is in order here. The proposed spectrum monitoring technique is not contingent upon the use of energy detector for spectrum sensing. In case another spectrum sensing method such as the cyclostationary detector, [13], or the autocorrelation-based detector [25] is used, the detection probabilities $\hat{p}_d(i), i = 0, 1, \cdots, K_S - 1$, should be replaced with the appropriate values.

To evaluate detection delay, we define two events. The first event, denoted $\mathcal{X}_1$, is when the PU emerges at the beginning of the SSI, namely in state 0, or in any of

the SMI states, namely state i for $K_S \leq i < K_S + K_M$. The second event, denoted $\mathcal{X}_2$, is when the PU emerges at the beginning of one of the intermediate states of SSI, namely state i for $1 \leq i < K_S$. Because the transmission time of each packet is assumed to be fixed, we evaluate the detection delay in terms of the number of packets.

Conditioned on the event $\mathcal{X}_1$, it can be shown that the probability of transition from each state to another is independent of past states and is determined by whether the system is in spectrum sensing or spectrum monitoring. Consequently, under hypothesis H_1, and conditioned on $\mathcal{X}_1$, we can model the system by a Markov chain as shown in Fig. 4.3. The probability transition matrix for this chain, which we refer to as Detection Delay Markov Chain (DDMC), is given by (4.9) where $p_m = 1 - p_d$ and $\hat{p}_m = 1 - \hat{p}_d(0)$ are the probabilities of misdetection in spectrum monitoring and spectrum sensing, respectively. In the following we denote $\hat{p}_d(0)$ by $\hat{p}_d$.

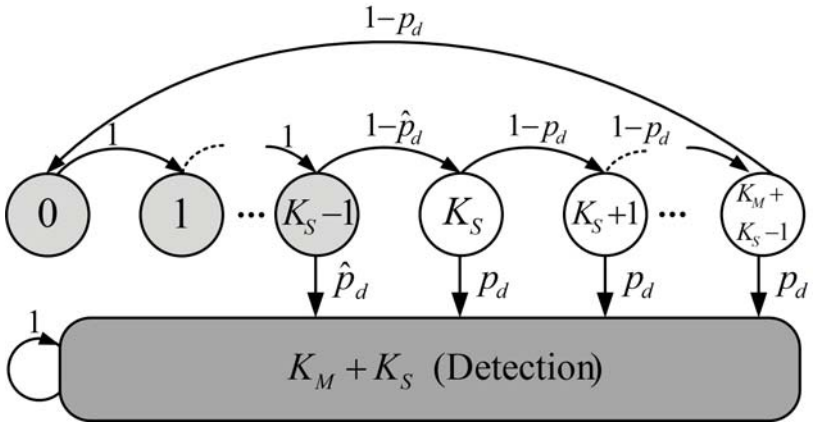

FIGURE 4.3. Markov chain model for detection delay given $\mathcal{X}_1$.

We note that in DDMC, state $K_M + K_S$ is an absorbing state and all other states are transient.

$$P_{DDMC} = \tag{4.9}$$

States	0	1	···		K_S	$K_S{+}1$	···	$K_S{+}K_M{-}1$	$K_S{+}K_M$
0	0	1			0	0	···	0	0
1	⋮		⋱		⋮	⋮	⋱	⋮	⋮
⋮	0	···	0	1	0				0
$K_S{-}1$	0	···		0	$\hat{p}_m$	0	···	0	$\hat{p}_d$
K_S	0	···			0	p_m		0	p_d
⋮	⋮	⋱			⋮	0	⋱		⋮
	0				0	⋮		p_m	
$K_S{+}K_M{-}1$	p_m	0	···		0	0	···	0	p_d
$K_S{+}K_M$	0	0	···		0	0	···	0	1

Let $f_k(i)$ be the probability of going in k steps from state i to state $K_S + K_M$. Then, from Chapman-Kolmogorov equation [66],

$$f_{k+1}(i) = \sum_{j=0}^{K_M+K_S-1} P_{DDMC}(i,j) f_k(j) \tag{4.10}$$

Define the vector $\underline{f}_k$ of length $K_M + K_S$ as,

$$\underline{f}_k \triangleq [f_k(0), f_k(1), \cdots, f_k(K_M + K_S - 1)]^T \tag{4.11}$$

where T denotes the transpose operation. Then

$$\underline{f}_{k+1} = G\underline{f}_k = G^k \underline{f}_1 \tag{4.12}$$

where the matrix G is obtained by removing the last row and column of P_{DDMC}, and where

$$\underline{f}_1 = [\overbrace{0 \quad \cdots \quad 0}^{K_S-1} \quad \hat{p}_d \quad \overbrace{p_d \quad \cdots \quad p_d}^{K_M}]^T \tag{4.13}$$

The average number of steps to reach the detection state, $K_M + K_S$, starting from state i, denoted as $F(i)$, is now given by,

$$F(i) \triangleq \sum_{k=1}^{\infty} k f_k(i) = \sum_{k=0}^{\infty} (k+1) \left[G^k \underline{f}_1 \right]_{(i)} \tag{4.14}$$

where $[\mathbf{y}]_{(i)}$ denotes the ith component of the vector $\mathbf{y}$. Detection delay is now given by

$$D1 = \sum_{i=0}^{K_M+K_S-1} F(i)\kappa(i) \tag{4.15}$$

where $\kappa(i)$ is the conditional probability that given the event $\mathcal{X}_1$, the PU emerges in state i. Let $\underline{\kappa} = [\kappa(0), \kappa(1), \cdots, \kappa(K_M + K_S - 1)]$. We have,

$$\underline{\kappa} = [\frac{1}{K_M+1} \overbrace{0 \cdots 0}^{K_S-1} \overbrace{\frac{1}{K_M+1} \cdots \frac{1}{K_M+1}}^{K_M}]^T \tag{4.16}$$

Substituting (4.14) for $F(i)$ in (4.15) and after some manipulations, detection delay conditioned on $\mathcal{X}_1$ can be written as,

$$D_1 = \underline{\kappa}^T (I - G)^{-2} \underline{f}_1 \tag{4.17}$$

where I is an identity matrix of size $(K_M + Ks) \times (K_M + K_S)$. We have evaluated the inverse of $I - G$ in Appendix B.

Given $\mathcal{X}_2$, the PU emerges in state i, $1 < i < K_S$, with probability $\frac{1}{K_S-1}$. In this case the PU will be detected at the end of the SSI with probability $\hat{p}_d(i)$ and detection delay is equal to $K_S - i$. On the other hand if the PU is not detected at the end of SSI, then detection delay is equal to $K_S - i$ plus detection delay given $\mathcal{X}_1$ when the primary user emerges in state K_S. Consequently, detection delay given $\mathcal{X}_2$ is given by,

$$\begin{aligned} D_2 = & \frac{1}{K_S - 1} \sum_{i=1}^{K_S-1} \{\hat{p}_d(i)(K_S - i) \\ & + (1 - \hat{p}_d(i))(K_S - i + \underline{\mathbf{1}}_{K_S+1} (I - G)^{-2} \underline{f}_1) \Big\} \end{aligned} \tag{4.18}$$

where $\underline{\mathbf{1}}_{K_S+1} = [\ \overbrace{0\ \cdots\ 0}^{K_S}\ \ 1\ \ \overbrace{0\ \cdots\ 0}^{K_M-1}\ ]^T$. Finally the total detection delay is given by,

$$\begin{aligned} D &= D_1 P(\mathcal{X}_1) + D_2 P(\mathcal{X}_2) \\ &= \frac{K_M+1}{K_S+K_M} D_1 + \frac{K_S-1}{K_S+K_M} D_2. \end{aligned} \tag{4.19}$$

4.6 System Assessment

In this section, we assess the limits of spectrum monitoring in terms of achievable regions for channel utilization and detection delay. It is assumed that a spectrum sensing algorithm with a fixed duration $K_S T_p$ and (fixed) probabilities of false alarm, $\hat{p}_f$, and detection, $\hat{p}_d$, is employed.

Considering (4.8) and the fact that p_f is a decreasing function of μ, channel utilization is an increasing function of K_M and μ. Therefore for a fixed μ and for a fixed K_M channel utilization is bounded as

$$\frac{1-\hat{p}_f}{1-\hat{p}_f+K_S} \leq U < \frac{1-\hat{p}_f}{1-\hat{p}_f+K_S p_f(\mu)} \tag{4.20}$$

$$\frac{1-\hat{p}_f}{1-\hat{p}_f+K_S} \leq U \leq \frac{1-\hat{p}_f}{1-\hat{p}_f+K_S/K_M}, \tag{4.21}$$

respectively. For most spectrum sensing algorithms, a packet time is sufficiently long for spectrum sensing to provide acceptable false alarm and detection probabilities. In this case detection delay is given by $D = D_1$ for which an alternative representation is given in appendix C.

In general the performance of spectrum sensing algorithms is better than spectrum monitoring, i.e., for a fixed SNR and probability of false alarm, $p_d < \hat{p}_d$. Considering this and the fact that for $K_S = 1$, p_d is a decreasing function of μ, one can verify that D_1 in (6.11) is an increasing function of K_M and μ. So, for a fixed

μ and $1 \leq K_M < \infty$, detection delay is bounded by

$$\frac{2 + (1 - \hat{p}_d) + (1 - p_d(\mu))}{2(1 - (1 - \hat{p}_d)(1 - p_d(\mu)))} \leq D \leq \frac{1}{p_d(\mu)} \tag{4.22}$$

On the other hand for a fixed K_M and different values of μ, detection delay is bounded by

$$1 + \frac{1 - \hat{p}_d}{1 + K_M} \leq D \leq \frac{2 + (2 - \hat{p}_d)K_M}{2\hat{p}_d} \tag{4.23}$$

4.6.1 Optimization of Channel Utilization

The two parameters of spectrum monitoring, namely K_M and μ can be chosen to maximize channel utilization subject to an upper bound on detection delay. As is shown in (4.20)–(4.23), both channel utilization and detection delay are increasing functions of K_M and μ for $K_S = 1$. Therefor a constrained optimization problem can be formulated as follows.

$$\begin{aligned} &\text{Maximize } U(K_M, \mu), \\ &\text{Subject to } D(K_M, \mu) \leq D_{\max} \end{aligned} \tag{4.24}$$

where $D_{\max}$ is the maximum acceptable detection delay. Since $p_d(\mu) \in [0, 1]$, is a finite decreasing sequence of μ, by setting $p_d(N + 1) = 0$, it follows that for any given $1 \leq D_{\max} < \infty$ there exists μ_0 such that,

$$\frac{1}{p_d(\mu_0)} \leq D_{\max} < \frac{1}{p_d(\mu_0 + 1)}. \tag{4.25}$$

The probability of detection is a function of the time offset between the received signals from the SU and the PU. Therefore to solve the optimization problem, we consider the minimum value of p_d which guarantees that the detection delay constraint in (4.24) is not violated. Setting $\partial p_d / \partial \tau = 0$ results in

$$\frac{\partial}{\partial \tau} \left(\psi^2(-\tau) + \psi^2(T_s - \tau) \right) = 0 \tag{4.26}$$

For the pulse shapes of interest (e.g., raised cosine, rectangular), (4.26) results in $\tau = T_s/2$. This is intuitive as for a timing offset of $\tau = T_s/2$, each symbol of SU receives equal interference from two symbols of the PU resulting in the minimum p_d. Subsequently we use this worst-case value for τ. To find the maximum value of μ which does not violate (4.24), we consider the upper bound in (4.22), and also the fact that $\mu \leq t$, to obtain the maximum value of the threshold, μ_0, given by

$$\mu_0 = \min\left(t, \left\lfloor Q^{-1}(\frac{1}{D_{\max}})\sigma_1 + Np_{b,1} \right\rfloor\right), \tag{4.27}$$

Let us define two regions, $\Omega_1 = [0, \mu_0]$ and $\Omega_2 = [\mu_0, t]$. We have,

$$\forall K_M, \forall \mu \in \Omega_1, \quad D(K_M, \mu) \leq D_{\max} \tag{4.28}$$

$$U(K_M, \mu) \leq U(K_M, \mu_0) \tag{4.29}$$

Consequently, μ_0 is the optimum solution in Ω_1, and by increasing K_M, channel utilization will increase up to its upper bound in (4.20). For $\mu \in \Omega_2$, the probability of false alarm is small, so, the channel utilization in (4.8) is approximated by,

$$U(K_M, \mu) \approx \frac{K_M(1-\hat{p}_f)}{K_M(1-\hat{p}_f) + K_S} \tag{4.30}$$

Treating K_M and μ as continuous variables, the gradient of $U(K_M, \mu)$ can be written as,

$$\nabla U(K_M, \mu) = \left(\frac{K_S(1-\hat{p}_f)}{(K_S + K_M(1-\hat{p}_f))^2}, 0\right)^T, \tag{4.31}$$

where $(.)^T$ denotes transpose. (4.31) implies that for all $\mu \in \Omega_2$, channel utilization is almost constant. Consequently in region Ω_2, the maximum channel utilization is not a function of μ and is achieved for the largest value of K_M. Moreover, from (4.22) and (4.25), for $\mu > \mu_0$, $D_{\max} < D(\infty, \mu)$ which implies that to satisfy (4.24), for each $\mu > \mu_0$ there is a maximum acceptable K_M which is finite. The maximum K_M satisfying (4.24) for $\mu > \mu_0$ is evaluated in appendix D. As a

result, in region Ω_2 the highest channel utilization is achieved for $\mu = \mu_0$ and $K_M \longrightarrow \infty$. In conclusion, the optimum solution to (4.24) is obtained for $\mu = \mu_0$ and for $K_M \longrightarrow \infty$, for which channel utilization increases without violating the constraint in (4.24).

4.7 Numerical Results

Numerical results on the performance of spectrum monitoring evaluated through analysis and simulation are presented here, and the advantages of joint spectrum sensing and spectrum monitoring compared to pure spectrum sensing is demonstrated. The simulation results are obtained by repeating each experiment at least 10^4 times, and all pulse shapes are rectangular.

Fig. 4.4 illustrates the ROCs from simulation and analysis for $N = 511$, $\gamma_s = 3$ dB, different values of γ_u and two cases of $\tau = 0$ and $\tau = T_s/2$. The simulation results are obtained using two different forward error correcting codes: a rate 1/2 convolutional code with generator matrix $[g^{(0)} = (716502)_8 \ ; \ g^{(1)} = (514576)_8]$, [67], and a $(511, 304)$ binary BCH code. We also employed a CRC-8 with the generator polynomial $x^8+x^7+x^6+x^4+x^2+1$. The SU employs QPSK, and the PU uses 16-QAM signaling. It is also evident from the graphs that the performance of the system is independent of utilized FEC technique. As shown in Fig. 4.4, the performance of spectrum monitoring degrades from $\tau = 0$ to $\tau = T_s/2$. In particular, for $p_f = 0.1$ and $\gamma_u = -4$ dB, probability of detection is 0.92 and 0.61 for $\tau = 0$ and $\tau = T_s/2$, respectively. Recall that as discussed in Section 4.6, $\tau = T_s/2$ is the worst case for detection delay. We should point out that when the detection and false alarm probabilities from simulation and analysis are close as illustrated by Fig. 4.4, the channel utilization and detection delay will also be close since the latter are only determined by the former. Similar conclusions can be derived from Fig. 4.5 which shows the simulation results when the SU uses a

16-QAM modulation scheme and the PU uses 64-QAM. The $(511, 304)$ BCH code and CRC-8 described above are used and $\gamma_s = 5$dB is assumed.

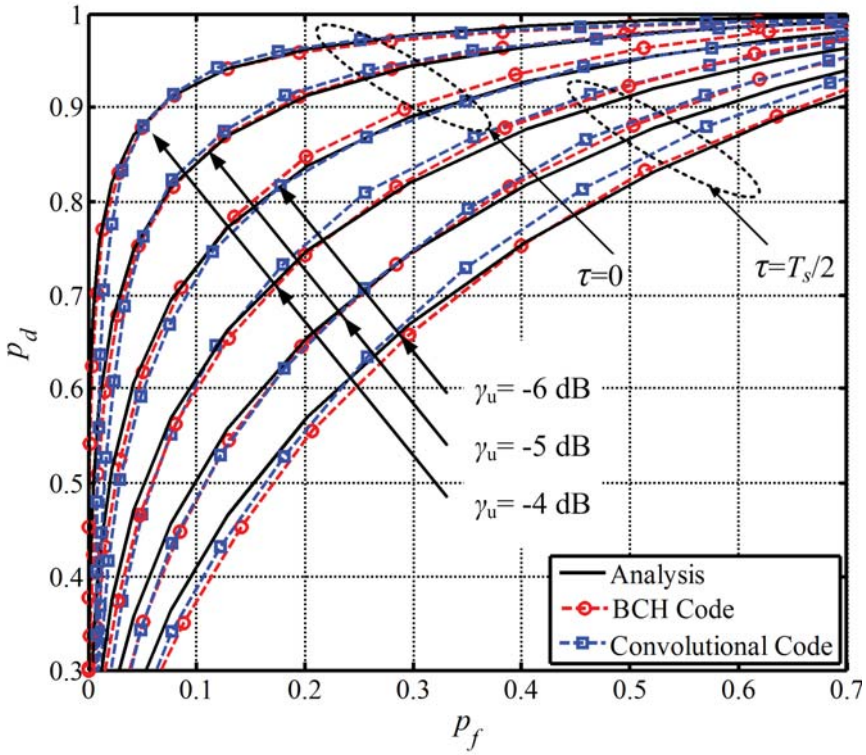

FIGURE 4.4. ROC for $N = 511$, $\gamma_s = 3$dB, different γ_u, and $\tau = 0, T_s/2$.

In the remainder of this section we evaluate CU and DD in terms of the false alarm and detection probabilities p_f and p_d. Figs. 4.6 and 4.7 illustrate channel utilization versus p_f and p_d, respectively, for different values of K_M and K_S, and $N = 256$, $\gamma_s = 3$dB, $\gamma_u = -3.5$dB, and $\hat{p}_f = 0.1$. As illustrated in these figures and evident from Fig. 4.2, increasing p_f (or p_d), increases the probability that the secondary user stops transmission (returns to state 0), resulting in lower channel utilization. Moreover, it can be seen from Fig. 4.6 and Fig. 4.7 that increasing K_S results in lower channel utilization because the system spends more time in spectrum sensing where the SU cannot use the channel. On the other hand, channel utilization increases with K_M. For a fixed value of K_S, a larger K_M implies that the SU spends more time transmitting and less time in spectrum sensing.

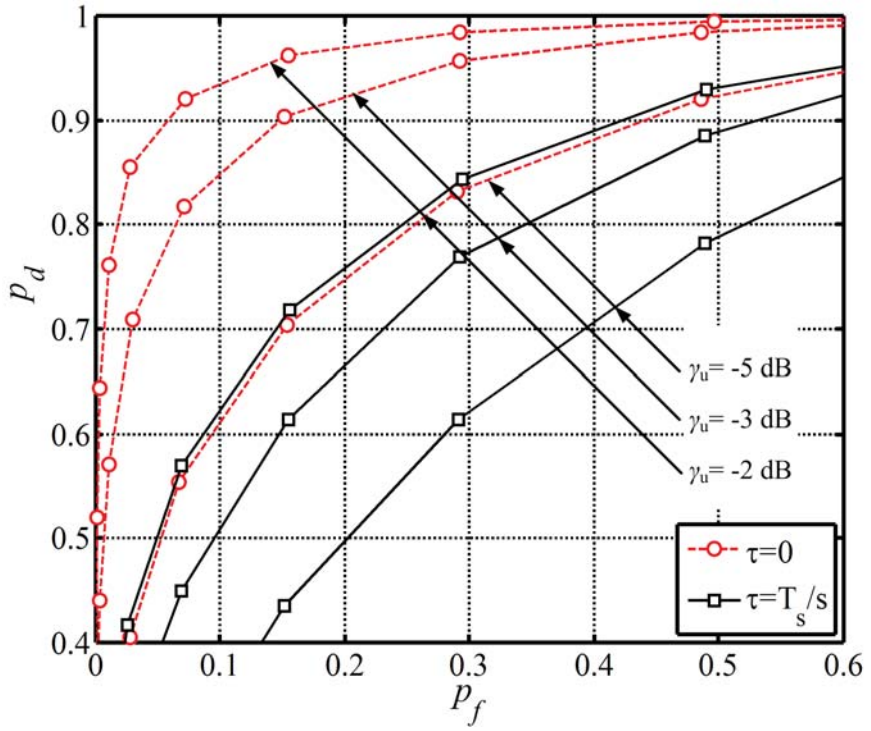

FIGURE 4.5. ROC for $(511, 304)$-BCH code, CRC-8, 16-QAM and 64-QAM for the SU and the PU, $\gamma_s = 5$dB, different γ_u, and $\tau = 0, T_s/2$.

Figs. 4.6 and 4.7 illustrate that in the case of $K_M = 1$ and for a fixed K_S, channel utilization is not a function of p_d and p_f. This is due the fact that there is only a single spectrum monitoring state and regardless of the decision in that state, the system moves into the spectrum sensing state. Therefore channel utilization is only a function of the decision in the spectrum sensing state. This statement can also be verified from (4.8) for $K_M = 1$ and the lower bound in (4.20).

Fig. 4.8 shows detection delay versus p_d from analysis and simulation for $K_S = 1, 5$, $K_M = 1, 2, 5, 10, 25$, $N = 256$, $\gamma_s = 3$dB, $\gamma_u = -6$dB, and $\hat{p}_f = 0.1$. Energy detector is assumed to be used for spectrum sensing. The probability of detection for energy detector when the PU emerges during SSI is derived in Appendix E. We should point out that the proposed spectrum monitoring technique is not contingent upon the use of energy detector for spectrum sensing and that energy detector is used here as an example only. It is well known that energy detectors,

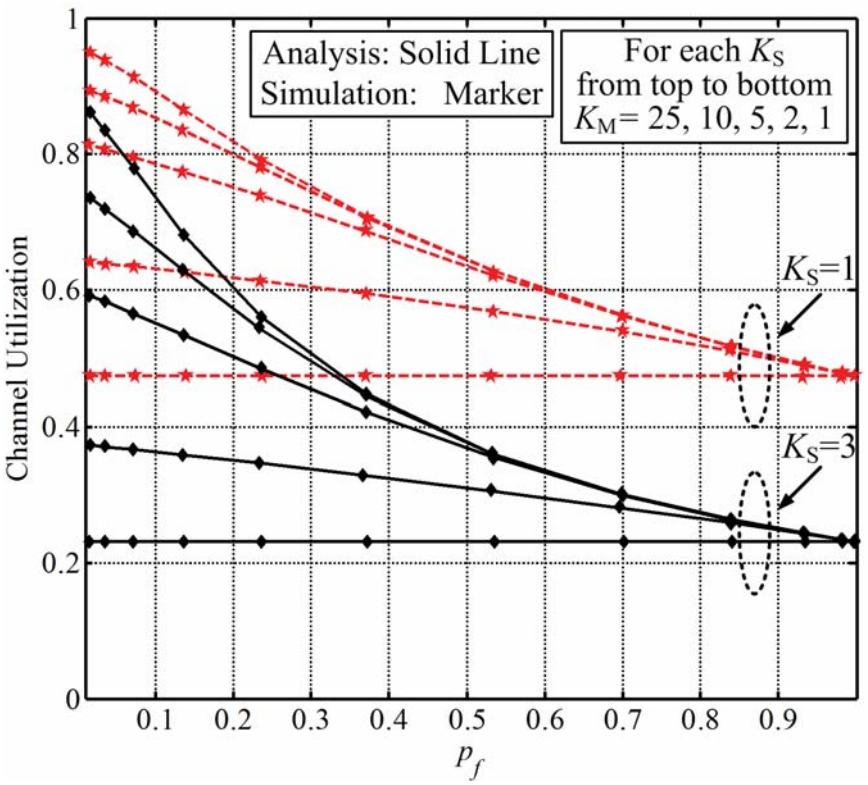

FIGURE 4.6. Channel utilization vs p_f for different values of K_M and K_S, $N = 256$, $\gamma_s = 3$dB, $\gamma_u = -3.5$dB and $\hat{p}_f = 0.1$.

while easy to implement, suffer from some drawbacks such as "SNR wall" [20]. In case another spectrum sensing method such as the cyclostationary detector, [13], or the autocorrelation-based detector [25] is used, the detection probabilities $\hat{p}_d(i), i = 0, 1, \cdots, K_S - 1$, should be replaced with the appropriate values.

It can be seen that in the case of $K_S = 1$, detection delay is an increasing function of K_M. This is due to the following. In general for fixed system parameters, spectrum sensing is more effective in detecting the presence of the PU than spectrum monitoring. Smaller values of K_M result in shorter time between visits to state 0 in DDMC where, with a high probability $\hat{p}_d$, the detection of PU occurs after a single packet time ($K_S = 1$). For larger values of K_M, subsequent visits to state 0 take longer and although spectrum monitoring attempts to detect the pres-

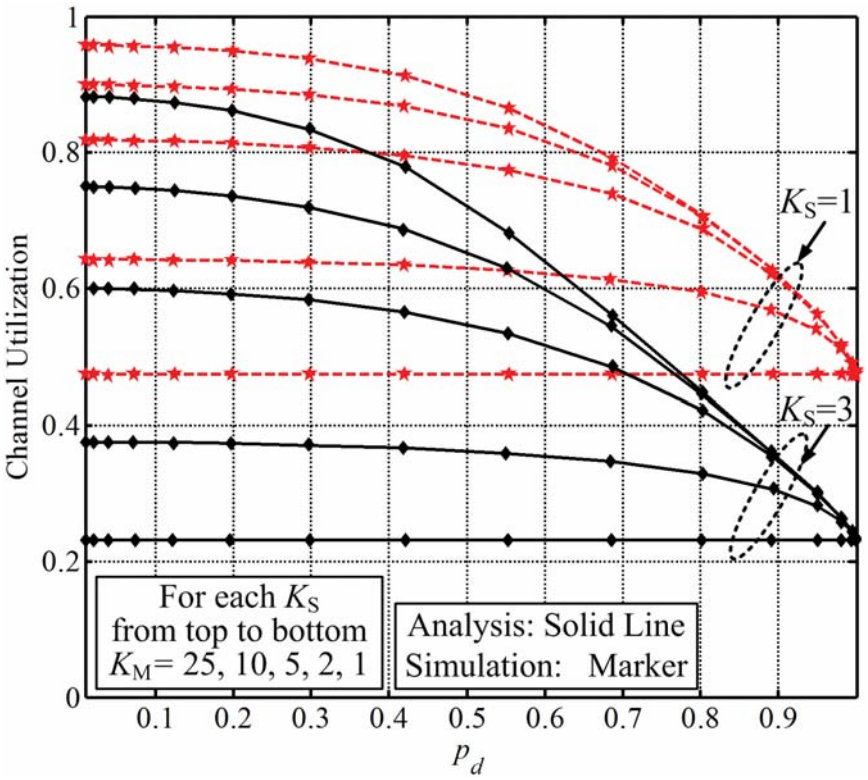

FIGURE 4.7. Channel utilization vs p_d for different values of K_M and K_S, $N = 256$, $\gamma_s = 3$dB, $\gamma_u = -3.5$dB and $\hat{p}_f = 0.1$.

ence of PU, it is not as effective as spectrum sensing, resulting in longer detection delay. Therefore in this case ($K_S = 1$), detection delay increases with K_M.

When $K_S > 1$, the spectrum sensing decision is made after state $K_S - 1$, whereas the spectrum monitoring decision is made after each packet. For small values of the spectrum monitoring detection probability, p_d, the chance of detecting the PU in the SMI is small, and with a high probability, the detection of PU will occur in the SSI. Therefore detection delay increases with K_M. On the other hand for larger values of p_d, the detection is made faster if it is made during the SMI. Consequently detection delay decreases with K_M. Note that as expected for large values of p_d, (e.g., $p_d > 0.7$ in this example), a detection delay of one (packet) can be achieved by increasing K_M (independent of the value K_S). Fig. 4.8 also shows that for $K_S = 1$ and fixed K_M, the detection delay is a decreasing function of p_d.

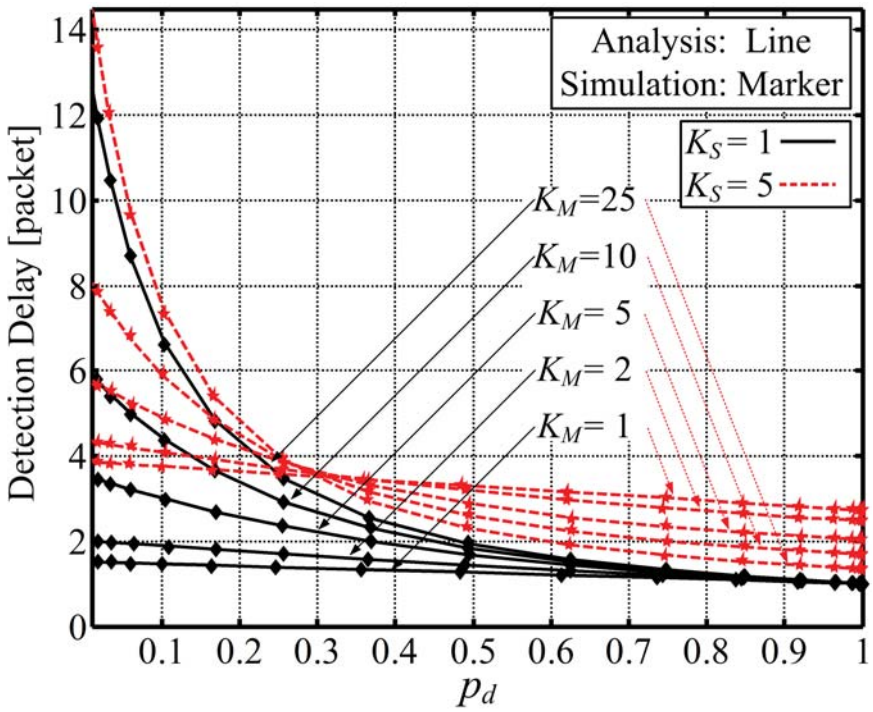

FIGURE 4.8. Detection delay vs p_d for different values of K_M and K_S, $N = 256$, $\gamma_s = 3$dB, $\gamma_u = -6$dB and $\hat{p}_f = 0.1$.

In Figs. 4.9 and 4.10 we evaluate channel utilization versus detection delay for two values of $\tau = 0$ and $\tau = T_s/2$, when $K_S = 1$, $N = 256$, $\gamma_s = 0$dB, $\gamma_u = -2.3$dB, and for the spectrum sensing algorithm, $\hat{p}_d = 0.95$ and $\hat{p}_f = 0.1$. The bounds in these figures can be found from (4.20), (4.21), (4.22) and (4.23). For any K_M, detection delay is an increasing function of μ. For fixed channel utilization, the worst detection delay corresponds to $p_f = p_d = 0$, i.e., the system uses spectrum sensing alone and no spectrum monitoring is performed. This implies that spectrum monitoring improves the performance of the system regardless of the values of K_M and μ.

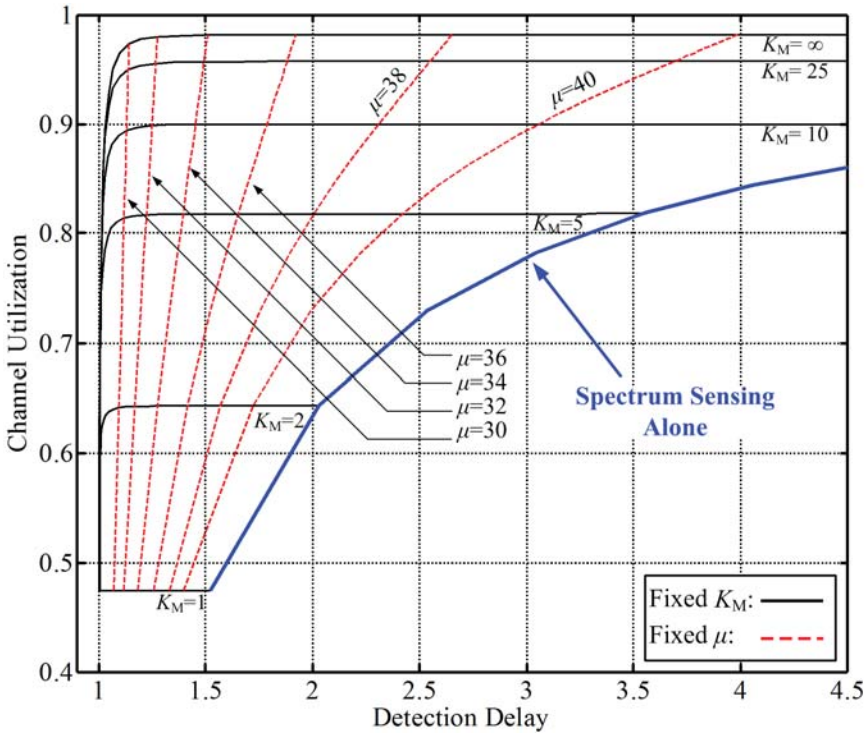

FIGURE 4.9. Channel utilization vs detection delay for $\tau = 0$, $K_S = 1$, $N = 256$, $\hat{p}_d = 0.95$, $\hat{p}_f = 0.1$, $\gamma_s = 0$dB and $\gamma_u = -2.3$dB.

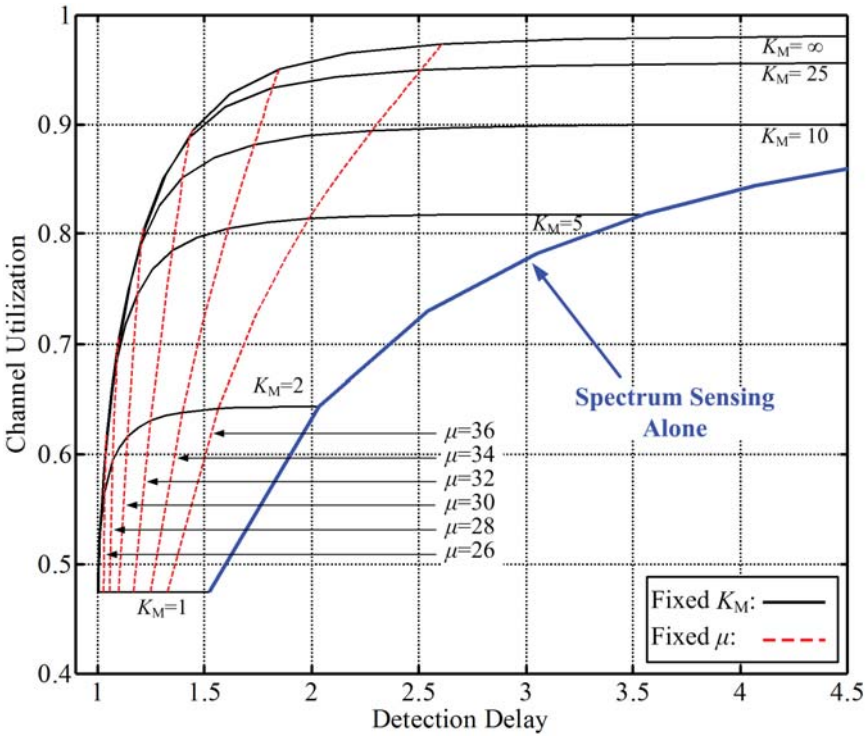

FIGURE 4.10. Channel utilization vs detection delay for $\tau = T_s/2$, $K_S = 1$, $N = 256$, $\hat{p}_d = 0.95$, $\hat{p}_f = 0.1$, $\gamma_s = 0$dB and $\gamma_u = -2.3$dB.

Chapter 5

Blind Spectrum Sensing Using Antenna Arrays and Path Correlation

5.1 Introduction and Background

In this Chapter we present a blind spectrum sensing technique for a secondary receiver equipped with a multiple-antenna system. Our approach exploits the channel path correlation among the signals received at different antenna elements. Correlation of channel paths coefficients has been established in a number of papers [68, 69, 70, 71, 72]. In particular it is shown that, in general, the path correlations increase as the beamwidth of the signals is reduced. A typical scenario is when the transmitter antenna, located on a high tower, has a LOS to the vicinity of the receiver where local scatterers may be present. Consequently the multi-path signals arrive within a certain range of angles resulting in highly correlated channel coefficients, [69, 70]. An example of this includes cases for which IEEE 802.22 standard has been developed to allow for reuse of underutilized licensed TV bands [5, 73]. Another scenario is the so-called keyhole or pinhole channels, in which, due to a large number of scatterers, there is only a small aperture through which all the signals can arrive at the receiver [71, 72]. Path correlation has also been considered in [74] in the design of MIMO predcoders.

In [75] the authors have studied the effects of path correlation on the performance of ED in a multi-antenna system. They have shown that in the presence of this correlation the system performance is degraded. In this paper, on the other hand, our goal is to exploit the path correlation for spectrum sensing. Our proposed algorithm is totally blind in that it does not require any knowledge of the primary signal parameters, the noise power or the channel fading coefficients. Our

decision statistic is based on the estimate of the cross-correlations among the received signals at different antenna elements. We evaluate the performance of the proposed algorithm through analysis and simulation and compare our results to several spectrum sensing techniques that utilize multi-antenna systems [28, 29, 21], It is shown that the proposed algorithm outperforms these methods.

5.2 System Model

Consider a SU receiver equipped with a linear antenna array of M equally spaced elements. Let h_k denote the channel fading coefficient from the PU transmitter to the kth antenna. It is assumed that h_k is a circularly symmetric Gaussian random variable with unit variance. Moreover, the channel undergoes block fading in that h_k remains unchanged during the spectrum sensing. For each antenna, the primary user's signal is assumed to arrive within a given range of angles or beamwidth. Assuming that the angle of arrival is uniformly distributed in the interval $[\theta - \theta_{\max}, \theta + \theta_{\max}]$, it is shown in [69] that the correlation between the channel coefficients h_k and h_l is given by

$$\begin{aligned}\phi_{hh}^{RR}(k-l) &\triangleq E[h_k^R h_l^R] = E[h_k^I h_l^I] = J_0(z(k-l))/2 \\ &+ \sum_{m=1}^{\infty} J_{2m}(z(k-l)) \cos(2m\theta) \frac{\sin(2m\theta_{\max})}{2m\theta_{\max}} \end{aligned} \tag{5.1}$$

and

$$\begin{aligned}\phi_{hh}^{RI}(k-l) &\triangleq E[h_k^R h_l^I] = -E[h_k^I h_l^R] \\ &= \sum_{m=0}^{\infty} J_{2m+1}(z(k-l)) \sin((2m+1)\theta) \frac{\sin((2m+1)\theta_{\max})}{(2m+1)\theta_{\max}} \end{aligned} \tag{5.2}$$

where $z = 2\pi\frac{D}{\lambda}$, and where D and λ are the antenna spacing and the wavelength, respectively. Here and subsequently, the superscripts R and I represent the real and imaginary parts of the complex variables, respectively.

Since (5.1) and (5.2) hold where the SU's are far from the PU's, the incident angle θ is usually very small. Thus in the following we assume that $\theta = 0$ which leads to

$$\phi_{hh}^{RR}(l) = J_0(zl)/2 + \sum_{m=1}^{m=\infty} J_{2m}(zl)\frac{\sin(2m\theta_{\max})}{2m\theta_{\max}} \tag{5.3}$$

and

$$\phi_{hh}^{RI}(l) = 0 \tag{5.4}$$

The extension to the case where $\theta \neq 0$ is somewhat straightforward. Also note that for the case of $\theta_{\max} = \pi$, the above reduces to Clark's model, [76, 77]. Fig. 5.1 shows the correlation $\phi_{hh}^{RR}(l)$ vs. the normalized distance $z = D/\lambda$ for several values of $\theta_{\max}$.

5.3 Correlation of Received Signals

We assume that the received signal at each antenna is down converted and sampled at the rate of one sample per symbol. In other words no oversampling is assumed. Let $r_{k,m}$ denote the mth sample of the complex envelope of the received signal at the kth antenna. Then

$$r_{k,m} = \eta h_k s_m + v_{k,m} \qquad k = 0, 1, \cdots, M-1 \tag{5.5}$$

where $\{s_m\}$ is the independent and identically distributed (iid) sequence of transmitted symbols, and where the noise sequences $\{v_{k,m}\}$ are assumed to be independent sequences of iid, circularly symmetric Gaussian random variables with variance N_0. The assumption of the independence of the noise sequences for different antenna elements k and l is discussed in section 5.5. Finally, $\eta \in \{0, 1\}$ indicates the presence ($\eta = 1$) or absence ($\eta = 0$) of the PU signal. In the following these two hypotheses are also denoted by $H_\eta, \eta = 0, 1$.

In the following we derive the statistical properties of the sequence $\{r_{k,n}\}$. Assuming that $E[s_m] = 0$, it is easy to see that

$$\begin{aligned} &E\left[r_{k,n}|H_\eta\right] = 0 \\ &E\left[r_{k,n}r^*_{k,m}|H_\eta\right] = 0 \qquad \forall m \neq n \end{aligned} \tag{5.6}$$

The correlation of $r_{k,n}$ and $r_{l,n}$ under H_0 is given by

$$E[r_{k,n}r^*_{l,n}|H_0] = E[v_{k,n}v^*_{l,n}] = N_0\delta(k-l) \tag{5.7}$$

The real and imaginary parts of the cross-correlation between $\{r_{k,n}\}$ and $\{r_{l,n}\}$ under H_1 are, respectively, given by

$$\begin{aligned} &E[\Re\{r_{k,n}r^*_{l,n}\}|H_1] = \\ &E\left[(h^R_k s^R_n - h^I_k s^I_n)(h^R_l s^R_n - h^I_l s^I_n) + (h^R_k s^I_n + h^I_k s^R_n)(h^R_l s^I_n + h^I_l s^R_n)\right] + N_0\delta(k-l) \\ &= 2\phi^{RR}_{hh}(k-l)\ \varepsilon_s + N_0\delta(k-l), \end{aligned} \tag{5.8}$$

and,

$$\begin{aligned} &E[\Im\{r_{k,n}r^*_{l,n}\}|H_1] = \\ &E\left[(h^R_k s^I_n + h^I_k s^R_n)(h^R_l s^R_n - h^I_l s^I_n) - (h^R_k s^R_n - h^I_k s^I_n)\times\right. \\ &\left.\left(h^R_l s^I_n + h^I_l s^R_n\right)\right] = 2\phi^{RI}_{hh}(k-l)\ \varepsilon_s = 0, \end{aligned} \tag{5.9}$$

where $\varepsilon_s = E[|s_m|^2]$, and where $\Re\{.\}$ and $\Im\{.\}$ represent the real and imaginary parts, respectively. To simplify notation subsequently we let

$$\mathcal{A}_\eta(k-l) \triangleq E[\Re\{r_{k,m}r^*_{l,m}\}|H_\eta] \tag{5.10}$$

Note that for Clark's model we have

$$\mathcal{A}_\eta(k-l) = \eta J_0(z(k-l))\varepsilon_s + N_0\delta(k-l) \tag{5.11}$$

5.4 Decision Statistics

5.4.1 Decision Statistics: Special Case

Spectrum sensing is performed using N consecutive samples of the received signal from each antenna, i.e., $\mathbf{r}_k = \{r_{k,0}, r_{k,1}, r_{k,2}, \cdots, r_{k,N-1}\}$, $k = 0, 1, \cdots, M-1$. In this section we consider the special case where the cross-correlation of $\mathbf{r}_0$ and $\mathbf{r}_l$, $l = 1, \cdots, M-1$, is used in our decision statistic. The estimate of the cross-correlation between $\mathbf{r}_0$ and $\mathbf{r}_l$ is given by

$$\hat{R}_{\text{sp}}(l) \triangleq \frac{1}{N} \sum_{m=0}^{N-1} \left(r_{l,m} r_{0,m}^* \right), \quad 0 \leq l \leq M-1 \tag{5.12}$$

In view of (5.9) in the following we only use the real part of (5.12) in the our decision statistic. Let

$$\psi_{\text{sp}}(l) \triangleq \Re\{\hat{R}_{\text{sp}}(l)\}. \tag{5.13}$$

The proposed decision statistic is now defined by

$$T_{\text{sp}}(L) \triangleq \frac{\sum_{l=1}^{L} w_{\text{sp}}(l)\psi_{\text{sp}}(l)}{\psi_{\text{sp}}(0)} \underset{H_0}{\overset{H_1}{\gtrless}} \lambda, \tag{5.14}$$

where $L = M-1$, and $w_{\text{sp}}(l), l = 1, 2, \cdots, L$, are a set of coefficients selected to improve the system performance. It is clear that they must be chosen to ensure the constructive addition of the terms in (5.14) under the H_1 hypothesis. It is shown in Appendix G that in the low SNR regime, the optimal choice for $w_{\text{sp}}(l)$ (which maximizes the probability of detection for a fixed probability of false alarm), is given by $w_{\text{sp}}^{opt}(l) = \phi_{hh}^{RR}(l)$. We note that the values of $\phi_{hh}^{RR}(l)$ are known from the channel coefficient statistics given by (5.3). In particular, for the Clark's model we get $w_{\text{sp}}^{opt}(l) = J_0(\frac{2\pi D}{\lambda} l)$, for $l = 1, 2, \cdots, L$.

The system performance is evaluated in terms of probability of false alarm, P_0, and probability of detection,P_1, given by

$$P_\eta \triangleq Pr\left\{T_{\text{sp}}(L) > \lambda | H_\eta\right\} = Pr\left\{\sum_{l=1}^{L} w_{\text{sp}}(l)\psi_{\text{sp}}(l) > \lambda\psi_{\text{sp}}(0) | H_\eta\right\}. \tag{5.15}$$

In the following section we evaluate P_η for $\eta = 0, 1$. In order to calculate P_η, we first need to find the mean and covariance matrix of $\{\psi_{\rm sp}(l)\}_{l=0}^{L}$ given H_η.

5.4.2 Performance Analysis

To evaluate the false alarm and detection probabilities, we assume that the samples $r_{l,m}$ are Gaussian random variables. This assumption is true when the modulation scheme used by the PU is MPSK (see Appendix I) and it is approximately true for other modulation schemes with a large signal constellation. In addition, by the central limit theorem, for a large N, $\psi_{\rm sp}(l), l = 0, 1, \cdots, L$, are jointly Gaussian (the accuracy of these assumptions/approximations has been verified in Section 5.6). Therefore it is sufficient to evaluate the conditional mean of $\{\psi_{\rm sp}(l)\}_{l=0}^{L}$ and covariance of $\{\psi_{\rm sp}(l), \psi_{\rm sp}(k)\}_{l,k=0}^{L}$ given H_η, denoted by $m_{\rm sp}(l|H_\eta)$ and $\mathcal{C}_{\rm sp}(l, k|H_\eta)$, respectively. It is shown in Appendix F that

$$m_{\rm sp}(l|H_\eta) \triangleq E[\psi_{\rm sp}(l)|H_\eta] = \mathcal{A}_\eta(l) \tag{5.16}$$

and

$$\begin{aligned}\mathcal{C}_{\rm sp}(l, k|H_\eta) &\triangleq {\rm cov}[\psi_{\rm sp}(l)\psi_{\rm sp}(k)|H_\eta] \\ &= \frac{1}{2N}\left\{\mathcal{A}_\eta(l)\mathcal{A}_\eta(k) + \mathcal{A}_\eta(l-k)\mathcal{A}_\eta(0)\right\}\end{aligned} \tag{5.17}$$

For the case of Clark's model we get

$$m_{\rm sp}(l|H_0) = N_0\delta(l) \tag{5.18}$$

$$m_{\rm sp}(l|H_1) = J_0(zl)\varepsilon_s + N_0\delta(l) \tag{5.19}$$

$$\begin{aligned}\mathcal{C}_{\rm sp}(l, k|H_0) &= \frac{N_0^2}{2N}[\delta(l)\delta(k) + \delta(l-k)] \\ \mathcal{C}_{\rm sp}(l, k|H_1) &= \frac{1}{2N}\{\,[J_0(zl)\varepsilon_s + N_0\delta(l)][J_0(zk)\varepsilon_s + \\ & N_0\delta(k)] + [J_0(z(l-k))\varepsilon_s + N_0\delta(l-k)][\varepsilon_s + N_0]\,\}\end{aligned} \tag{5.20}$$

Let

$$Y_L \triangleq \sum_{l=1}^{L} w_{\rm sp}(l)\psi_{\rm sp}(l) - \lambda\psi_{\rm sp}(0). \tag{5.21}$$

Then $P_\eta = Pr(Y_L > 0|H_\eta)$. Since Y_L is Gaussian, P_η can be evaluated from the mean and variance of Y_L conditioned on H_η and denoted by $m_{Y_L|H_\eta}$, and $\sigma^2_{Y_L|H_\eta}$, respectively. Using (5.16), (5.17) and (5.21) we get

$$m_{Y_L|H_\eta} \triangleq E[Y_L|H_\eta] = \sum_{l=1}^{L} w_{\rm sp}(l)\mathcal{A}_\eta(l) - \lambda\mathcal{A}_\eta(0), \tag{5.22}$$

and,

$$\begin{aligned}\sigma^2_{Y_L|H_\eta} \triangleq {\rm var}(Y_L|H_\eta) = &\sum_{l=1}^{L}\sum_{k=1}^{L} w_{\rm sp}(l)w_{\rm sp}(k)\mathcal{C}_{\rm sp}(l,k|H_\eta) \\ &+ \lambda^2\, \mathcal{C}_{\rm sp}(0,0|H_\eta) - 2\lambda\sum_{l=1}^{L} w_{\rm sp}(l)\mathcal{C}_{\rm sp}(0,l|H_\eta).\end{aligned} \tag{5.23}$$

Finally, the detection and false alarm probabilities are given by

$$P_\eta = Q\left(-\frac{m_{Y_L|H_\eta}}{\sigma_{Y_L|H_\eta}}\right) \tag{5.24}$$

One can verify that the probability of false alarm does not depend on the noise power and is given by

$$P_0 = Q\left(\frac{\lambda\sqrt{N}}{\sqrt{\Omega^2_{\rm sp} + \lambda^2}}\right) \tag{5.25}$$

where

$$\Omega^2_{\rm sp} \triangleq \frac{1}{2}\sum_{l=1}^{L} w^2_{\rm sp}(l) \tag{5.26}$$

Therefore for a given probability of false alarm $P_0 = \epsilon$, the threshold λ_ϵ can be computed as

$$\lambda_\epsilon = \frac{\Omega_{\rm sp}Q^{-1}(\epsilon)}{\sqrt{N - [Q^{-1}(\epsilon)]^2}} \tag{5.27}$$

where $Q^{-1}(.)$ is the inverse of the Q function.

5.4.3 Decision Statistics: The General Case

In the previous section we considered a decision statistic based on the cross-correlation between the signals from antenna 0 and antennas $l = 1, 2, \cdots, L$. This can be extended to include the cross-correlation among all pairs of antennas. Let

$$\hat{R}_{\rm ge}(l) \triangleq \sum_{k=0}^{M-l-1} \frac{1}{N} \sum_{m=0}^{N-1} \left(r_{k+l,m} r_{k,m}^* \right) \qquad 0 \le l \le M-1 \tag{5.28}$$

denote the estimate of the *cumulative cross-correlation* of the received signals and let $\psi_{\rm ge}(l) \triangleq \Re\{\hat{R}_{\rm ge}(l)\}$. The new decision statistic is given by

$$T_{\rm ge}(L) \triangleq \frac{\sum_{l=1}^{L} w_{\rm ge}(l)\psi_{\rm ge}(l)}{\psi_{\rm ge}(0)} \underset{H_0}{\overset{H_1}{\gtrless}} \lambda \tag{5.29}$$

Clearly $L = M-1$ implies that the signals from all the antenna elements are used in the decision statistic; however, since the envelope of the correlation for two antenna elements is a decreasing function of their distance (see Fig. 5.1), we may choose $L < M-1$ when this correlation becomes negligible.

Derivation of false alarm and detection probabilities follow those in Section 5.4. In particular, let $m_{\rm ge}(l|H_\eta)$ and $\mathcal{C}_{\rm ge}(l,k|H_\eta)$, respectively, denote the mean and covariance of $\psi_{\rm ge}(l)$ given H_η. Then

$$m_{\rm ge}(l|H_\eta) \triangleq E[\psi_{\rm ge}(l)|H_\eta] = (M-l)\mathcal{A}_\eta(l) \tag{5.30}$$

and

$$\begin{aligned} \mathcal{C}_{\rm ge}(l,k|H_\eta) &\triangleq \mathrm{cov}[\psi_{\rm ge}(l)\psi_{\rm ge}(k)|H_\eta] \\ &= \frac{1}{2N} \sum_{p=0}^{M-l-1} \sum_{q=0}^{M-k-1} \mathcal{A}_\eta(p+l-q)\mathcal{A}_\eta(q+k-p) \\ &\quad + \mathcal{A}_\eta(l-k+p-q)\mathcal{A}_\eta(q-p) \end{aligned} \tag{5.31}$$

The proof of (5.30) and (5.31) is given in Appendix F. To find the probabilities of detection and false alarm, define

$$Y_L \triangleq \sum_{l=1}^{L} w_{\rm ge}(l)\psi_{\rm ge}(l) - \lambda\psi_{\rm ge}(0). \tag{5.32}$$

The conditional mean and variance of Y_L are given by

$$m_{Y_L|H_\eta} = \sum_{l=1}^{L}(M-l)w_{\text{ge}}(l)\mathcal{A}_\eta(l) - M\lambda\mathcal{A}_\eta(0) \tag{5.33}$$

$$\sigma^2_{Y_L|H_\eta} = \sum_{l=1}^{L}\sum_{k=1}^{L} w_{\text{ge}}(l)w_{\text{ge}}(k)\mathcal{C}_{\text{ge}}(l,k|H_\eta) + \lambda^2\mathcal{C}_{\text{ge}}(0,0|H_\eta) - 2\lambda\sum_{l=1}^{L} w_{\text{ge}}(l)\mathcal{C}_{\text{ge}}(0,l|H_\eta) \tag{5.34}$$

In the low SNR regime the optimal weighting coefficients are calculated in appendix G and are given by

$$w_{\text{ge}}^{opt}(l) = (M-l)\phi_{hh}^{RR}(l) \qquad 1 \le l \le L \tag{5.35}$$

Finally, P_η is given by (5.24).

5.5 Antenna Spacing

It is clear from (5.3) that, in general, the correlation of channel coefficients decreases with increases in inter-element spacing of the multi-antenna system. Since our decision statistics rely on this correlation, evidently closer spacing of the antenna elements would improve the performance of the proposed spectrum sensing technique. However, as discussed in [78, 79, 80, 81, 82], small inter-element spacing results in mutual coupling between the antennas. This coupling results in a parasitic correlation of the signals (for both transmitted signal and thermal noise components) among the antennas for spacings below one wavelength. According to [79, Fig. 5(b)] the correlation caused by the signal coupling, particularly for low SNR, does not change the channel correlation expressed in (5.3). However, the presence of noise correlation due to antenna coupling complicates the task of an autocorrelation-based spectrum sensing technique such as that proposed in this paper. Therefore we must ensure that noise sequences on different antenna elements remain uncorrelated by selecting an appropriate value for D. From [79, Fig. 5(b)],

it can be seen that noise coupling between adjacent antennas will be negligible for values of D satisfying $D/\lambda = 0.39, 0.91$ and $D/\lambda \geq 1$. On the other hand D must be chosen so that the correlation among channel coefficients, as described by (5.3) remains high. These two conditions together provide the guideline for selecting the values of D. In Fig. 5.1 we have plotted the channel correlation coefficients vs. the normalized inter-element spacing D/λ for different values of $\theta_{\max}$ (using (5.1) with $\theta = 0$). It can be seen that for the case of Clark's model where $\theta_{max} = \pi$, selecting $D/\lambda = 0.39$ or 0.91 leads to very low correlation among the channel coefficients. Therefore, we must consider $D/\lambda \geq 1$. In this case the maximum channel correlation is obtained for $D = 1.1\lambda$.

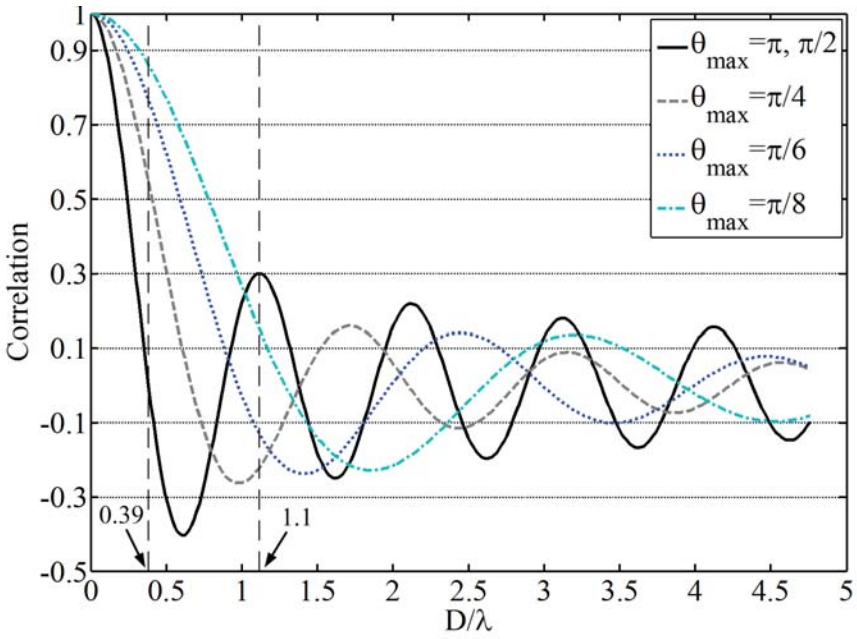

FIGURE 5.1. Correlation between channel coefficients vs. D/λ.

On the other hand when $\theta_{max} = \pi/k$ for $k \geq 4$, large correlation among channel coefficients can be achieved by choosing $D/\lambda = 0.39$. This will clearly enhance the performance of our proposed method. However, it should be noted that the distance between antenna elements separated by $2D$ will be 0.78λ. Unfortunately

in this case the noise processes in these two subsystems will be correlated due to the mutual coupling between the two antennas (see [79, Fig. 5(b)]). [1] To get around this problem, in the decision statistics in (5.14) or (5.29) we set the second coefficient ($w_{\rm sp}(2)$ or $w_{\rm ge}(2)$) to zero and ignore the correlations among antenna elements that are $2D$ apart. The simulation results verify that this does not degrade the system performance significantly.

5.6 Simulation and Numerical Results

In this section, we present our numerical results from simulation and analysis. First we verify the accuracy of the Gaussian assumptions in Section 5.4.2. Next we compare our performance results with several recently-published blind spectrum techniques.

The system model used in the simulation is based on the description of section 5.2. The channel coefficients are zero mean complex Gaussian random variables with covariance matrix based on (5.1) (with $\theta = 0$). The modulation systems considered are 16 PSK, and 16 and 256 QAM. The simulation results are obtained by repeating each experiment at least 10^4 times.

In Section 5.4.2 we assumed that the received signal samples $r_{l,m}$ are Gaussian. Under H_0, this assumption is always true. Under H_1, it is not hard to show that this assumption is true for MPSK or any other modulation scheme for which all the signals in the constellation are of equal magnitude. However, this assumption is approximately true for other modulation schemes. In Fig. 5.2 we show the ROC curves for 16 PSK, and 16 and 256 QAM. It can be seen that there is no significant difference between the numerical results obtained from analysis which rely on the Gaussian assumption and those obtained from simulation.

[1] Note that this will not be an issue for antennas separated by a distance of $3D$ or larger.

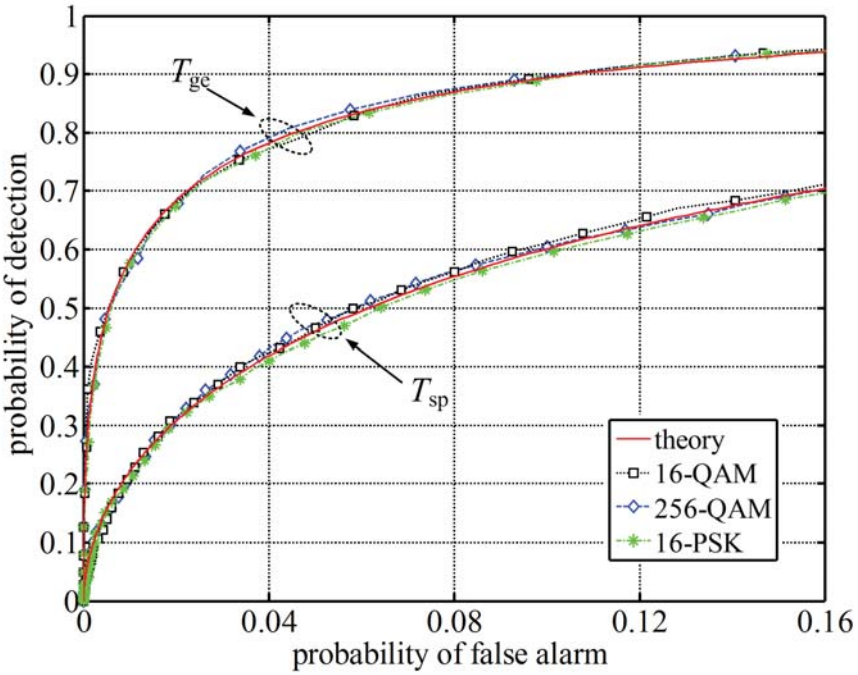

FIGURE 5.2. ROC curves for the the two proposed methods for $M = 4, L = 3, N = 1024$, SNR$= -12$, $\theta_{max} = \pi/4$.

Invoking the central limit theorem, we also assumed in Section 5.4.2 that the estimated correlations of the received signal is Gaussian. To verify the accuracy of this assumption for small values of N, in Fig. 5.3 we plot the detection probability P_1 vs. SNR obtained from simulation and analysis for $N = 10, 32, 64, 100$. It can be seen the Gaussian assumption is accurate even for values of N as small as 10.

Figs. 5.4 and 5.5 demonstrate the probability of detection P_1 vs. SNR for a fixed probability of false alarm ($P_0 = 0.1$) under Clark's model and a quarter-space model ($\theta_{\max} = \pi/4$), respectively. As expected, the performance of the system improves as the number of antennas (M) increases. For the special case considered in Section 5.4.1 we reach a point of diminishing return due to the fact that only the correlation between a single antenna and its neighbors are considered and that the paths correlations decrease with distance. On the other hand, for the general case in Section 5.4.3, the improvement is considerable even when increasing M from 6 to 8. In this case a larger M results in a larger number of antenna elements

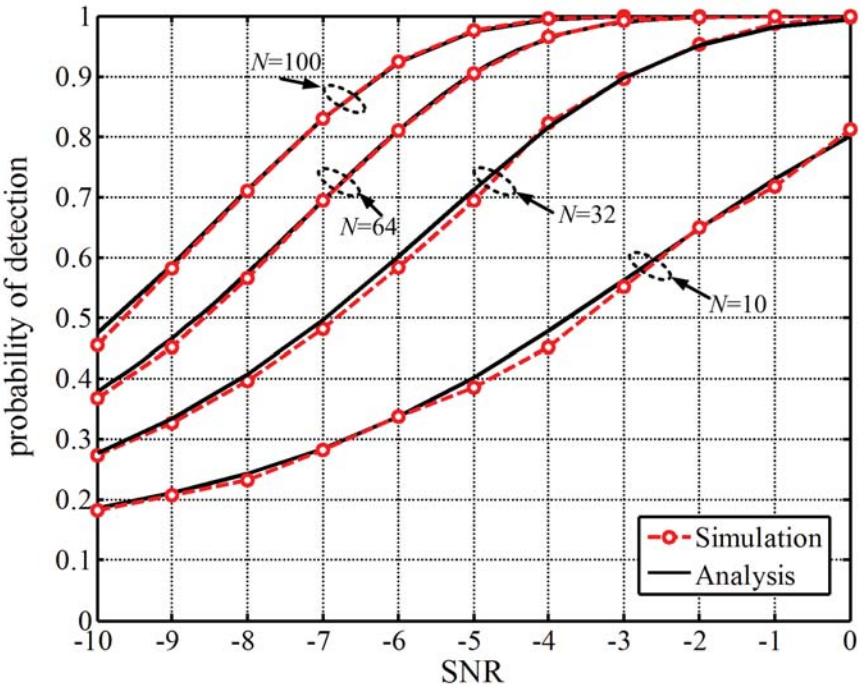

FIGURE 5.3. Probability of detection vs. SNR using $T_{\text{ge}}$for $M = 4, L = 3, P_0 = 0.1$, $\theta_{max} = \pi/4$ and different values of N.

with close distance and high path correlation resulting in improved performance. In particular we note that using $M = 8$ antenna elements, the proposed method can achieve a detection probability of 0.9 for $N = 1024$ samples and SNR values of -12 and -14 dB for the Clark and quarter-space models, respectively.

Fig. 5.6 shows the detection probability P_1 versus SNR for $M = 4$ antennas for different values of $\theta_{\max}$ using the test statistic for the general case. As expected (from (5.4)), Clark's model ($\theta_{max} = \pi$) and the half-space model ($\theta_{\max} = \pi/2$) have the same performance. However, smaller values of $\theta_{\max}$ result in significant improvements over Clark's model. In particular for $P_1 = 0.9$, $\theta_{\max} = \pi/16$ shows an improvement of more than 5 dB over $\theta_{\max} = \pi$.

In the remainder of this section we compare simulation results from our algorithms with those from three blind spectrum sensing techniques, namely the *arithmetic to geometric mean* (AGM) of [29], the *generalized likelihood Ratio Detector-3*

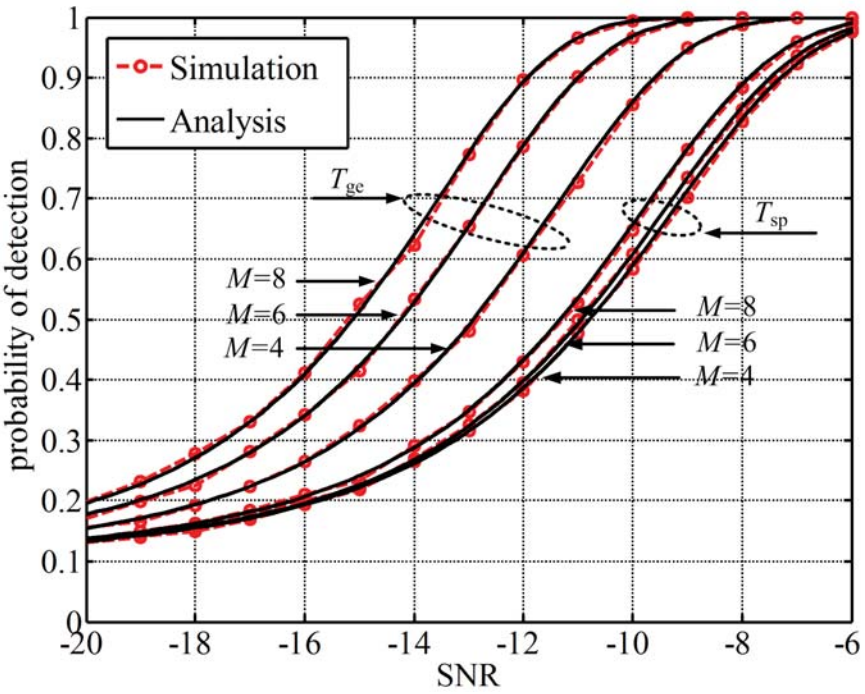

FIGURE 5.4. Detection probability vs. SNR for Clark or half-space model ($\theta_{max} = \pi$ or $\theta_{max} = \pi/2$), $P_0 = 0.1$, $N = 1024$ and $L = M - 1$.

(GLRD3) of [28], and the *maximum-to-minimum eigenvalue* (MME) of [21]. Interested readers can find a brief overview of these algorithms in Appendix H. We should point out that the GLRT method of [30] is identical to the GLRD3 of [28] and therefore has not been included in the comparisons.

Figs. 5.7 and 5.8 show the probability of detection versus SNR for $M = 4$, $P_0 = 0.1$ and $N = 1024$ under Clark's model and quarter-space model, respectively, and compare the results with from the three algorithms mentioned above. It can be seen that our proposed method outperforms all the other algorithms. In particular for $P_1 = 0.9$, in the case of Clark's model the proposed method ($T_{\text{ge}}(L)$) outperforms the other methods by 2.8 dB . In the case of quarter-space model the improvement is 2.7 dB over AGM and 3.7 dB over GLRD3.

A remark is in order here. Although the three algorithms AGM, GLRD3 and MME do not seem to depend on the channel paths correlations, the results in Figs.

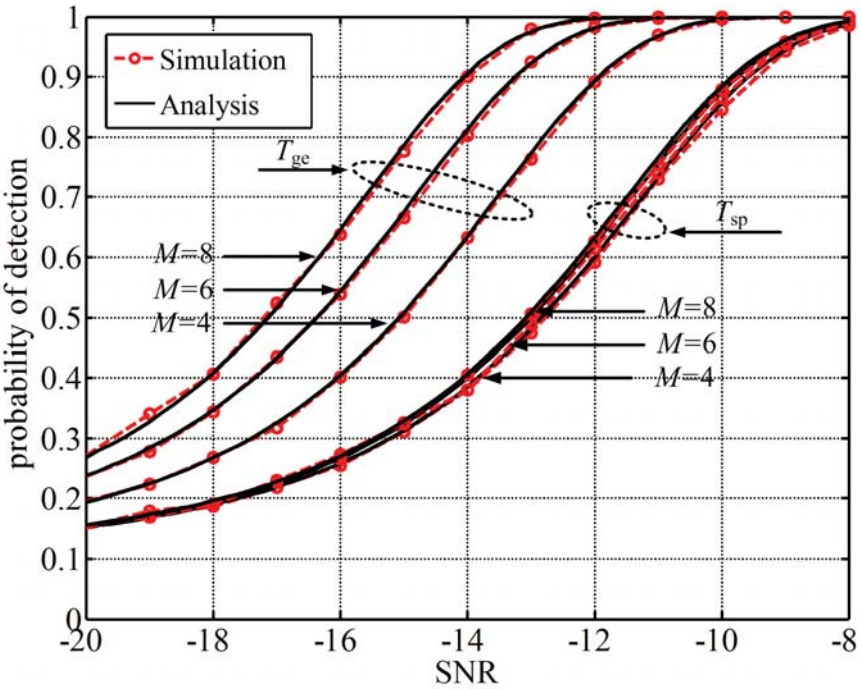

FIGURE 5.5. Detection probability vs. SNR for quarter-space model ($\theta_{max} = \pi/4$) with $P_0 = 0.1$, $N = 1024$ and $L = M - 1$.

5.7 and 5.8 show otherwise. This is due to the fact that the paths correlations depend on the beamwidth $\theta_{\max}$. As a result the correlations between the rows of $\mathbf{r}$ in (6.35) vary with $\theta_{\max}$. Therefore the matrix $\mathcal{R}_\eta$ in (6.36) and its eigenvalues also depend on $\theta_{\max}$. Consequently, the performance of these algorithms also changes slightly depending on the beamwidth $\theta_{\max}$.

Finally in Figs. 5.9 and 5.10 we show the complementary ROC for $M = 4$ and $N = 64$ when $SNR = 0$ dB and $SNR = -5$ dB under Clark's model and quarter-space model, respectively, and compare the results to the three algorithms in [29, 28, 21].

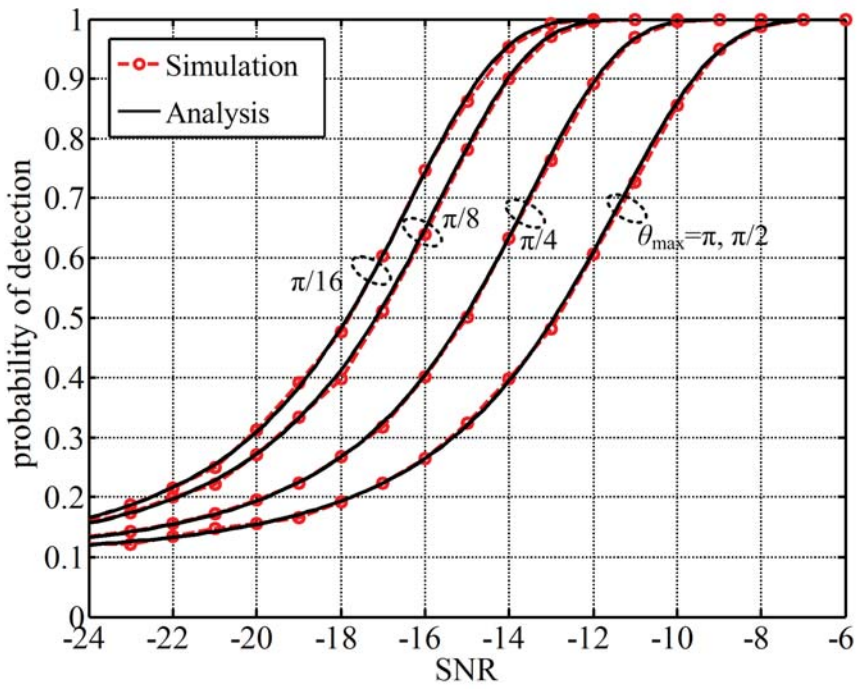

FIGURE 5.6. Detection probability vs. SNR using $T_{\text{ge}}(L)$ for different values of $\theta_{\max}$, with $M = 4$, $L = 3$, $P_0 = 0.1, N = 1024$.

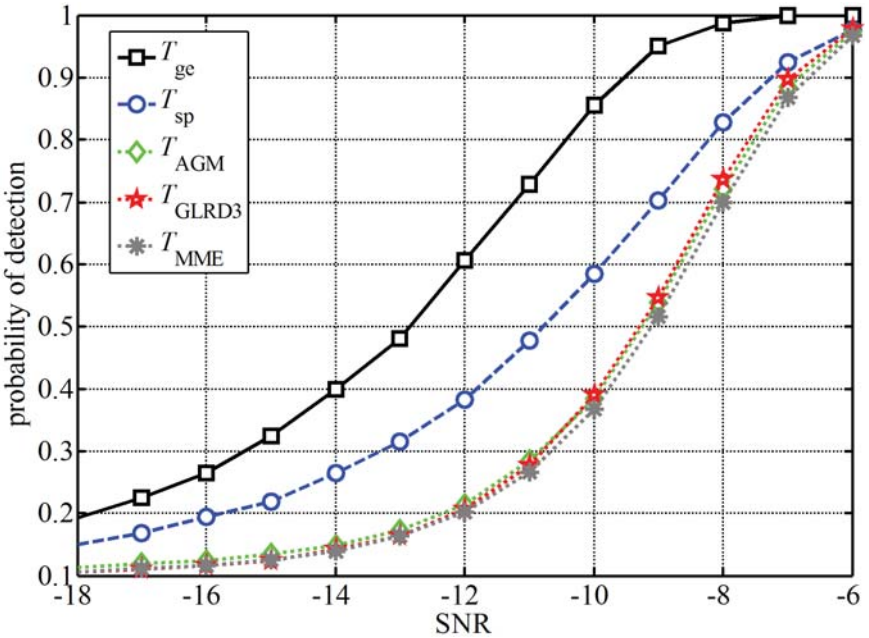

FIGURE 5.7. Comparison of the performance of the proposed methods with three other blind sensing techniques for $M = 4$, $L = 3$, $P_0 = 0.1, N = 1024$ and Clark's Model.

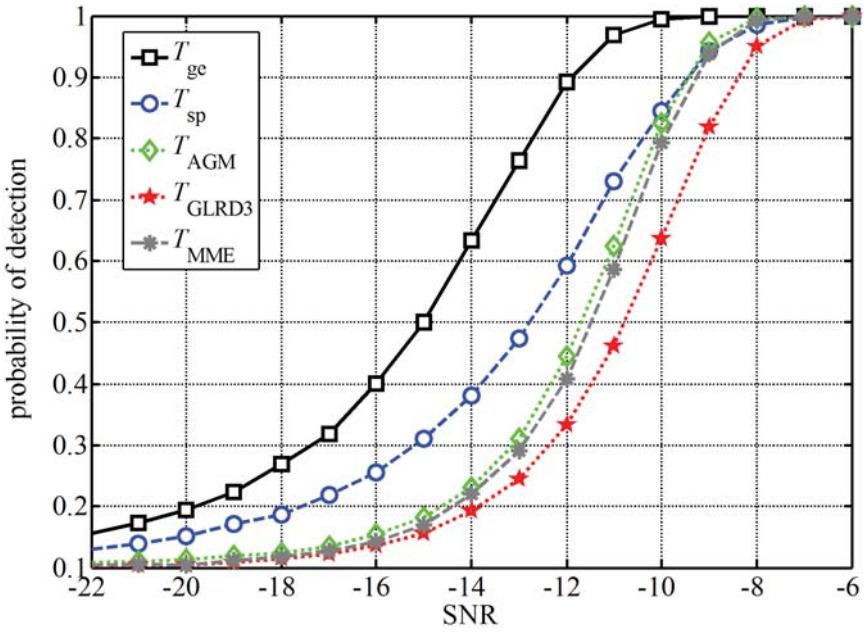

FIGURE 5.8. Comparison of the performance of the proposed methods with three other blind sensing techniques for $M = 4$, $L = 3$, $P_0 = 0.1, N = 1024$ and quarter-space model.

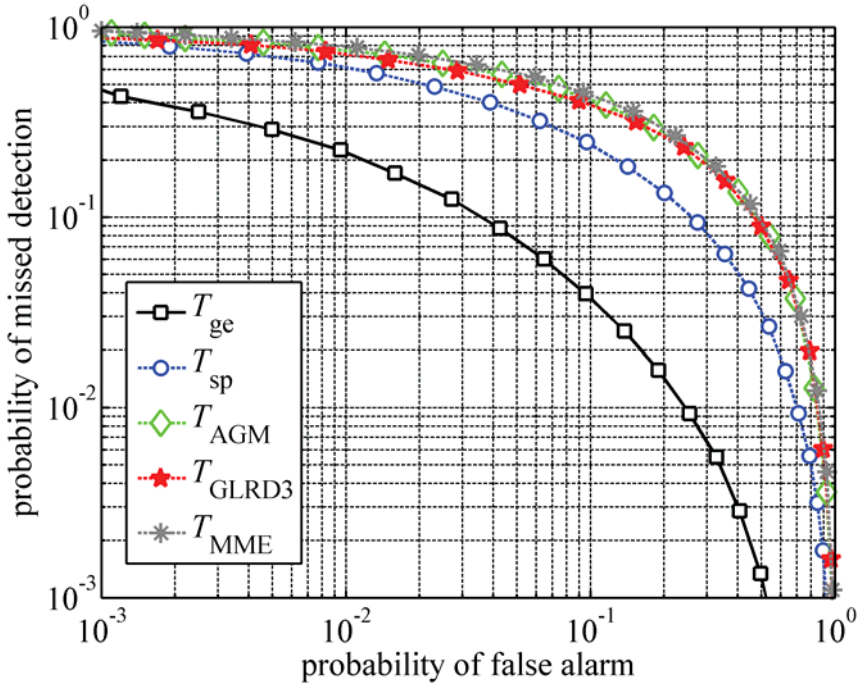

FIGURE 5.9. Comparison of the complementary ROC curves for the proposed method and three other blind sensing techniques for $M = 4$, $L = 3$, $SNR = 0$ dB, $N = 64$ and Clark's Model.

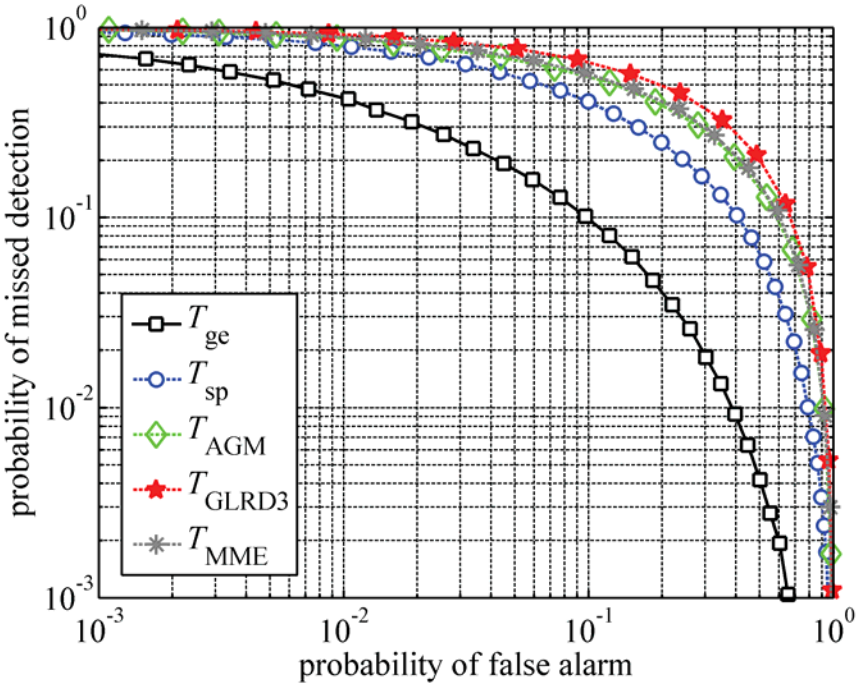

FIGURE 5.10. Comparison of the complementary ROC curves for the proposed method and three other blind sensing techniques for $M = 4$, $L = 3$, $SNR = -5$ dB, $N = 64$ and quarter-space model.

Chapter 6
Conclusion

The ever increasing demand for wireless services and the static spectrum allocation led to spectrum scarcity in wireless communications. On the other side, studies have shown that most of the allocated radio frequencies are under-utilized. Recently, CRs have been introduced as a potential solution to this problem. The CR network has to be able to detect the presence of the PUs signals, so as to avoid interfering with it. Therefore, SS plays a crucial role in the successful deployment of CRs.

In Chapter 2, a SS technique is proposed for signaling schemes with controlled intersymbol interference in the transmitter. Examples include correlative coding or partial response signaling techniques which have an inherent memory in the transmitted signal. A decision statistic is introduced based on the autocorrelation of the received signal and its performance in terms of the probabilities of false alarm and detection is evaluated for AWGN and Rayleigh fading channels. It is shown that the proposed method is a constant false alarm detector. The numerical results from simulation and analysis are presented to demonstrates the accuracy of our analysis.

In Chapter 3, we consider the effect of co-channel interference on a desired signal by a careful examination of the samples at the output of the matched filter receiver. We show that the timing offset between the interference and the desired signals may results in the correlation of adjacent sample. We evaluate the bit error probability resulting from CCI as well as the distribution of the total number of errors in a packet. It is shown that the bit error probability is largest when the interference and the desired signals are synchronized. Our results can be employed

for more accurate evaluation of CCI effects and in developing techniques for CCI mitigation such as designing precoders or forward error correction codes.

In Chapter 4, we introduce a novel decision statistic for spectrum monitoring based on the receiver error count. Detection and false alarm probabilities of this decision statistic are evaluated from analysis and simulation. Using two Markov chain models we derive closed form formulas for channel utilization of the secondary users and detection delay of primary users. The limits of channel utilization and detection delay under the proposed method are derived and an optimization problem is solved to maximize channel utilization with a constraint on detection delay. Numerical results are presented from analysis and simulation which show that the hybrid spectrum sensing/spectrum monitoring technique significantly outperforms spectrum sensing alone.

And in Chapter 5, we present a blind spectrum sensing technique for cognitive radios equipped with a multi-antenna systems. The decision statistic is based on an estimate of the cross-correlation of the signals received at different antennas which is a result of the correlation of the channel path coefficients from the primary user transmitter to different elements in the antenna array. The performance of the proposed methods is evaluated using an asymptotic analysis and compared with simulation results. It is shown that the proposed methods outperform several recently-proposed techniques for blind spectrum sensing with multi-antenna systems.

References

[1] J. Yang, "Spatial channel characterization for cognitive radios," MS Thesis, UC Berkeley, 2004.

[2] D. Cabric, S. Mishra, and R. Brodersen, "Implementation issues in spectrum sensing for cognitive radios," in *Signals, Systems and Computers, 2004. Conference Record of the Thirty-Eighth Asilomar Conference on*, vol. 1, nov. 2004, pp. 772 – 776 Vol.1.

[3] F. N. 03-322, "Notice of proposed rule making and order," *Federal Communications Commission*, Dec. 2003.

[4] J. Mitola, "Cognitive radio: An integrated agent architecture for software defined radio," Doctor of Technology Dissertation, Royal Inst. of Technology, Stockholm, Sweden, 2000.

[5] "Ieee draft standard for information technology -telecommunications and information exchange between systems - wireless regional area networks (wran) - specific requirements - part 22: Cognitive wireless ran medium access control (mac) and physical layer (phy) specifications: Policies and procedures for operation in the tv bands," *IEEE P802.22/D1.0, December 2010*, pp. 1 –598, 20 2010.

[6] S. Haykin, "Cognitive radio: brain-empowered wireless communications," *IEEE J. Sel. Areas Commun.*, vol. 23, no. 2, pp. 201–220, 2005.

[7] C. Cordeiro, K. Challapali, D. Birru, and N. Sai Shankar, "Ieee 802.22: the first worldwide wireless standard based on cognitive radios," in *New Frontiers in Dynamic Spectrum Access Networks, 2005. DySPAN 2005. 2005 First IEEE International Symposium on*, nov. 2005, pp. 328 –337.

[8] B. Wang and K. Liu, "Advances in cognitive radio networks: A survey," *Selected Topics in Signal Processing, IEEE Journal of*, vol. 5, no. 1, pp. 5 –23, feb. 2011.

[9] I. F. Akyildiz, W.-Y. Lee, M. C. Vuran, and S. Mohanty, "Next generation/dynamic spectrum access/cognitive radio wireless networks: A survey," *Computer Networks*, vol. 50, no. 13, pp. 2127–2159, 2006.

[10] E. D. N. 02-135, "Spectrum Policy Task Force Report," *Federal Communications Commission*, 2002.

[11] Z. Quan, S. Shellhammer, W. Zhang, and A. Sayed, "Spectrum sensing by cognitive radios at very low snr," in *Global Telecommunications Conference, 2009. GLOBECOM 2009. IEEE*, 30 2009-dec. 4 2009, pp. 1 –6.

[12] T. Yucek and H. Arslan, "A survey of spectrum sensing algorithms for cognitive radio applications," *Communications Surveys Tutorials, IEEE*, vol. 11, no. 1, pp. 116 –130, 1st quarter 2009.

[13] A. V. Dandawaté and G. B. Giannakis, "Statistical tests for presence of cyclostationarity," *IEEE Trans. Signal Process.*, vol. 42, no. 9, pp. 2355–2369, 1994.

[14] W. A. Gardner and C. M. Spooner, "Signal interception: performance advantages of cyclic-feature detectors," *IEEE Trans. Commun.*, vol. 40, no. 1, pp. 149–159, 1992.

[15] J. Lundén, V. Koivunen, A. Huttunen, and H. V. Poor, "Spectrum sensing in cognitive radios based on multiple cyclic frequencies," in *CrownCom 2007*, Orlando, FL, 2007.

[16] J. Lunden, V. Koivunen, A. Huttunen, and H. Poor, "Collaborative cyclostationary spectrum sensing for cognitive radio systems," *Signal Processing, IEEE Transactions on*, vol. 57, no. 11, pp. 4182 –4195, 2009.

[17] J. Lunden, S. Kassam, and V. Koivunen, "Robust nonparametric cyclic correlation-based spectrum sensing for cognitive radio," *Signal Processing, IEEE Transactions on*, vol. 58, no. 1, pp. 38 –52, 2010.

[18] H. Urkowitz, "Energy detection of unknown deterministic signals," *Proc. IEEE*, vol. 55, no. 4, pp. 523–531, 1967.

[19] F. F. Digham, M. S. Alouini, and M. K. Simon, "On the energy detection of unknown signals over fading channels," *IEEE Trans. on Commun.*, vol. 55, no. 1, pp. 21–24, 2007.

[20] R. Tandra and A. Sahai, "SNR walls for signal detection," *IEEE J. Sel. Topics Signal Process.*, vol. 2, no. 1, pp. 4–17, 2008.

[21] T. J. Lim, R. Zhang, Y. C. Liang, and Y. Zeng, "Glrt-based spectrum sensing for cognitive radio," in *Global Telecommunications Conference, 2008. IEEE GLOBECOM 2008. IEEE*, Nov. 30-dec. 4 2008, pp. 1 –5.

[22] S. Chaudhari, V. Koivunen, and H. Poor, "Autocorrelation-based decentralized sequential detection of ofdm signals in cognitive radios," *Signal Processing, IEEE Transactions on*, vol. 57, no. 7, pp. 2690 –2700, july 2009.

[23] ——, "Distributed autocorrelation-based sequential detection of ofdm signals in cognitive radios," in *Cognitive Radio Oriented Wireless Networks and Communications, 2008. CrownCom 2008. 3rd International Conference on*, may 2008, pp. 1 –6.

[24] Y. Zeng and Y.-C. Liang, "Covariance based signal detections for cognitive radio," in *IEEE DySPAN*, Dublin, Ireland, 2007, pp. 202–207.

[25] M. Naraghi-Pour and T. Ikuma, "Autocorrelation-based spectrum sensing for cognitive radios," *Vehicular Technology, IEEE Transactions on*, vol. 59, no. 2, pp. 718 –733, 2010.

[26] ——, "Diversity techniques for spectrum sensing in fading environments," in *Military Communications Conference, 2008. MILCOM 2008. IEEE*, nov. 2008, pp. 1 –7.

[27] Y. Zeng and Y.-C. Liang, "Spectrum-sensing algorithms for cognitive radio based on statistical covariances," *Vehicular Technology, IEEE Transactions on*, vol. 58, no. 4, pp. 1804 –1815, May 2009.

[28] A. Taherpour, M. Nasiri-Kenari, and S. Gazor, "Multiple antenna spectrum sensing in cognitive radios," *Wireless Communications, IEEE Transactions on*, vol. 9, no. 2, pp. 814 –823, feb. 2010.

[29] R. Zhang, T. Lim, Y.-C. Liang, and Y. Zeng, "Multi-antenna based spectrum sensing for cognitive radios: A GLRT approach," *Communications, IEEE Transactions on*, vol. 58, no. 1, pp. 84 –88, jan. 2010.

[30] P. Wang, J. Fang, N. Han, and H. Li, "Multiantenna-assisted spectrum sensing for cognitive radio," *Vehicular Technology, IEEE Transactions on*, vol. 59, no. 4, pp. 1791 –1800, May 2010.

[31] A. Parsa, A. Gohari, and A. Sahai, "Exploiting interference diversity for event-based spectrum sensing," oct. 2008, pp. 1 –12.

[32] G. L. Stuber, "Principles of mobile communication," New York, 2002.

[33] P. Kabal and S. Pasupathy, "Partial-response signaling," *Communications, IEEE Transactions on*, vol. 23, no. 9, pp. 921 – 934, sep 1975.

[34] J. G. Proakis, "Digital communications, fourth edition," McGraw-Hill Higher Education, 2001.

[35] S. Parsaeefard and A. Sharafat, "Robust worst-case interference control in underlay cognitive radio networks," *Vehicular Technology, IEEE Transactions on*, vol. 61, no. 8, pp. 3731 –3745, oct. 2012.

[36] T. Vanhatupa, M. Hnnikinen, and T. D. Hmlinen, "Evaluation of throughput estimation models and algorithms for wlan frequency planning," *Computer Networks*, vol. 51, no. 11, pp. 3110 – 3124, 2007. [Online]. Available: http://www.sciencedirect.com/science/article/pii/S1389128607000114

[37] P. Tiwary, N. Maskey, S. Khakurel, and G. Sachdeva, "Effects of co-channel interference in wlan and cognitive radio based approach to minimize it," in *Advances in Recent Technologies in Communication and Computing (ARTCom), 2010 International Conference on*, oct. 2010, pp. 158 –160.

[38] G. Fang, E. Dutkiewicz, K. Yu, R. Vesilo, and Y. Yu, "Distributed inter-network interference coordination for wireless body area networks," in *GLOBECOM 2010, 2010 IEEE Global Telecommunications Conference*, dec. 2010, pp. 1 –5.

[39] A. Abbosh and D. Thiel, "Performance of mimo-based wireless sensor networks with cochannel interference," in *Intelligent Sensors, Sensor Networks and Information Processing Conference, 2005. Proceedings of the 2005 International Conference on*, dec. 2005, pp. 115 – 119.

[40] R. Muammar and S. Gupta, "Cochannel interference in high-capacity mobile radio systems," *Communications, IEEE Transactions on*, vol. 30, no. 8, pp. 1973 – 1978, aug 1982.

[41] R. Muammar, "Co-channel interference in microcellular mobile radio system," in *Vehicular Technology Conference, 1991. Gateway to the Future Technology in Motion., 41st IEEE*, may 1991, pp. 198 –203.

[42] A. Attar, V. Krishnamurthy, and O. Gharehshiran, "Interference management using cognitive base-stations for umts lte," *Communications Magazine, IEEE*, vol. 49, no. 8, pp. 152 –159, august 2011.

[43] Y. Wen, S. Loyka, and A. Yongacoglu, "Asymptotic analysis of interference in cognitive radio networks," *Selected Areas in Communications, IEEE Journal on*, vol. 30, no. 10, pp. 2040 –2052, november 2012.

[44] Y.-U. Jang, "Performance analysis of cognitive radio networks based on sensing and secondary-to-primary interference," *Signal Processing, IEEE Transactions on*, vol. 59, no. 11, pp. 5663 –5668, nov. 2011.

[45] M. Elalem, L. Zhao, and Z. Liao, "Interference mitigation using power control in cognitive radio networks," in *Vehicular Technology Conference (VTC 2010-Spring), 2010 IEEE 71st*, may 2010, pp. 1 –5.

[46] D. Hu and S. Mao, "Co-channel and adjacent channel interference mitigation in cognitive radio networks," in *MILITARY COMMUNICATIONS CONFERENCE, 2011 - MILCOM 2011*, nov. 2011, pp. 13 –18.

[47] A. Giorgetti, "Interference mitigation technique by sequence design in uwb cognitive radio," in *Applied Sciences in Biomedical and Communication Technologies (ISABEL), 2010 3rd International Symposium on*, nov. 2010, pp. 1 –5.

[48] S.-M. Cheng, W. C. Ao, and K.-C. Chen, "Efficiency of a cognitive radio link with opportunistic interference mitigation," *Wireless Communications, IEEE Transactions on*, vol. 10, no. 6, pp. 1715 –1720, june 2011.

[49] M. Orooji, E. Soltanmohammadi, and M. Naraghi-Pour, "Performance analysis of spectrum monitoring for cognitive radios," *To appear MILITARY COMMUNICATIONS CONFERENCE, 2012 - MILCOM 2012*, Oct 2012.

[50] E. Soltanmohammadi, M. Orooji, and M. Naraghi-Pour, "Spectrum monitoring for cognitive radios in rayleigh fading channel," *To appear MILITARY COMMUNICATIONS CONFERENCE, 2012 - MILCOM 2012*, Oct 2012.

[51] D. Rawat and D. Popescu, "Joint precoder and power adaptation for cognitive radios in interference systems," in *Performance Computing and Communications Conference (IPCCC), 2009 IEEE 28th International*, dec. 2009, pp. 425 –430.

[52] K.-J. Lee, H. Sung, and I. Lee, "Linear precoder designs for cognitive radio multiuser mimo downlink systems," in *Communications (ICC), 2011 IEEE International Conference on*, june 2011, pp. 1 –5.

[53] P. Billingsley, *Probability and Measure (Third ed.)*. New York: John Wiley & Sons, 1995.

[54] H. Cramer, "On the composition of elementary errors, second paper: Statistical applications," *Skand. Aktuarietidskrift*, vol. 11, pp. 13–74, 1928.

[55] R. von Mises, *Wahrscheinliehkeitsrechnung und ihre Anwendung in der Statistik und Theoretischen Physik*. F. Duticke, Ed. Vienna, Austria: Leipzig, 1931.

[56] Y.-C. Liang, Y. Zeng, E. Peh, and A. T. Hoang, "Sensing-throughput tradeoff for cognitive radio networks," *Wireless Communications, IEEE Transactions on*, vol. 7, no. 4, pp. 1326 –1337, april 2008.

[57] S. Zarrin and T. J. Lim, "Throughput-sensing tradeoff of cognitive radio networks based on quickest sensing," in *Communications (ICC), 2011 IEEE International Conference on*, june 2011, pp. 1 –5.

[58] S. Stotas and A. Nallanathan, "Overcoming the sensing-throughput tradeoff in cognitive radio networks," in *Communications (ICC), 2010 IEEE International Conference on*, may 2010, pp. 1 –5.

[59] A. Hoang, Y.-C. Liang, and Y. Zeng, "Adaptive joint scheduling of spectrum sensing and data transmission in cognitive radio networks," *Communications, IEEE Transactions on*, vol. 58, no. 1, pp. 235 –246, january 2010.

[60] Q. Zhao, S. Geirhofer, L. Tong, and B. Sadler, "Opportunistic spectrum access via periodic channel sensing," *Signal Processing, IEEE Transactions on*, vol. 56, no. 2, pp. 785 –796, feb. 2008.

[61] S. W. Boyd, J. M. Frye, M. B. Pursley, and T. C. Royster IV, "Spectrum monitoring during reception in dynamic spectrum access cognitive radio networks," *Communications, IEEE Transactions on*, vol. 60, no. 2, pp. 547 –558, february 2012.

[62] A. Leon-Garcia and I. Widjaja, *Communication Networks: Fundamental Concepts and Key Architectures*, 2nd ed. New York: McGraw Hill, 2004.

[63] G. Castagnoli, S. Brauer, and M. Herrmann, "Optimization of cyclic redundancy-check codes with 24 and 32 parity bits," *Communications, IEEE Transactions on*, vol. 41, no. 6, pp. 883 –892, jun 1993.

[64] P. Koopman, "32-bit cyclic redundancy codes for internet applications," in *Dependable Systems and Networks, 2002. DSN 2002. Proceedings. International Conference on*, 2002, pp. 459 – 468.

[65] K. Witzke and C. Leung, "A comparison of some error detecting crc code standards," *Communications, IEEE Transactions on*, vol. 33, no. 9, pp. 996 – 998, sep 1985.

[66] S. M. Ross, *Introduction to Probability Models*, 10th ed. United State of America: Academic Press, 2010.

[67] S. B. Wicker, *Error Control Systems for Digital Communication and Storage*, 1st ed. Upper Saddle River, New Jersey: Prentice-Hall, 1995.

[68] W.-Y. Lee, "Effects on correlation between two mobile radio base-station antennas," *Vehicular Technology, IEEE Transactions on*, vol. 22, no. 4, pp. 130 – 140, nov. 1973.

[69] J. Salz and J. Winters, "Effect of fading correlation on adaptive arrays in digital mobile radio," *Vehicular Technology, IEEE Transactions on*, vol. 43, no. 4, pp. 1049 –1057, Nov. 1994.

[70] D.-S. Shiu, G. Foschini, M. Gans, and J. Kahn, "Fading correlation and its effect on the capacity of multielement antenna systems," *Communications, IEEE Transactions on*, vol. 48, no. 3, pp. 502 –513, mar. 2000.

[71] D. Chizhik, G. Foschini, M. Gans, and R. Valenzuela, "Keyholes, correlations, and capacities of multielement transmit and receive antennas," *Wireless Communications, IEEE Transactions on*, vol. 1, no. 2, pp. 361 –368, apr 2002.

[72] H. Xu, D. Chizhik, H. Huang, and R. Valenzuela, "A generalized space-time multiple-input multiple-output (mimo) channel model," *Wireless Communications, IEEE Transactions on*, vol. 3, no. 3, pp. 966 – 975, may 2004.

[73] C. Stevenson, G. Chouinard, Z. Lei, W. Hu, S. Shellhammer, and W. Caldwell, "Ieee 802.22: The first cognitive radio wireless regional area network standard," *Communications Magazine, IEEE*, vol. 47, no. 1, pp. 130 –138, january 2009.

[74] H. Bahrami and T. Le-Ngoc, "MIMO precoder designs for frequency-selective fading channels using spatial and path correlation," *Vehicular Technology, IEEE Transactions on*, vol. 57, no. 6, pp. 3441 –3452, nov. 2008.

[75] S. Kim, J. Lee, H. Wang, and D. Hong, "Sensing performance of energy detector with correlated multiple antennas," *Signal Processing Letters, IEEE*, vol. 16, no. 8, pp. 671 –674, aug. 2009.

[76] R. H. Clarke, "A statistical theory of mobile-radio reception," *Bell Labs Technical Journal*, vol. 4, pp. 957 –1000, 1968.

[77] W. C. Jakes, "Microwave mobile communications," New York, 1994.

[78] S. Krusevac, P. Rapajic, and R. Kennedy, "Channel capacity of multi-antenna communication systems with closely spaced antenna elements," in *Personal, Indoor and Mobile Radio Communications, 2005. PIMRC 2005. IEEE 16th International Symposium on*, vol. 4, sept. 2005, pp. 2366 –2370 Vol. 4.

[79] C. Domizioli, B. Hughes, K. Gard, and G. Lazzi, "Noise correlation in compact diversity receivers," *Communications, IEEE Transactions on*, vol. 58, no. 5, pp. 1426 –1436, May 2010.

[80] S. Krusevac and P. Rapajic, "Channel capacity of mimo systems with closely spaced terminated antennas," in *Information Theory, 2007. ISIT 2007. IEEE International Symposium on*, june 2007, pp. 1076 –1080.

[81] J. Wallace and M. Jensen, "Mutual coupling in mimo wireless systems: a rigorous network theory analysis," *Wireless Communications, IEEE Transactions on*, vol. 3, no. 4, pp. 1317 – 1325, july 2004.

[82] T. Svantesson and A. Ranheim, "Mutual coupling effects on the capacity of multielement antenna systems," in *Acoustics, Speech, and Signal Processing, 2001. Proceedings. (ICASSP '01). 2001 IEEE International Conference on*, vol. 4, may 2001, pp. 2485 –2488 vol.4.

[83] P. Janssen and P. Stoica, "On the expectation of the product of four matrix-valued gaussian random variables," *Automatic Control, IEEE Transactions on*, vol. 33, no. 9, pp. 867 –870, sep. 1988.

[84] R. A. Horn and C. R. Johnson, *Matrix Analysis*. Cambridge University Press, 1990.

Appendix A: Values of $\Gamma_{\hat{\xi}|\eta}$ and $\Gamma_{\hat{\chi}|\eta}$

Janssen and Stocia proved in [83] that if a, b, c and d are four Gaussian random variables, the expectation of the product of that four Gaussian random variables holds in the following equation.

$$\begin{aligned} E[abcd] &= E[ab]E[cd] + E[ac]E[bd] \\ &\quad + E[ad]E[bc] - 2E[a]E[b]E[c]E[d] \end{aligned} \tag{6.1}$$

Also it can be seen that,

$$\begin{aligned} &\Phi_{rr}^{(\eta)}(i)\Phi_{rr}^{(\eta)}(k) + \Phi_{rr}^{(\eta)}(-i)\Phi_{rr}^{(\eta)}(-k) \\ &= 2\xi^{(\eta)}(i)\xi^{(\eta)}(k) - 2\chi^{(\eta)}(i)\chi^{(\eta)}(k). \end{aligned} \tag{6.2}$$

Using (6.1) and after some manipulations for low SNR-regime, one can drive (6.3) and (6.4),

$$\begin{aligned} &\gamma_{\hat{\xi}|\eta}(i,k) \triangleq \Omega_i^{(R)}\Omega_k^{(R)} E\left[\ \hat{\xi}(i)\hat{\xi}(k)\Big|\ H_\eta\right] \\ &= \frac{\Omega_i^{(R)}\Omega_k^{(R)}}{4(N-i)(N-k)} \sum_{n=0}^{N-i-1}\sum_{m=0}^{N-k-1} \\ &\quad + E[r_{n+i}r_n^* r_{m+k}r_m^* \mid H_\eta] + E[r_{n+i}^* r_n r_{m+k}r_m^* \mid H_\eta] \\ &\quad + E[r_{n+i}r_n^* r_{m+k}^* r_m \mid H_\eta] + E[r_{n+i}^* r_n r_{m+k}^* r_m \mid H_\eta] \\ &= \frac{\Omega_i^{(R)}\Omega_k^{(R)}}{4(N-i)(N-k)} \sum_{n=0}^{N-i-1}\sum_{m=0}^{N-k-1} \Phi_{rr}^{(\eta)}(i)\Phi_{rr}^{(\eta)}(k) \\ &+ \Phi_{rr}^{(\eta)}(n+i-m)\Phi_{rr}^{(\eta)}(m+k-n) + \Phi_{rr}^{(\eta)}(i)\Phi_{rr}^{(\eta)}(-k) \\ &+ \Phi_{rr}^{(\eta)}(n+i-m-k)\Phi_{rr}^{(\eta)}(m-n) + \Phi_{rr}^{(\eta)}(-i)\Phi_{rr}^{(\eta)}(k) \\ &+ \Phi_{rr}^{(\eta)}(-n-i+m+k)\Phi_{rr}^{(\eta)}(-m+n) + \Phi_{rr}^{(\eta)}(-i)\Phi_{rr}^{(\eta)}(-k) \\ &+ \Phi_{rr}^{(\eta)}(-n-i+m)\Phi_{rr}^{(\eta)}(-m-k+n) \\ &= \Omega_i^{(R)}\Omega_k^{(R)}\xi^{(\eta)}(i)\xi^{(\eta)}(k) + \frac{\Omega_i^{(R)}\Omega_k^{(R)}}{2(N-i)(N-k)} \sum_{n=0}^{N-i-1}\sum_{m=0}^{N-k-1} \\ &\quad \xi^{(\eta)}(n+i-m)\xi^{(\eta)}(m+k-n) \\ &+ \xi^{(\eta)}(n+i-m-k)\xi^{(\eta)}(n-m) \\ &- \chi^{(\eta)}(n+i-m)\chi^{(\eta)}(m+k-n) \\ &- \chi^{(\eta)}(n+i-m-k)\chi^{(\eta)}(m-n) \end{aligned} \tag{6.3}$$

Using the same approach one can show that,

$$\gamma_{\hat{\chi}|\eta}(i,k) \triangleq \Omega_i^{(I)}\Omega_k^{(I)} E\left[\ \hat{\chi}(i)\hat{\chi}(k)|\, H_\eta\right] \tag{6.4}$$

$$= \Omega_i^{(I)}\Omega_k^{(I)}\chi^{(\eta)}(i)\chi^{(\eta)}(k) + \frac{\Omega_i^{(I)}\Omega_k^{(I)}}{2(N-i)(N-k)} \sum_{n=0}^{N-i-1}\sum_{m=0}^{N-k-1}$$

$$\xi^{(\eta)}(n+i-m)\xi^{(\eta)}(m+k-n)$$

$$-\xi^{(\eta)}(n+i-m-k)\xi^{(\eta)}(n-m)$$

$$-\chi^{(\eta)}(n+i-m)\chi^{(\eta)}(m+k-n)$$

$$+\chi^{(\eta)}(n+i-m-k)\chi^{(\eta)}(m-n)$$

Appendix B:
Inverse of the matrix $(I - G)$

One can verify that the eigenvalues of G, obtained from the solutions of the characteristic equation $\det(\lambda I - G) = 0$, are given by

$$\lambda_k = [(1-\hat{p}_d)(1-p_d)^{K_M}]^{1/(K_S+K_M)} \exp(\frac{2\pi jk}{K_S+K_M}) \tag{6.5}$$

where $0 \leq k < K_S + K_M$, and $j = \sqrt{-1}$. It can be seen that if $p_d \neq 0$ and $\hat{p}_d \neq 0$, then for all k $(0 \leq k < K_S + K_M)$, $|\lambda_k| \neq 1$. This implies that the inverse of $I - G$ exists.

Each row and column of G has exactly one nonzero entry implying that G is a generalized permutation matrix which can be written as $G = G^0 C$, where

$$G^0 \triangleq \text{diag}(\overbrace{1 \quad \cdots \quad 1}^{K_S-1} \quad \hat{p}_m \quad \overbrace{p_m \quad \cdots \quad p_m}^{K_M}) \tag{6.6}$$

and where

$$C = \begin{bmatrix} 0 & 1 & 0 & \cdots & 0 \\ \vdots & 0 & 1 & & \vdots \\ & & \ddots & \ddots & \\ 0 & & & 0 & 1 \\ 1 & 0 & \cdots & & 0 \end{bmatrix} \tag{6.7}$$

is the basic circulant permutation matrix, [84]. When G is multiplied on the right by a matrix, say A, then each row of A will be (circularly) shifted up by one and multiplied by the corresponding element of the main diagonal of G^0. Therefore,

$$\begin{gathered} G^{(K_M+K_S)\ell+n} = \alpha^\ell G^n \\ 0 \leq n < K_S + K_M, \quad 0 \leq \ell \end{gathered} \tag{6.8}$$

where $\alpha = \hat{p}_m p_m^{K_M}$. Hence,

$$\begin{aligned} (I-G)^{-1} = \sum_{k=0}^{\infty} G^k &= \sum_{n=0}^{K_S+K_M-1} G^n \sum_{\ell=0}^{\infty} \alpha^\ell \\ &= \frac{1}{1-\alpha} \sum_{n=0}^{K_S+K_M-1} G^n \end{aligned} \tag{6.9}$$

Consequently, the inverse of $I - G$ can be easily computed as the sum of a finite number of terms.

Appendix C: Detection Delay for $K_S = 1$

In this section, an alternative formula is derived for detection delay in the case of $K_S = 1$. From (4.19), when the length of SSI is one, detection delay is equal to D_1 in (4.17). Therefore, $\sum_{n=0}^{K_M} G^n$ can be represented by (6.10).

$$\sum_{n=0}^{K_M} G^n = \begin{bmatrix} 1 & \hat{p}_m & \hat{p}_m p_m & \hat{p}_m p_m^2 & \cdots & \hat{p}_m p_m^{K_M-1} \\ p_m^{K_M} & 1 & p_m & p_m^2 & \cdots & p_m^{K_M-1} \\ p_m^{K_M-1} & \hat{p}_m p_m^{K_M-1} & 1 & p_m & \cdots & p_m^{K_M-2} \\ \vdots & \vdots & \ddots & \ddots & \ddots & \vdots \\ p_m^2 & \hat{p}_m p_m^2 & \cdots & \hat{p}_m p_m^{K_M-1} & 1 & p_m \\ p_m & \hat{p}_m p_m & \hat{p}_m p_m^2 & \cdots & \hat{p}_m p_m^{K_M-1} & 1 \end{bmatrix} \tag{6.10}$$

Assuming $K_S = 1$ and substituting (6.10) into (6.9) and (4.17), one can verify that,

$$\begin{aligned} D = D_1 &= \frac{1}{1-\hat{p}_m p_m^{K_M}} + \\ &\frac{1}{(1-\hat{p}_m p_m^{K_M})(1+K_M)} \left(\sum_{n=1}^{K_M} n \hat{p}_m p_m^{n-1} + \sum_{n=1}^{K_M} n p_m^{K_M-n+1} \right) \\ &= \frac{1}{1-\hat{p}_m p_m^{K_M}} + \frac{1}{(1-\hat{p}_m p_m^{K_M})(1+K_M)} \times \\ &\left(\frac{K_M(p_m - \hat{p}_m p_m^{K_M})}{1-p_m} + \frac{(1-p_m^{K_M})(\hat{p}_m - p_m^2)}{(1-p_m)^2} \right) \end{aligned} \tag{6.11}$$

For small value of p_m, D is approximated by

$$D \approx 1 + \frac{1}{1+K_M} \left(\frac{\hat{p}_m - p_m^2}{(1-p_m)^2} + \frac{K_M p_m}{1-p_m} \right) \tag{6.12}$$

Appendix D:
Maximum K_M for $\mu > \mu_0$

From (4.24) and (6.12) and after some manipulations we get,

$$K_M \left(\frac{1}{p_d(\mu)} - D_{\max} \right) \leq \left(\frac{\hat{p}_d}{p_d^2(\mu)} - \frac{2}{p_d(\mu)} + D_{\max} \right) \tag{6.13}$$

As p_d is a decreasing function of μ followed by (4.25),

$$D_{\max} < \frac{1}{p_d(\mu)}, \quad \text{for} \;\; \mu > \mu_0 \tag{6.14}$$

So,

$$K_{M,\max} = \left\lfloor \frac{1/p_d(\mu) - D_{\max}}{\hat{p}_d/p_d^2(\mu) - 2/p_d(\mu) + D_{\max}} \right\rfloor \tag{6.15}$$

where $K_{M,\max}$ is maximum K_M for $\mu > \mu_0$ that does not violate (4.24).

Appendix E:
The values of $\hat{p}_d(i)$ for ED

The decision statistics decides in favor of H_1 when the total energy of the received signal during the SSI exceeds a threshold, say ψ_{ED}. Let us define $\zeta^{(i)}$ as the SNR in the SSI when the primary user emerges in the state i, $0 \leq i < K_S$. Then, $\zeta^{(i)} = \frac{Ks-i}{Ks}\zeta^{(0)}$ and, [19],

$$\hat{p}_d(i) = Q_{NK_S}(\sqrt{2NK_S\zeta^{(i)}}, \sqrt{\mu_{ED}}) \tag{6.16}$$

where $Q_m(\alpha, \beta)$ is the generalized Marcum Q-Function.

Appendix F: Derivation of the moments

It is easy to verify that

$$E[\psi_{\rm ge}(l)|H_\eta] = \sum_{k=0}^{M-l-1} \frac{1}{N} \sum_{m=0}^{N-1} \Re\left\{E\left[r_{k+l,m} r_{k,m}^* | H_\eta\right]\right\} = (M-l)\mathcal{A}_\eta(l) \tag{6.17}$$

from which it follows that

$$E[\psi_{\rm sp}(l)|H_\eta] = \frac{1}{N} \sum_{m=0}^{N-1} \Re\left\{E\left[r_{l,m} r_{0,m}^* | H_\eta\right]\right\} = \mathcal{A}_\eta(l) \tag{6.18}$$

Furthermore,

$$E[\psi_{\rm ge}(l)\psi_{\rm ge}(k)|H_\eta] = \frac{1}{N^2} \sum_{p=0}^{M-l-1} \sum_{q=0}^{M-k-1} \sum_{m=0}^{N-1} \sum_{n=0}^{N-1} E\left[\Re\left\{r_{p+l,m} r_{p,m}^*\right\} \Re\left\{r_{q+k,n} r_{q,n}^*\right\} | H_\eta\right] \tag{6.19}$$

In the following the correlation of $\psi_{\rm ge}(l)$ and $\psi_{\rm ge}(k)$ is first derived for an arbitrary angle θ. Let $\rho_\eta(l-k) \triangleq E[r_{l,m} r_{k,m}^* | H_\eta]$. It follows that

$$\rho_\eta(l-k) = \mathcal{A}_\eta(l-k) + j\mathcal{B}_\eta(l-k), \tag{6.20}$$

where $\mathcal{B}_\eta(k-l) \triangleq E[\Im\{r_{k,m} r_{l,m}^*\}|H_\eta]$. For the case of $\theta = 0$, we get $\mathcal{B}_\eta(l) = 0$ for all l. Using the assumption that the received signal samples are Gaussian, we get,

$$\begin{aligned}
&E[\psi_{\rm ge}(l)\psi_{\rm ge}(k)|H_\eta] = \frac{1}{4N^2} \sum_{p=0}^{M-l-1} \sum_{q=0}^{M-k-1} \sum_{m=0}^{N-1} \sum_{n=0}^{N-1} \\
&E\left[r_{p+l,m} r_{p,m}^* r_{q+k,n} r_{q,n}^* + r_{p+l,m} r_{p,m}^* r_{q+k,n}^* r_{q,n} \right. \\
&\left. + r_{p+l,m}^* r_{p,m} r_{q+k,n} r_{q,n}^* + r_{p+l,m}^* r_{p,m} r_{q+k,n}^* r_{q,n} | H_\eta\right] \\
&= \frac{1}{4N^2} \sum_{p=0}^{M-l-1} \sum_{q=0}^{M-k-1} \sum_{m=0}^{N-1} \sum_{n=0}^{N-1} \\
&[\rho_\eta(l)\rho_\eta(k) + \rho_\eta(l)\rho_\eta(-k) + \rho_\eta(-l)\rho_\eta(k) + \rho_\eta(-l)\rho_\eta(-k)] \\
&+ [\rho_\eta(p+l-q)\rho_\eta(q+k-p) + \rho_\eta(p+l-q-k)\rho_\eta(q-p) \\
&+ \rho_\eta(q+k-p-l)\rho_\eta(p-q) \\
&+ \rho_\eta(q-p-l)\rho_\eta(p-q-k)\,]\,\delta(m-n)
\end{aligned} \tag{6.21}$$

Now by considering the fact that

$$\rho_\eta(l)\rho_\eta(k) + \rho_\eta(-l)\rho_\eta(-k) = 2\mathcal{A}_\eta(l)\mathcal{A}_\eta(k) - 2\mathcal{B}_\eta(l)\mathcal{B}_\eta(k),$$

and

$$\rho_\eta(l)\rho_\eta(-k) + \rho_\eta(-l)\rho_\eta(k) = 2\mathcal{A}_\eta(l)\mathcal{A}_\eta(k) + 2\mathcal{B}_\eta(l)\mathcal{B}_\eta(k),$$

equation (6.21) reduces to,

$$\begin{aligned} &E[\psi_{\rm ge}(l)\psi_{\rm ge}(k)|H_\eta] = (M-l)(M-k)\mathcal{A}_\eta(l)\mathcal{A}_\eta(k) \\ &-\frac{1}{2N}\sum_{p=0}^{M-l-1}\sum_{q=0}^{M-k-1}[\mathcal{A}_\eta(p+l-q)\mathcal{A}_\eta(q+k-p)+ \\ &\mathcal{A}_\eta(p+l-q-k)\mathcal{A}_\eta(q-p) - \mathcal{B}_\eta(p+l-q)\mathcal{B}_\eta(q+k-p) \\ &-\mathcal{B}_\eta(p+l-q-k)\mathcal{B}_\eta(q-p)] \end{aligned} \tag{6.22}$$

Equation (5.31) now follows from (6.22) and (6.17) by setting $\theta = 0$. Finally from (6.22) we get

$$\begin{aligned} &E[\psi_{\rm sp}(l)\psi_{\rm sp}(k)|H_\eta] = \mathcal{A}_\eta(l)\mathcal{A}_\eta(k) \\ &-\frac{1}{2N}[\mathcal{A}_\eta(l)\mathcal{A}_\eta(k) + \mathcal{A}_\eta(l-k)\mathcal{A}_\eta(0) \\ &-\mathcal{B}_\eta(l)\mathcal{B}_\eta(k) - \mathcal{B}_\eta(l-k)\mathcal{B}_\eta(0)], \end{aligned} \tag{6.23}$$

from which (5.17) follows by setting $\theta = 0$.

Appendix G: Optimization of the weighting coefficients

Our goal is to choose the coefficients

$$\mathbf{w} \triangleq (w_{\rm sp}(1), w_{\rm sp}(2), \cdots, w_{\rm sp}(L)),$$

so as to optimize the system performance. Since both false-alarm and detection probabilities are a function of these coefficients, we formulate this problem as a constrained optimization problem, whereby we attempt to minimize the detection probability with a constraint on the false-alarm probability (a Neyman-Pearson type criterion). Examination of (5.21)-(5.24) reveals that scaling the coefficients $w_{\rm sp}(l)$ by the same factor does not change the probabilities of false alarm and detection. Therefore, to obtain a unique solution, the value of $\Omega_{\rm sp}$ in (5.26) is selected to be a constant. The optimization problem is now formulated as follows.

$$\begin{aligned} &\text{Maximize :} \quad P_1(\mathbf{w}), && (6.24)\\ &\text{Subject to :} \\ &\qquad P_0(\mathbf{w}) \leq \epsilon, && (6.25)\\ &\qquad \frac{1}{2}\sum_{l=1}^{L} w_{\rm sp}^2(l) = \Omega_0, && (6.26) \end{aligned}$$

where the dependence of $P_1(\mathbf{w})$ and $P_0(\mathbf{w})$ on $\{w_{\rm sp}(l)\}_{l=1}^{L}$ is shown explicitly. It is easy to verify that for the optimal solution, the inequality in (6.25) is satisfied with equality. Then we can evaluate the value of the threshold λ as in (5.27). Since the Q function is monotone decreasing, the optimization problem can be restated as

$$\begin{aligned} &\text{Maximize :} \quad J \triangleq \frac{m_{Y_L|H_1}(\mathbf{w})}{\sigma_{Y_L|H_1}(\mathbf{w})}, && (6.27)\\ &\text{Subject to :} \quad \frac{1}{2}\sum_{l=1}^{L} w_{\rm sp}^2(l) = \Omega_0, \end{aligned}$$

where $m_{Y_L|H_1}(\mathbf{w})$ and $\sigma_{Y_L|H_1}(\mathbf{w})$ are given by (5.22) and (5.23), respectively, and the value of λ in (5.22) and (5.23) is given by (5.27). The above problem is difficult to solve because of the complexity of the cost function J. However, we note that for small SNR values ($\varepsilon_s << N_0$), the standard deviation $\sigma_{Y_L|H_1}$ can be approximated by

$$\sigma_{Y_L|H_1} \approx \sqrt{\frac{N_0^2(\Omega_0^2 + \lambda^2)}{N}} \qquad (6.28)$$

Then using (6.28) the optimization problem in (6.27) can be replaced by

$$\begin{aligned} &\text{Maximize}: \quad \tilde{J} = c_1 \sum_{l=1}^{L} w_{\text{sp}}(l) A_1(l) - c_2 \\ &\text{Subject to}: \quad \frac{1}{2} \sum_{l=1}^{L} w_{\text{sp}}^2(l) = \Omega_0 \end{aligned} \tag{6.29}$$

where $c_1 = 1/\sigma_{Y_L|H_1}$ and $c_2 = Q^{-1}(\epsilon)$ are constants. The above problem can be solved using the Lagrange multipliers method. The Lagrangian is given by

$$\mathcal{J} = c_1 \sum_{l=1}^{L} w_{\text{sp}}(l) A_1(l) - c_2 - \zeta(\frac{1}{2} \sum_{l=1}^{L} w_{\text{sp}}^2(l) - \Omega_0) \tag{6.30}$$

Evaluating the partial derivative of $\mathcal{J}$ with respect to $w_{\text{sp}}(l)$ we obtain

$$\frac{\partial \mathcal{J}}{\partial w_{\text{sp}}}(l) = c_1 A_1(l) - \zeta w_{\text{sp}}(l) \qquad 1 \le l \le L \tag{6.31}$$

Setting (6.31) to zero and solving for $\{w_{\text{sp}}(l)\}_{l=1}^{L}$, we get the optimal solution:

$$w_{\text{sp}}^{opt}(l) = \frac{c_1}{\zeta} A_1(l) \qquad 1 \le l \le L \tag{6.32}$$

Substituting (6.32) in (6.26) we get

$$w_{\text{sp}}^{opt}(l) = \frac{\Omega_0 A_1(l)}{\sqrt{2 \sum_{l=1}^{L} A_1(l)^2}} \qquad 1 \le l \le L \tag{6.33}$$

From (6.33) we see that the optimal coefficients $w_{\text{sp}}^{opt}(l)$ are proportional to the correlations $A_1(l)$. Since Ω_0 is an arbitrary parameter, we can select it such that $w_{\text{sp}}^{opt}(l) = \frac{A_1(l)}{2\varepsilon_s} = \phi_{hh}^{RR}(l)$ for $1 \le l \le L$. We use these values in our simulations.

For the general case the mean of Y_L under H_1 is given by (5.33). Therefore, in the low SNR regime (6.27) reduces to

$$\begin{aligned} &\text{Maximize}: \quad \tilde{J} = c_1 \sum_{l=1}^{L} w_{\text{ge}}(l)(M-l) A_1(l) - c_2 \\ &\text{Subject to}: \quad \frac{1}{2} \sum_{l=1}^{L} w_{\text{ge}}^2(l) = \Omega_0 \end{aligned} \tag{6.34}$$

where c_1 and c_2 are as before. Following the same approach as above we get (5.35).

Appendix H: Available Blind Spectrum Sensing Algorithms

As described in the introduction, energy detector based spectrum sensing techniques have a good performance as long as they can precisely estimate the power of the noise, the power of the transmitted signal and the channel fading coefficients [28]. To get around these requirements, several authors have considered GLRT-based algorithms. A brief description of three of these approaches is given in the following. Consider the received signal

$$\mathbf{r} \triangleq \{r_{m,n}\}, \quad 0 \leq n \leq N-1, \quad 0 \leq m \leq M-1. \tag{6.35}$$

Define the matrix $\hat{\mathcal{R}}$ by,

$$\hat{\mathcal{R}} \triangleq \frac{1}{N}\mathbf{r}\mathbf{r}^H \tag{6.36}$$

By applying the singular value decomposition (SVD) to $\hat{\mathcal{R}}$ we get

$$\hat{\mathcal{R}} = \hat{\mathbf{U}}\hat{\mathbf{\Lambda}}\hat{\mathbf{V}} \tag{6.37}$$

where $\hat{\mathbf{\Lambda}} \triangleq \text{Diag}\{\hat{\lambda}_m\}, 0 \leq m \leq M-1$, and where $\{\hat{\lambda}_m\}$ is the set of eigenvalues of $\hat{\mathcal{R}}$. Suppose the eigenvalues are sorted in descending order. The decision statistics of the three algorithms are given in the following.

Arithmetic to Geometric Mean (AGM)

[29]

$$T_{AGM} \triangleq \frac{\frac{1}{M}\sum_{m=0}^{M-1}\hat{\lambda}_m}{(\prod_{m=0}^{M-1}\hat{\lambda}_m)^{1/M}}$$

Generalized Likelihood Ratio Detector-3 (GLRD3)

[28]

$$T_{GLRD3} \triangleq \frac{\hat{\lambda}_0}{\sum_{m=1}^{M-1}\hat{\lambda}_m}$$

Maximum to Minimum Eigenvalue (MME)

[21]

$$T_{MME} \triangleq \frac{\hat{\lambda}_0}{\hat{\lambda}_{M-1}}$$

Appendix I:
Distribution of received symbols

Lemma 3. *Suppose the primary users' transmitted symbols have zero mean and consider the received symbols under hypothesis H_1. If the PU signal constellation has constant modulus (as in MPSK), then the received symbols are circularly symmetric Gaussian random variables.*

Proof. Under H_1, we have $r_{k,m} = h_k s_m + v_{k,m}$. In light of the fact that by assumption $v_{k,m}$ is Gaussian, it is sufficient to show that $\nu_{k,m} = h_k s_m$ is Gaussian. Note that h_k is assumed to be a a circularly symmetric Gaussian random variable with unit variance. Conditioned on $s_m = s$, we get $\nu_{k,m} = sh_k$. Then clearly $\nu_{k,m}$ is Gaussian with variance $|s|^2$, i.e., for $\mathbf{x} = (x_1, x_2)$

$$f_{\nu_{k,m}|s_m}(\mathbf{x}|s) = \frac{1}{\pi|s|^2} e^{-\frac{|\mathbf{x}|^2}{|s|^2}}. \tag{6.38}$$

Now if the signal constellation has constant modulus such that $|s_m| = a$ for all m and some constant a, then the PDF of $\nu_{k,m}$ is given by

$$f_{\nu_{k,/m}}(\mathbf{x}) = \frac{1}{\pi a^2} e^{-\frac{|\mathbf{x}|^2}{a^2}} \tag{6.39}$$

□

In the case where the constellation does not have a constant modulus, the distribution of $\nu_{k,m}$ is a mixture of several zero-mean Gaussian distributions with different variances.

Vita

Mahdi Orooji was born in Tehran, Iran, in 1980. He received B.Sc. and M.Sc. degree in electrical engineering from the University of Tehran in 2003, and from Iran University of Science and Technology in 2006, respectively. He is currently working toward the Ph.D. degree in Electrical Engineering with the School of Electrical Engineering and Computer Sciences at the Louisiana State University (LSU), Baton Rouge. He is expected to graduate by May 2013.

Mr. Orooji worked as a graduate assistant at LSU from 2009 to present. He has been working under the supervision of Prof. Morteza Naraghi Pour. During his PhD in LSU, he has published three IEEE transaction papers, submitted one paper to IEEE transaction, and one paper to IEEE Signal Processing Letters. He also published one Globecom-2011 conference papers, three Milcom-2012 conference paper. He also submitted two other papers to ICASSP-2013.

His research interests are wireless communication and statistical signal processing. Mr. Orooji is the recipient of the H. D. Perkins Doctoral Fellowship Award from LSU during 2009-2013.